

学位論文

Theoretical analyses of Ru oxides on the basis of
a conserving approximation

(保存近似に基づくRu酸化物の理論解析)

平成25年12月博士(理学)申請

東京大学大学院理学系研究科

物理学専攻

荒川 直也

Abstract

In this thesis, I study the in-plane resistivity, ρ_{ab} , and the Hall coefficient, R_H , in the weak-field limit for the Ru t_{2g} orbital Hubbard model on a two-dimensional square lattice by using fluctuation-exchange approximation including the Maki-Thompson (MT) current vertex correction (CVC). In particular, I consider the cases near and away from the incommensurate (IC) antiferromagnetic (AF) quantum-critical point (QCP), where the spin fluctuation (SF) located at $\mathbf{Q}_{\text{IC-AF}} = (2\pi/3, 2\pi/3)$ is strongly enhanced.

I obtain six principal results. (i) ρ_{ab} shows the T -linear dependence near the IC AF QCP, while the T^2 dependence is obtained away from the IC AF QCP. This change arises from the stronger momentum dependence of the quasi-particle (QP) damping near the IC AF QCP. (ii) The effect of the MT CVC on the power of the temperature dependence of ρ_{ab} is negligible, although this leads to an increase of the value of ρ_{ab} as a result of a decrease of the current. (iii) The $d_{xz/yz}$ orbital gives the dominant contribution to the in-plane longitudinal conductivity, while the contribution of the d_{xy} orbital is very small. This is due to the combination of the smaller QP damping of the $d_{xz/yz}$ orbital and the momentum dependence of the band velocity. (iv) R_H is less affected by the self-energy of electrons. (v) The signs of the transverse conductivities of the $d_{xz/yz}$ and the d_{xy} orbitals are opposite in the model of Sr_2RuO_4 . As a result, R_H of this model without the MT CVC becomes nearly zero. (vi) The negative enhancement of R_H is induced by the MT CVC not only near but also away from the IC AF QCP, although in the latter case this enhancement is strongly suppressed at low temperatures. This negative enhancement arises from the bend of the current of the $d_{xz/yz}$ orbital due to the MT CVC of the non-diagonal SF between this and the d_{xy} orbitals at $\mathbf{Q}_{\text{IC-AF}}$. The strong suppression of R_H obtained away from the IC AF QCP arises from the cancellation between this negative enhancement and the positive enhancement arising from the bend of the current of the d_{xy} orbital due to the MT CVC of the diagonal SF of that orbital at $\mathbf{Q}'_{\text{IC-AF}} = (\pi, 2\pi/3)$.

From these results, I deduce the following conclusions. One is that ρ_{ab} of Ru oxides is determined almost by the $d_{xz/yz}$ orbital since the QP damping of that orbital will remain smaller than that of the d_{xy} orbital even in other Ru oxides. In particular, ρ_{ab} shows the T -linear dependence near the IC AF QCP due to the characteristic momentum dependence of the QP damping of the $d_{xz/yz}$ orbital. The other conclusion is that R_H of the model of Sr_2RuO_4 does not show the Curie-Weiss (CW) like temperature dependence even near the IC AF QCP since the bends of the currents of the $d_{xz/yz}$ and the d_{xy} orbitals due to the MT CVC lead to the opposite-sign contributions to R_H . The situation will be changed in other Ru oxides, where the occupation number of each orbital and/or a ratio of the QP damping of the d_{xy} orbital to that of the $d_{xz/yz}$ orbital are/is different from those/that of the model of Sr_2RuO_4 .

I propose that ρ_{ab} of Ru oxides can give information about the structure of the magnetic fluctuations not of the d_{xy} orbital but of the $d_{xz/yz}$ orbital, and that R_H of the Ru oxides in the weak-field limit can capture a characteristic transport property of a multi-orbital effect, which arises from the bend of the current of the $d_{xz/yz}$ orbital due to the MT CVC of the non-diagonal SF between that and the d_{xy} orbital at $\mathbf{Q}_{\text{IC-AF}}$.

I believe that the results obtained in this thesis not only lead to a deeper understanding of the transport properties of Ru oxides but also open a new door in the transport properties of multi-orbital strongly correlated electron systems (SCESs) since the similar mechanism will be realized in other multi-orbital SCESs where several sheets of the Fermi surface's are located near each other and the dimensionalities of the orbital characters are different.

Contents

1	Introduction	1
1.1	Outline of this thesis	1
1.2	Experimental review	2
1.2.1	Basis of the electronic structure	3
1.2.2	Unusual properties	6
1.3	Theoretical review	8
1.3.1	Electronic structure	8
1.3.2	Magnetic properties	12
1.3.3	Transport properties	13
1.4	Motivation	16
2	Formalism	19
2.1	Effective model of Sr_2RuO_4	20
2.2	FLEX approximation for multi-orbital systems	22
2.2.1	General derivation	22
2.2.2	Applicability	24
2.3	Transport coefficients on the basis of the microscopic FL theory	26
2.3.1	Resistivity	27
2.3.2	Hall coefficient in the weak-field limit	37
2.4	Irreducible four-point VF in the FLEX approximation	46
3	Results	53
3.1	QP damping	54
3.2	Dynamical property of SFs	56
3.3	In-plane resistivity	61
3.4	Hall coefficient in the weak-field limit	65
4	Discussion	71
4.1	Comparisons with other theoretical results	71
4.2	Correspondences with experimental results	73
5	Conclusions and remaining issues	75

Chapter 1

Introduction

In this chapter, after showing the outline of this thesis in §1.1, I briefly review experimental and theoretical results of Sr_2RuO_4 in §1.2 and §1.3, respectively, and explain motivations of the analyses of this thesis in §1.4. In these experimental and theoretical reviews, we focus on the electronic structure and the magnetic and the transport properties only in the paramagnetic (PM) phase of Sr_2RuO_4 . I do not show the results in the superconducting (SC) phase appearing below 1K [1] since the focus of this thesis is the transport properties in the PM phase. However, I believe that understanding the properties in the PM phase leads to a deep understanding of those in the SC phase.

1.1 Outline of this thesis

This thesis is organized as follows.

In Chapter 1, I give experimental and theoretical reviews of Sr_2RuO_4 , and explain the motivations of the analyses of this thesis. For the experimental review in §1.2, the basis of the electronic structure and five unusual properties are explained. For the theoretical review in §1.3, I present the results of some previous theoretical studies, discuss their correspondences to the experimental results, and explain some remaining issues. In particular, I argue that two of the five unusual properties can be explained in the fluctuation-exchange (FLEX) approximation [2], where spatial correlation is taken into account beyond the mean-field approximation (MFA) [3].

Next, in Chapter 2, I explain the method used for the calculations of resistivity and Hall coefficient in the weak-field limit, which are the transport properties focused, by using an effective model of Sr_2RuO_4 . First, in §2.1, I show an effective model of Sr_2RuO_4 , i.e., the Ru t_{2g} orbital Hubbard model on a two-dimensional (2D) square lattice. The parameters of the non-interacting part are determined so as to reproduce the electronic structure obtained in the local-density approximation (LDA) [4, 5]. The interacting part of this effective model is treated in the FLEX approximation [3], whose explanation is given in §2.2 following the discussion in Refs. [6, 7]. Section 2.3 is devoted to the general derivations of the resistivity and the Hall coefficient in the weak-field limit for multi-orbital systems. In these derivations, only the most divergent contributions with respect to the quasi-particle (QP) lifetime are taken into account [8, 9]. As a result, we see that the resistivity is inversely proportional to the QP lifetime, and the Hall coefficient is independent of that. In §2.4, I give the general derivation of the irreducible electron-hole four-point vertex function (VF), resulting in the correction to the

current, i.e. the current vertex correction (CVC) [10, 11], by using the self-energy of electrons in the FLEX approximation.

Then, in Chapter 3, I present numerical results near and away from the incommensurate (IC) antiferromagnetic (AF) quantum-critical point (QCP), which exists in the effective model of Sr_2RuO_4 [2], by using the FLEX approximation including the Maki-Thompson (MT) CVC [12, 13]. For simplicity, I neglect the Aslamasov-Larkin (AL) CVCs [14] since these are of higher order with respect to the QP damping than the MT CVC and these become negligible [11, 15] in the cases considered in this thesis.

Before showing the results of the transport coefficients, I present the momentum dependence of the QP damping in §3.1 and the dynamical property of spin fluctuations (SFs) in §3.2. Both the QP damping and the imaginary part of the effective interaction of the FLEX approximation, mediated by fluctuations in spin and charge sectors, are used in the kernel of the MT CVC. In §3.1, I analyze the role of each Ru t_{2g} orbital in the QP damping and discuss whether the phenomenological Fermi liquid (FL) description works or not. Here, the phenomenological FL description means that the single-particle Green's function can be approximated by the standard form of the coherent part [10, 16]. This description works when the QP damping is smaller than temperature considered [10]. In §3.2, I analyze the effects of U and T as well as the roles of the Ru t_{2g} orbitals on the dynamical property of SFs, and discuss how that dynamical property affects the current of each orbital through the MT CVC.

Sections 3.3 and 3.4 are devoted to the temperature dependence of the resistivity and of the Hall coefficient in the weak-field limit, respectively. In particular, I analyze the effects both of the momentum dependence of the self-energy of electrons and of the temperature dependence of the electron-hole four-point VF. Also, the roles of each Ru t_{2g} orbital and of each fluctuation (SF, orbital and spin-orbital combined fluctuations [17]) are investigated.

In Chapter 4, I compare the obtained results with other theoretical results in a single-orbital Hubbard model [11] on a 2D square lattice by the same approximation used in this thesis and in a tight-binding model of Sr_2RuO_4 by using the phenomenological theory [18]. I also address the correspondences with experimental results for Ru oxides.

Finally, in Chapter 5, I summarize principal results and conclusions drawn from this study, and I explain remaining issues for future study.

1.2 Experimental review

In this section, in order to explain basic properties of Sr_2RuO_4 , I briefly review several experimental studies for the PM phase of Sr_2RuO_4 [19].

As I will explain below in detail, there are five unusual properties, although extensive research has revealed that Sr_2RuO_4 can be regarded as a well-defined quasi-2D FL with moderately strong correlation. The five unusual properties are (1) the structure of magnetic fluctuations [20], (2) the orbital dependence of the mass enhancement [21], (3) the semiconductor-like temperature dependence of the out-of-plane resistivity in the high-temperature region [22], (4) the negative enhancement of the Hall coefficient at some temperatures due to tiny amount of nonmagnetic Al impurities [23], and (5) the T -linear in-plane resistivity appearing in the case of small substitution of Ti^{4+} for Ru^{4+} [24].

This section is organized as follows. I begin with the explanation of the basis of the electronic structure of Sr_2RuO_4 . After explaining the crystal structure [1] and the corresponding energy

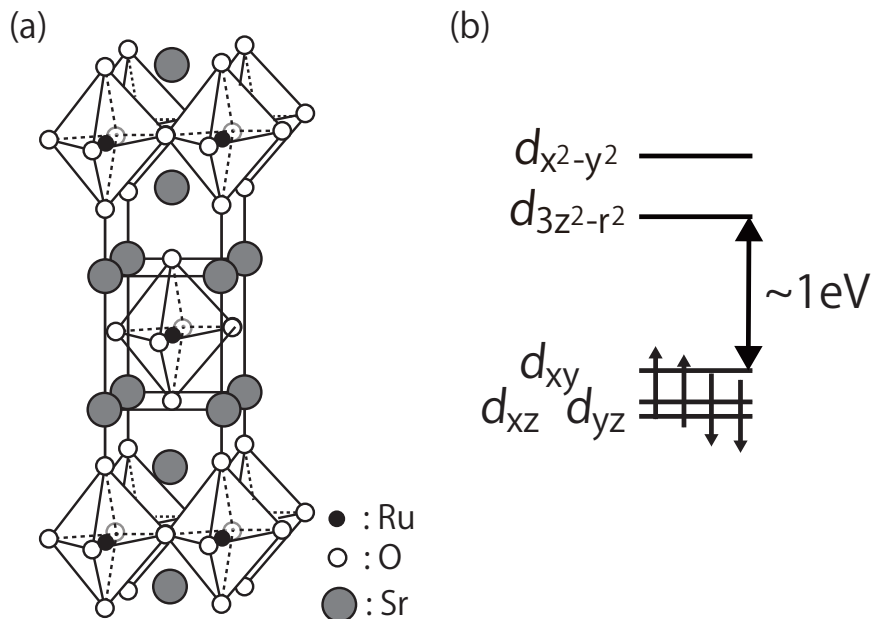


Figure 1.1: (a) Schematic crystal structure of Sr₂RuO₄ and (b) schematic energy levels of Sr₂RuO₄ for the Ru 4d orbitals. Up and down arrows in (b) represent spin-up and spin-down electrons, respectively.

levels for the Ru 4d orbitals, I present the Fermi surface (FS) observed experimentally [21, 25]. Next, I present several experimental results indicating the well-defined FL behaviors. These are transport properties [22, 26], the magnetic susceptibility [27], and the specific heat [27]. Then, I turn to several experimental results [19, 27, 28] which show the roles of electron correlation in Sr₂RuO₄. In particular, I argue that electron correlation is not so strong in Sr₂RuO₄ as in cuprates (i.e., copper oxides) but moderately strong, although electron correlation plays important roles. Finally, I explain the five unusual properties.

1.2.1 Basis of the electronic structure

By the extensive experimental research, it is well established that Sr₂RuO₄ can be regarded as a quasi-2D t_{2g} electron system.

According to a powder x-ray diffraction measurement [1], Sr₂RuO₄ is categorized as a layered perovskite oxide. The crystal structure has $I4/mmm$ body-centered tetragonal space-group symmetry. The schematic crystal structure is shown in Fig. 1.1 (a). In this crystal structure, only the d_{xz} and the d_{yz} orbitals are degenerate, as shown in Fig. 1.1 (b). Since Sr₂RuO₄ has the layered perovskite structure, the crystalline-electric-field (CEF) energy between the Ru e_g and the Ru t_{2g} orbitals is about 1 eV [28, 29]. Furthermore, the electronic conduction is anisotropic (e.g., quasi-2D), and the ratio of the in-plane resistivity to the out-of-plane resistivity at low temperature is about 10^{-3} [1]. The ratios at 2 K and 290 K are 1/850 and 1/220, respectively [1].

In addition, electrons occupying the Ru t_{2g} orbitals give the dominant contributions to the electronic conduction since a Ru ion is Ru⁴⁺, i.e. $(4d)^4$ configuration. Although the CEF energy between the Ru e_g and the Ru t_{2g} orbitals is large [Fig. 1.1 (b)], the CEF energy between the $d_{xz/yz}$ and the d_{xy} orbitals is small since the experimentally observed occupation numbers of these orbitals are nearly the same, i.e. 1.33 [21], due to the band overlap.

Actually, the measurement [21] of the de Haas-van Alphen (dHvA) effect has shown that

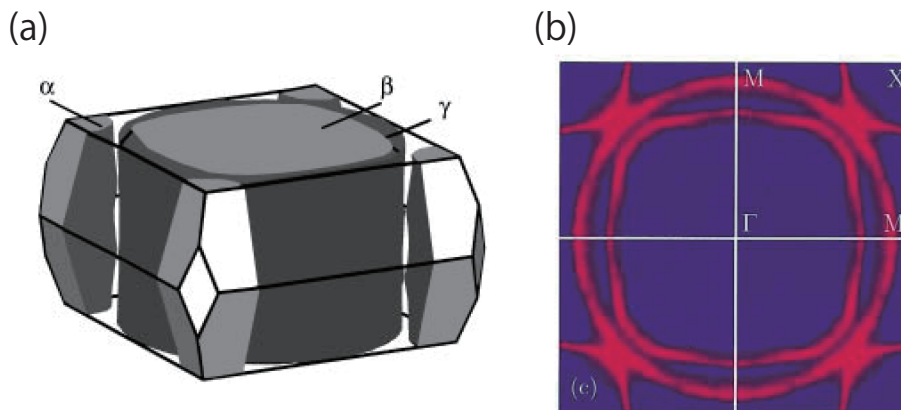


Figure 1.2: (a) Schematic picture of the FS of Sr_2RuO_4 observed by the dHvA effect [21] and (b) the FS observed by the ARPES [25]. (a) and (b) are reprinted from Ref. [21], “Copyright 1996 by the American Physical Society” and from Ref. [25], “Copyright 2000 by the American Physical Society”, respectively.

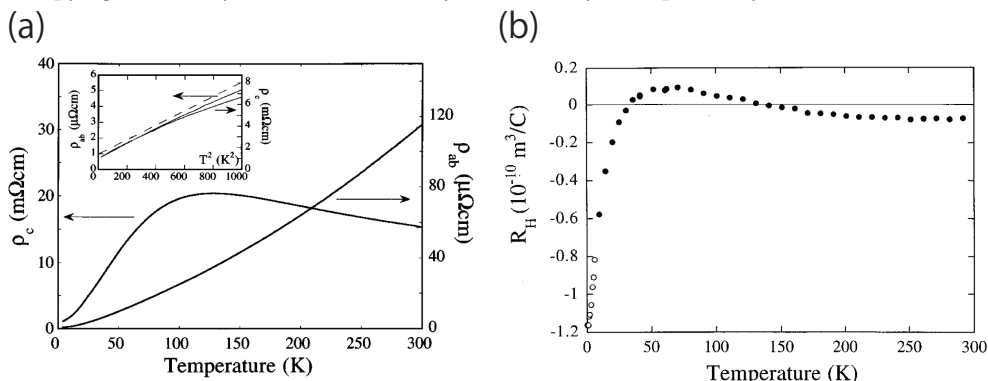


Figure 1.3: Temperature dependence of (a) the in-plane and the out-of-plane resistivities [22] of Sr_2RuO_4 and (b) the Hall coefficient [30] of Sr_2RuO_4 in a magnetic field of 2 T. The inset of (a) shows these resistivities below 32 K plotted against T^2 . (a) and (b) are reprinted from Ref. [22], “Copyright 1996 by the American Physical Society” and from Ref. [30], “Copyright 1996 by the American Physical Society”, respectively.

there are three cylindrical sheets of the FS’s consisting of the quasi-1D α and β sheets and the quasi-2D γ sheets. The schematic picture of the observed FS is shown in Fig. 1.2 (a). The $d_{xz/yz}$ and the d_{xy} orbitals form the quasi-1D and the quasi-2D sheets of the FS, respectively. This observation supports the above statement about the role of the Ru t_{2g} orbitals. Qualitatively the same result as the dHvA effect [21] has been obtained from angle-resolved photoemission spectroscopy (ARPES) measurement [25], as shown in Fig. 1.2 (b).

Extensive experimental research also reveals that Sr_2RuO_4 shows the following several well-defined FL behaviors. (The meaning of the well-defined FL has been described in §1.1.)

First, transport properties are consistent with the results obtained in the phenomenological FL theory [10]: the in-plane and the out-of-plane resistivities at low temperature show the T^2 dependence [22] as shown in Fig. 1.3 (a), and a Drude peak is observed below 30 K in the electric field applied both parallel and perpendicular to the RuO_2 planes [26]. Temperature dependence of the Hall coefficient [30] shown in Fig. 1.3 (b) is not so simple as in single-orbital systems. However, as I will explain in §1.3.3, this temperature dependence can be reproducible by a phenomenological theory [18] within the relaxation time approximation, assuming a typical

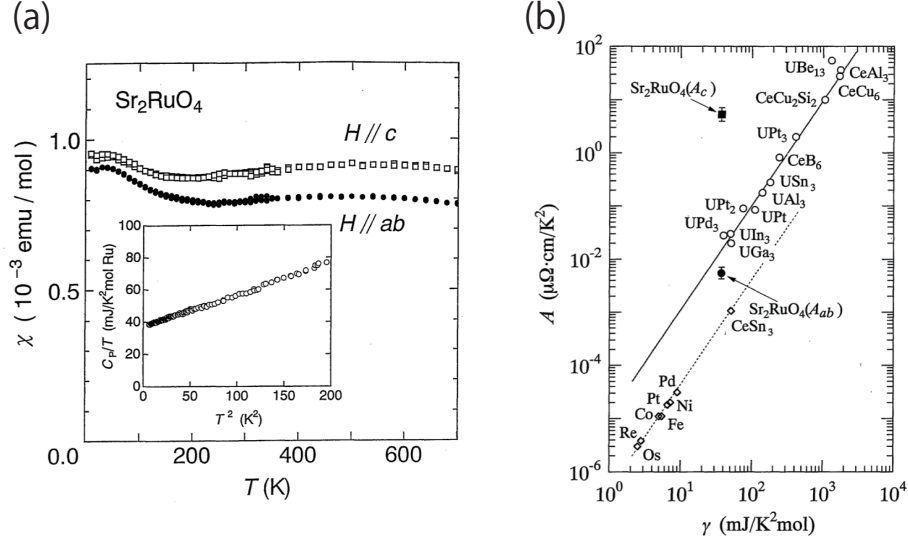


Figure 1.4: (a) Magnetic susceptibility of Sr_2RuO_4 in a magnetic field of 1 T and (b) the coefficient of the T^2 term of the in-plane and the out-of-plane resistivities of Sr_2RuO_4 against the coefficient of the electronic specific heat. Data shown in (a) are not corrected by diamagnetic contributions from the core electrons of -0.91×10^{-4} emu/mol. The inset in (a) shows the specific heat divided by temperature plotted against T^2 for a single crystal. The solid and the broken lines in (b) represent the Kadowaki-Woods ratio, a_0 , and $a_0/25$, respectively. Reprinted from Ref. [27], “Copyright 1997 by Physical Society of Japan”.

form [16] of the QP damping.

Second, as shown in Fig. 1.4 (a), the magnetic susceptibility in a magnetic field of 1 T shows very weak temperature dependence, indicating that the main contribution arises from Pauli paramagnetism [27]. Note that the temperature independent contribution arising from the Van Vleck term is very small compared with the observed value since the estimated contribution is approximately 1.5×10^{-4} emu/mol [31]. In addition, the Korringa behavior in the nuclear-magnetic-resonance (NMR) measurement [31].

Third, the temperature dependence of the specific heat, which is shown in the inset of Fig. 1.4 (a), is well fitted by the sum of the electron and the lattice contributions [27].

Next, I will explain that electron correlation is not so strong in Sr_2RuO_4 as in cuprates but moderately strong, although electron correlation plays important roles.

There are several evidences of the importance of electron correlation in Sr_2RuO_4 . One is the enhancement of the coefficient of the electronic specific heat [27]: the value is $37.5 \text{ mJ/K}^2 \text{ mol}$, which is about 3.6 times larger than that obtained in a band calculation [4]. In addition, the effective mass of each Ru t_{2g} orbital is about 3-5 times larger than that obtained in band calculations [4, 19]. Another is the Wilson ratio being larger than unity, which is the value for a free electron gas: the observed value is 1.7–1.9 [27]. Furthermore, as shown in Fig. 1.4 (b), the Kadowaki-Woods ratio for the in-plane conduction indicates the importance of electron correlation, i.e., the observed value is $0.3a_0$ – $0.5a_0$, which is not far from the value for typical heavy-fermion compounds (e.g., UPt_3 , CeCu_2Si_2) [27]. Here a_0 is the universal value, $1.0^{-5} \mu\Omega\text{cm}/(\text{mJ/K}^2)$.

On the other hand, a polarized O 1s x-ray absorption measurement [28] shows that the electron correlation of Sr_2RuO_4 is not so strong. Actually, the observed spectrum [28] can be reproduced within the unrestricted Hartree-Fock calculation for the two-site model, assuming

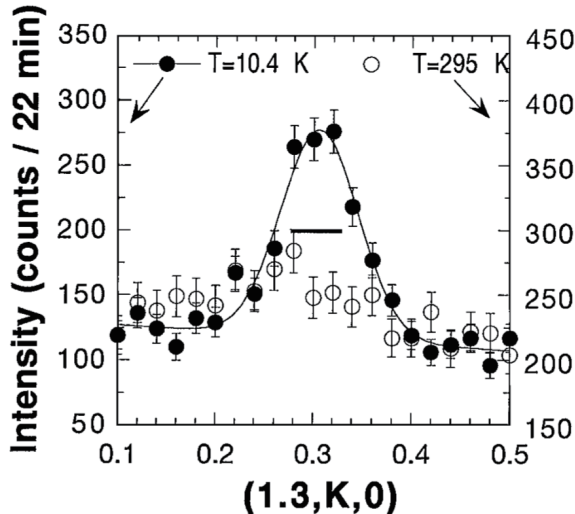


Figure 1.5: Intensity observed by INS measurement [20] of Sr_2RuO_4 at $\hbar\omega = 6.2$ meV around $\mathbf{Q} = \mathbf{q} + \mathbf{G} = (1.3, 0.3, 0)$ along $(0, 1, 0)$ direction, where $\mathbf{q} = (\pm 0.6\pi/a, \pm 0.6\pi/a, 0) = (\pm 0.3, \pm 0.3, 0)$ and \mathbf{G} is a zone center or a Z point (001) in the $(HK0)$ plane. The peak is originated not from the phonon but from the magnetic fluctuation since the lowest phonon frequency at \mathbf{q} is above 12 meV. Reprinted from Ref. [20], “Copyright 1999 by the American Physical Society”.

that the on-site intra-orbital Coulomb interaction of the Ru $4d$ orbitals is 2 eV. This value is about half of the total bandwidth of the Ru t_{2g} orbitals obtained in the band calculation [4, 44]. Thus, electron correlation of Sr_2RuO_4 is not so strong but moderately strong.

1.2.2 Unusual properties

In this section, I explain the five unusual properties of Sr_2RuO_4 . The first and the second unusual properties can be understood [2] if spatial correlation is taken into account beyond the MFA (see §1.3).

(1) The mechanism of the structure of magnetic fluctuations is unclear. As shown in Fig. 1.5, inelastic neutron scattering (INS) measurement [20] for Sr_2RuO_4 reveals the enhancement of IC AF SF located at $\mathbf{q} = (\pm 0.6\pi/a, \pm 0.6\pi/a, 0) = (\pm 0.3, \pm 0.3, 0)$ with a being the lattice constant along the a axis, while it does not find sizable ferromagnetic (FM) SFs. This result is unusual since the observed enhancement of the IC AF SF seems to arise from the nesting instability [32] of the $d_{xz/yz}$ orbital, of which the density-of-states (DOS) near the Fermi level is smaller than that of the d_{xy} orbital. Note that within the MFA, the primary contribution to the susceptibility arises from the orbitals having the largest DOS near the Fermi level. (As I will explain in §1.3, this magnetic structure cannot be reproduced even within the RPA for models with the experimentally observed occupation numbers [21].)

Since a polarized neutron measurement [33] for $\text{Ca}_{2-x}\text{Sr}_x\text{RuO}_4$ has revealed the role of each Ru t_{2g} orbital in the magnetic fluctuations, i.e. the primary contribution arises from the d_{xy} orbital, it is desirable to carry out similar analyses in Sr_2RuO_4 . Although there was a polarized neutron diffraction measurement [34] for Sr_2RuO_4 , this experiment did not discuss this issue since the aim was to analyze the symmetry of the Cooper pairing in the SC phase.

Although there was a controversial discussion about the inconsistency between the results of

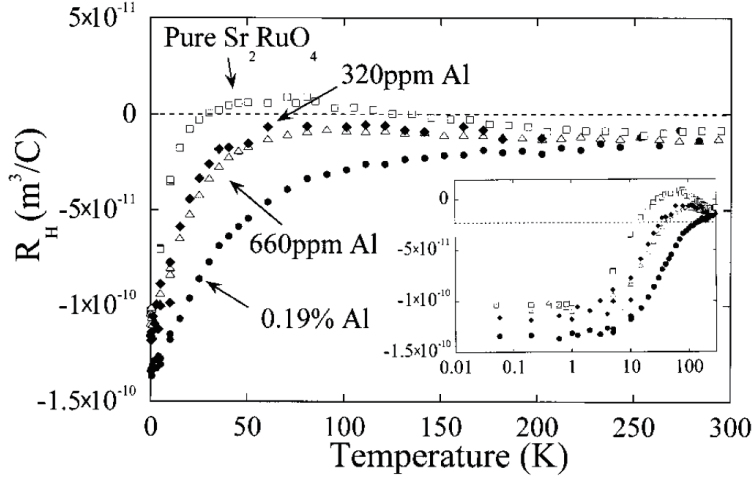


Figure 1.6: Temperature dependence of the Hall coefficient of Sr_2RuO_4 doped with Al [23] in the weak magnetic field. In this measurement, the magnetic field sweeps from -2 to 2 T for $T < 50$ K and from -3 to 3 T for $T > 50$ K. The inset shows the same data plotted in a logarithmic temperature scale in order to emphasize the low temperature behavior. Reprinted from Ref. [23], “Copyright 2001 by the American Physical Society”.

INS and NMR measurements, this has been resolved as follows. The authors of an early NMR measurement [35] for Sr_2RuO_4 have proposed that there will be no enhanced AF SF since the temperature dependence of the spin-lattice relaxation rate at Ru sites is the same as that at O sites. If commensurate AF SFs for Ru ions are enhanced, the amplitude should vanish at the magnetically symmetric O sites. However, the authors of a later NMR measurement [36] have pointed out that this result of the early NMR measurement [35] does not contradict with the evolution of the IC AF SF observed by INS measurement [20]. Thus, it is experimentally established that the IC AF SF located at $\mathbf{q} = (\pm 0.3, \pm 0.3, 0)$ is primary in Sr_2RuO_4 .

(2) Second unusual property is the orbital dependence of the mass enhancement. Combining the result of dHvA effect [21] and that of the band calculation, we can see that the mass enhancement of the γ band is larger than that of the α/β bands: the mass enhancements of α , β , γ bands are 3.0, 3.5, and 5.5, respectively [19]. This result seems to contradict with a simple theoretical argument that the mass enhancement is large when the bandwidth is small. In the case of Sr_2RuO_4 , the bandwidth of the quasi-1D $d_{xz/yz}$ orbital is smaller than that of the quasi-2D d_{xy} orbital.

(3) Third, as shown in Fig. 1.3 (a), the out-of-plane resistivity of Sr_2RuO_4 shows semiconductor-like behavior at high temperatures and has the maximum around 130 K, although it shows metallic behavior at low temperatures [22]. In contrast, the in-plane resistivity always shows metallic behavior [22]. This semiconductor-like behavior will arise from the incoherent conduction due to electron correlation (e.g. strong momentum dependence of the QP lifetime). Therefore, the roles of electron correlation in the transport properties of Sr_2RuO_4 should be analyzed on the basis of microscopic theory beyond the phenomenological FL theory, in which only the coherent conduction is treated [10].

(4) Fourth, tiny amount of nonmagnetic impurities of Al gives rise to unusual negative enhancement of the Hall coefficient [23] as shown in Fig. 1.6. This enhancement cannot be understood within a simple Born approximation for the nonmagnetic impurity scattering in

weakly correlated electron systems since in this case nonmagnetic impurities just give an additional QP damping [16]. In addition, in a single-orbital model, this enhancement cannot be reproduced even if the effects of strong electron correlation are taken into account. In this case, the weak nonmagnetic impurity scattering gives rise to a suppression of the absolute value of Hall coefficient from the value without impurities [37]. Thus, it is necessary to clarify the roles of orbital degrees of freedom in the transport properties in the presence of dilute nonmagnetic impurities.

(5) Fifth, the origin of the emergence of the T -linear in-plane resistivity [24] due to small substitution of Ti^{4+} for Ru^{4+} has not been clarified yet. The power of the temperature dependence of the in-plane resistivity changes from square in Sr_2RuO_4 to linear in $\text{Sr}_2\text{Ru}_{1-y}\text{Ti}_y\text{O}_4$ at $y = 0.025$, although the electronic structure of the latter is similar to that of Sr_2RuO_4 . Note that the Ti-substitution does not induce either the rotation or the tilting of RuO_6 octahedra [38], which give rise to drastic modifications of the electronic structure. From the results [11, 39] in single-orbital systems, we expect that this T -linear dependence will be related to the characteristic momentum dependence of the QP damping due to the enhanced fluctuations near an AF QCP. Actually, $\text{Sr}_2\text{Ru}_{1-y}\text{Ti}_y\text{O}_4$ at $y = 0.025$ is located near the IC AF QCP [24, 40, 41], whose magnetic fluctuations are nearly the same as those in Sr_2RuO_4 . Thus, it is desirable to investigate the in-plane resistivity in the presence of dilute nonmagnetic impurities not only in the case of Sr_2RuO_4 but also in the case near the IC AF QCP.

1.3 Theoretical review

In this section, I briefly review several theoretical studies for the PM phase of Sr_2RuO_4 , discuss their correspondence with the experimental results, and explain the remaining issues. In particular, I argue that spatial correlation beyond the MFA plays very important roles in discussing the electronic structure and the magnetic properties. Actually, the origins of two of the five unusual properties, shown in the previous section, have been clarified by an analysis [2] based on the FLEX approximation that takes account of spatial correlation beyond the MFA. Although there is a previous study [42] using the FLEX approximation, this previous study cannot explain the above two unusual properties. This previous study [42] uses a simplified effective interaction in which some contributions from SF have been neglected.

This section is organized as follows. I begin with previous theoretical results of the electronic structure on the basis of the band calculations in the LDA [4, 5, 43] and in the local-spin-density approximation (LSDA) [44], of the dynamical-mean-field theory (DMFT) [45, 46], and of the FLEX approximation [2]. We also compare these results with the experimental results and discuss their validities. Next, in §1.3.2, I present previous theoretical results of the magnetic properties on the basis of the mean-field type approximations [32, 47, 48, 49] and of the FLEX approximation [2]. I also give the comparisons with the experimental results and the discussions about their validities. Then, in §1.3.3, I present previous theoretical results of the transport properties on the basis of the phenomenological theory [18], discuss the validity, and explain the remaining issues.

1.3.1 Electronic structure

First, I show the results of the band calculations in the LDA [4, 5, 43] and in the LSDA [44], and discuss their validities.

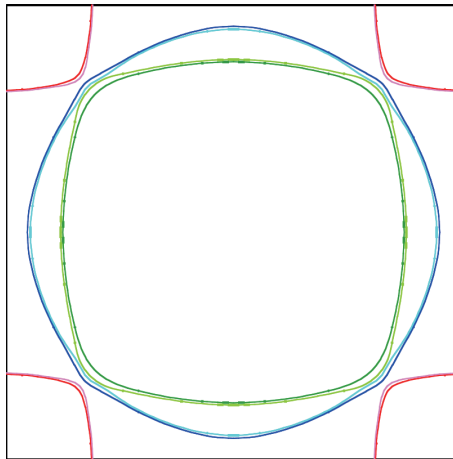


Figure 1.7: FS of Sr_2RuO_4 obtained in the LSDA on $k_z = 0$ in the range of $-\pi/a \leq k_x, k_y \leq \pi/a$ in the presence and the absence of the SOI [44]. Dark and light lines represent the FS sheets calculated in the presence and the absence of the SOI, respectively. In the absence of the SOI, the γ -FS (light blue) becomes very close to the inner sheet (light green) in the (π, π) direction. This contradicts with experiments [21, 25]. In the presence of the SOI, on the other hand, the γ -FS and the inner sheet separate, which is closer to the experimentally observed FS's. Reprinted from Ref. [44], "Copyright 2009 by Physical Society of Japan".

Basic properties of the electronic structure of Sr_2RuO_4 except several properties can be understood within the LDA. A band calculation [4] within the LDA just after the discovery [1] of Sr_2RuO_4 has revealed that the electronic structure near the Fermi level is essentially described by the antibonding bands of the Ru t_{2g} and the O $2p$ orbitals, and that the DOS near the Fermi level is originated mainly from that of the Ru t_{2g} orbitals. The similar results are obtained in other band calculations [5, 43, 44]. From the results of the LSDA [44], the spin-orbit interaction (SOI), which is estimated to be 0.167 eV for Ru atom, little affects the topology of the FS except the vicinity of $\mathbf{k} = (2\pi/3, 2\pi/3)$ and the energy dependence of the DOS. The FS obtained in the LSDA is shown in Fig. 1.7. The small value of the SOI is consistent with the experimental result [31] of the magnetic susceptibility.

However, the band calculations within the LDA cannot reproduce the experimentally observed occupation number of each Ru t_{2g} orbital. To be precise, the occupation numbers of the $d_{xz/yz}$ and the d_{xy} orbitals in the LDA are 1.39 and 1.23, respectively [45], which are different from the experimental values [21] of 1.33 and 1.33. This difference arises from a quantitative difference of the FS between the LDA and experiments [21, 25]: as shown in Fig. 1.7, the γ -FS becomes very close to the inner FS in the (π, π) direction. Furthermore, this occupation number is important in the magnetic properties discussed in §1.3.2. Thus, the LDA is inadequate to describe the properties of Sr_2RuO_4 , although the electronic structure obtained in the LDA is a good starting point in order to include effects of electron correlation.

Next, I discuss the results [45, 46] of the DMFT. The impurity solver used in Ref. [45] is not written, and that used in Ref. [46] is exact diagonalization.

The inconsistency in the occupation number is not resolved in a DMFT [45], although the values are improved. For example, in the case with the intra-orbital Coulomb interaction $U = 2.3$ eV and the Hund's rule coupling $J = 0.4$ eV, the occupation numbers of the $d_{xz/yz}$ and the d_{xy} orbitals are 1.36 and 1.29, respectively [45].

In the following, I explain the orbital dependence of the mass enhancement obtained in the DMFT [45] for Sr_2RuO_4 in detail.

Some authors of a DMFT [45] have proposed that the Hund's metal be the origin of the unusual orbital dependence of the mass enhancement of Sr_2RuO_4 since that can be reproduced only for large values of J . Here, the Hund's metal [50] is a metallic state with large effective mass due to a large value of J . The mass enhancement obtained in the DMFT arises mainly from local SF since the renormalization factors of the Ru t_{2g} orbitals show a monotonic J dependence.

Their results about the orbital dependence of the mass enhancement can be understood as the combination of the two effects explained below. One is a reduction of a critical value of U for a Mott transition, U_{MIT} , due to an increase of J . This arises from the J dependence [51] of the Mott gap for a t_{2g} orbital Hubbard model with $n_e = 4$, where n_e is the total occupation number. Namely, for a fixed value of U , an increase of J leads to the approaching the Mott transition. The other effect is that in all the parameters considered in Ref. [45], the occupation number of the d_{xy} orbital is nearer to 1 compared with that of the $d_{xz/yz}$ orbital, resulting in the smaller energy scale of local SF [52], i.e. the correlated Fermi temperature, of the d_{xy} orbital. Note that the mass enhancement is inversely proportional to a ratio of the correlated Fermi temperature to the non-interacting one. From these two effects, an increase of J gives rise to the larger mass enhancement of the d_{xy} orbital compared with that of the $d_{xz/yz}$ orbital [45].

However, this result [45] is drastically changed in a more realistic situation. First, the occupation numbers of the d_{xy} and the $d_{xz/yz}$ orbitals are the same experimentally [21]. Thus, for the model having the experimentally observed values of the occupation numbers, the correlated Fermi temperature of the d_{xy} ($d_{xz/yz}$) orbital becomes larger (smaller) than that obtained in this DMFT [45], resulting in the smaller (larger) mass enhancement of the d_{xy} ($d_{xz/yz}$) orbital. Second, on a 2D square lattice, if we take account of spatial correlation, we obtain a strong suppression of the mass enhancement compared with the DMFT results. Actually, in cellular DMFT [53, 54] for the single-orbital Hubbard model, the mass enhancement obtained in the DMFT is strongly suppressed by a partial account of spatial correlation. Note that in the cellular DMFT, the effects of spatial correlation are partially taken into account beyond the DMFT [55]. I expect that the similar result will be obtained for multi-orbital Hubbard models.

Furthermore, even within the DMFT, it is doubtful that a large value of J is important in order to obtain a larger mass enhancement of the d_{xy} orbital. Another DMFT [46] for Sr_2RuO_4 has revealed that for $J = (U/4)$, which is larger than that used in Ref. [45], the occupation number of the $d_{xz/yz}$ orbital becomes nearer to 1 at $U = 2.1$ eV, which is the same as that used in Ref. [45], than that of the d_{xy} orbital. In this case, the mass enhancement of the $d_{xz/yz}$ orbital will be larger than that of the d_{xy} orbital. This result contradicts the proposal of Ref. [45], i.e. the emergence of the Hund's metal in Sr_2RuO_4 . Thus, I doubt that the Hund's metal is realized in Sr_2RuO_4 , although there are some quantitative differences of the parameters of the non-interacting Hamiltonian between these previous studies [45, 46].

In order to understand the mass enhancement of Sr_2RuO_4 , I think that it is necessary to include spatial correlation.

Finally, I present the results of the FLEX approximation [2] and discuss its validity.

Similarly to the DMFT [45], the experimentally observed value of the occupation numbers cannot be reproduced in the FLEX approximation [2] for the model whose non-interacting FS is the same as the FS obtained in the LDA [4, 5], although the values are improved. To be precise, the occupation numbers of the $d_{xz/yz}$ and the d_{xy} orbitals are 1.357 and 1.284 at $U = 2.1$ eV

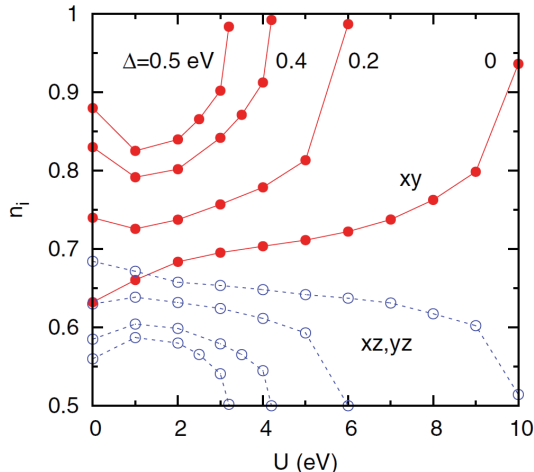


Figure 1.8: Occupation numbers of the d_{xy} and the $d_{xz/yz}$ orbitals per a spin as a function of U in a DMFT [46] of Sr_2RuO_4 at $J = U/4$ and $T = 0.02$ eV. It should be noted that $n_i = 1$ and 0.5 correspond to the full-filled and half-filled cases, respectively. Δ is the CEF energy between the d_{xy} and the $d_{xz/yz}$ orbitals. The result at $\Delta = 0$ eV corresponds to the case of Sr_2RuO_4 since the authors have used a tight-binding model of Sr_2RuO_4 , where Δ has been chosen as 0 eV for simplicity. Note that the impurity solver is exact diagonalization. Reprinted from Ref. [46], “Copyright 2007 by the American Physical Society”.

and $J = (U/6) = 0.35$ eV, while those at $U = 0$ eV are 1.375 and 1.249 .

In contrast to the occupation number, the larger mass enhancement of the d_{xy} orbital can be reproduced in the FLEX approximation in the range of $0 \leq J \leq (U/4)$, which is wider than in the DMFT [45]. Figures 1.9 (a) and (b) show the obtained renormalization factors of the $d_{xz/yz}$ and the d_{xy} orbitals, which are inversely proportional to the mass enhancements. The reason why the mass enhancement of the d_{xy} orbital is always larger than that of the $d_{xz/yz}$ orbital is that spatially broad SF of the d_{xy} orbital is strongly enhanced in all the cases considered [2].

As I show below, in contrast to the case of the DMFT [45], the results obtained in the FLEX approximation [2] will remain qualitatively the same even in a more realistic situation. First, I have checked in the FLEX approximation that, when the occupation number of each Ru t_{2g} orbital at $U = 0$ eV is chosen as the experimentally observed value [21], the mass enhancement of the d_{xy} orbital remains larger than that of the $d_{xz/yz}$ orbital [2]. In addition, we can expect that taking account of local correlation does not lead to a strong suppression of the mass enhancement obtained in the FLEX approximation. The reasons are as follows. (1) It is known that for the single-orbital Hubbard model on a 2D square lattice, the terms neglected in the FLEX approximation lead to a larger mass enhancement [56]. (2) The similar tendency will remain even for multi-orbital cases.

The difference between the FLEX approximation and the DMFT will be understood that on a 2D square lattice, the Mott transition is easily destabilized by spatial correlation, while an AF instability is hardly destabilized by local correlation.

From the above discussions, I conclude that a correct treatment of both local and spatial correlations is necessary to reproduce the experimentally observed value [21] of the occupation numbers if we regard the electronic structure obtained in the LDA [4, 5, 43] as a good starting point in order to include effects of electron correlation, and that spatial correlation plays

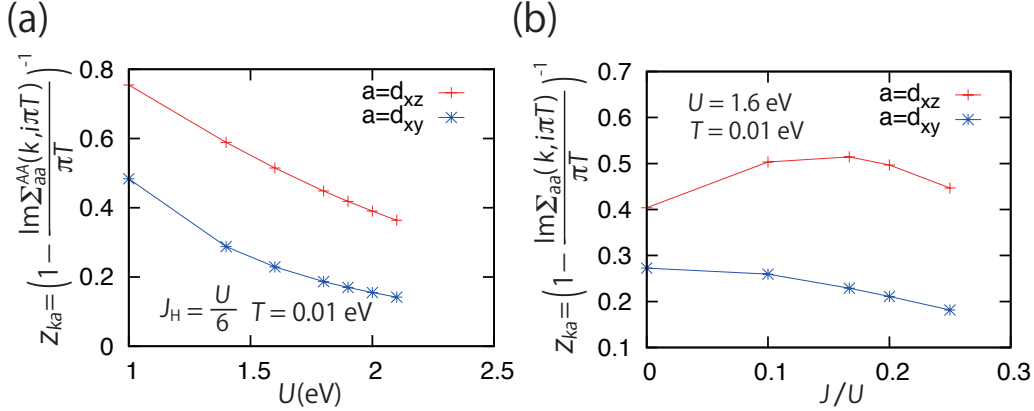


Figure 1.9: Renormalization factors of the d_{xz} and the d_{xy} orbitals at $\mathbf{k} = (3\pi/4, 21\pi/32)$ and $(7\pi/8, \pi/8)$ as functions of (a) U and (b) (J/U) in the FLEX approximation [2] for a 2D tight-binding model of Sr_2RuO_4 , where the non-interacting FS is the same as that obtained in the LDA [4, 5]. 64×64 meshes and 1024 Matsubara frequencies are used. For all the cases considered, the mass enhancement of the d_{xy} orbital is larger than that of the $d_{xz/yz}$ orbital. At other wave vectors, the similar relative magnitude is obtained. Note that the mass enhancement is inversely proportional to the renormalization factor.

more important roles in discussing the orbital dependence of the mass enhancement than local correlation does. In other words, the unusual orbital dependence of the mass enhancement is originated from the stronger enhancement of the spatially broad SF of the d_{xy} orbital than that of the $d_{xz/yz}$ orbital.

1.3.2 Magnetic properties

The authors of a band calculation [32] within the LDA have proposed the nesting instability for the $d_{xz/yz}$ orbital with $\mathbf{q} \approx (2\pi/3, 2\pi/3)$. This result seems to be consistent with the result of an INS measurement [20].

However, this result will be modified if the occupation number of each Ru t_{2g} orbital becomes the same as that observed experimentally [21]. (As described in §1.3.1, the occupation numbers of the $d_{xz/yz}$ and the d_{xy} orbitals in the LDA are 1.39 and 1.23, which are different from the experimental values, 1.33 [21].) The reason is as follows (see Fig. 1.10). The increase (decrease) of the occupation number of the d_{xy} ($d_{xz/yz}$) orbital means that the bands of the d_{xy} ($d_{xz/yz}$) orbital should be lower (higher). As a result, the DOS of the $d_{xz/yz}$ (d_{xy}) orbital near the Fermi level decreases (increases). Then, these changes of the DOS give rise to the decrease (increase) of the susceptibility of the $d_{xz/yz}$ (d_{xy}) orbital.

Actually, in the RPA [47, 48] for the model having the experimentally consistent occupation number [21], it is shown that the dominant contribution to the spin susceptibility arises from the d_{xy} orbital and the wave vector of the primary instability becomes $\mathbf{q} \approx (\pi, \pi/2)$, although for large values of the Hund's rule coupling there appears an enhancement of the IC AF SF located at $\mathbf{q} \approx (2\pi/3, 2\pi/3)$. The results in the RPA [48] are shown in Figs. 1.11 (a) and (b). (Note that there is a quantitative difference between Refs. [47] and [48] due to a slight difference of the choice of hopping parameters.) There is another previous study [49] in the RPA, showing that the primary contribution to the spin susceptibility arises from the $d_{xz/yz}$ orbital. However, this result is incorrect since the occupation numbers used in Ref. [49] are inconsistent with the

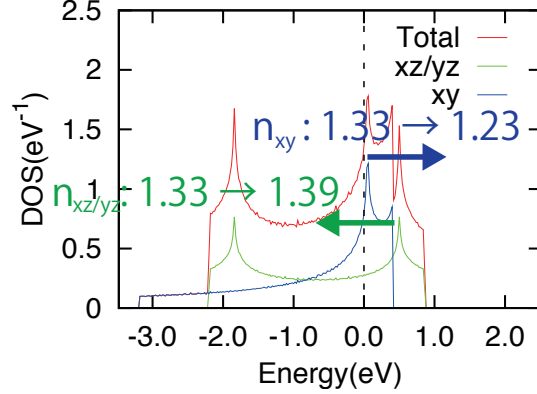


Figure 1.10: Non-interacting DOS of a 2D tight-binding model of Sr_2RuO_4 , where the occupation number of each Ru t_{2g} orbital is the experimentally consistent value, 1.33. Green and blue arrows represent the changes of the DOSs of the $d_{xz/yz}$ and the d_{xy} orbitals, as the occupation number becomes the value obtained in the LDA [4, 5, 43]. These changes lead to a decrease (an increase) of the DOSs of the $d_{xz/yz}$ (d_{xy}) orbital near the Fermi level.

experiment [21].

In contrast to the cases of the mean-field type approximation [32, 47, 48, 49], the IC AF SF located at $\mathbf{q} \approx (2\pi/3, 2\pi/3)$ is reproduced in the FLEX approximation [2] by using the model whose occupation number of each orbital without interactions is the same as the experimentally observed occupation number [48]. The similar result is obtained in another model whose non-interacting FS is the same as that obtained in the LDA [4, 5]. In the former (latter) model, electron correlation leads to the occupation number leaving (approaching towards) the value observed experimentally [21]. Namely, if spatial correlation is taken into account beyond the MFA, it is natural to reproduce the IC AF SF observed experimentally in a wide range of the parameters of the non-interacting Hamiltonian.

As revealed by the analysis of the FLEX approximation [2], the essential factor to understand the unusual magnetic property is the cooperative enhancement of SF for all the Ru t_{2g} orbitals, which is induced by the merging of the nesting vectors for the $d_{xz/yz}$ and the d_{xy} orbitals due to the deformation of the FS. In other words, the self-energy correction of electrons beyond the MFA plays significant roles in discussing the magnetic properties. Actually, we see from Figs. 1.12 (a)–(c) that when the peaks of SF for the $d_{xz/yz}$ and the d_{xy} orbitals are set to merge, the IC AF SF located at $\mathbf{q} = (2\pi/3, 2\pi/3)$ becomes primary.

Thus, I conclude that spatial correlation beyond the MFA is essential for understanding the magnetic properties of Sr_2RuO_4 .

1.3.3 Transport properties

In this section, I present the result of the transport property of Sr_2RuO_4 within the phenomenological theory [18]. A phenomenological theory [18] can reproduce the temperature dependence of the in-plane resistivity and the Hall coefficient, as shown in Figs. 1.13 (a) and (b). In this theory, these transport coefficients are calculated within the relaxation time approximation using a tight-binding model of Sr_2RuO_4 . Here the authors give the QP damping, $1/\tau_a$, by the following momentum-independent form with some ad hoc parameters: $1/\tau_a = \eta_a + \alpha_a T^2$, where $a = d_{xz}, d_{yz}, d_{xy}$, $\{\eta\} = (2.75, 2.75, 3.25)$, and $\{\alpha\} = (0.035, 0.04, 0.06)$. Note that this QP damping is

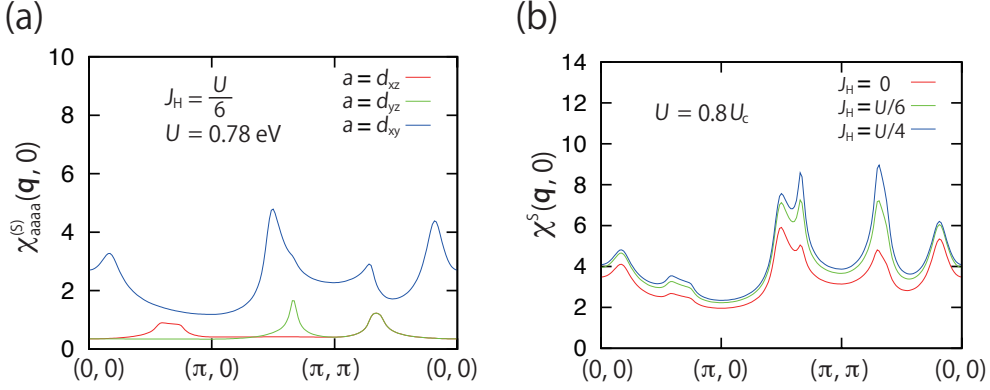


Figure 1.11: Momentum dependence of (a) the static susceptibility in a spin sector and (b) the static spin susceptibility, $\sum_{a,b} \chi_{aabb}^{(S)}(\mathbf{q}, 0)$, within the RPA at $T = 0.02$ eV for a 2D tight-binding model of Sr_2RuO_4 having the experimentally consistent occupation number [48]. 128×128 meshes and 1024 Matsubara frequencies are used. U_c is a critical value of the magnetic transition, which is $U_c = 0.975$ eV at $J_H = U/6$. The wave vector of the corresponding instability is $\mathbf{q} \approx (\pi, \pi/2)$. At a small (large) value of J_H , U_c is larger (smaller) than the value at J_H .

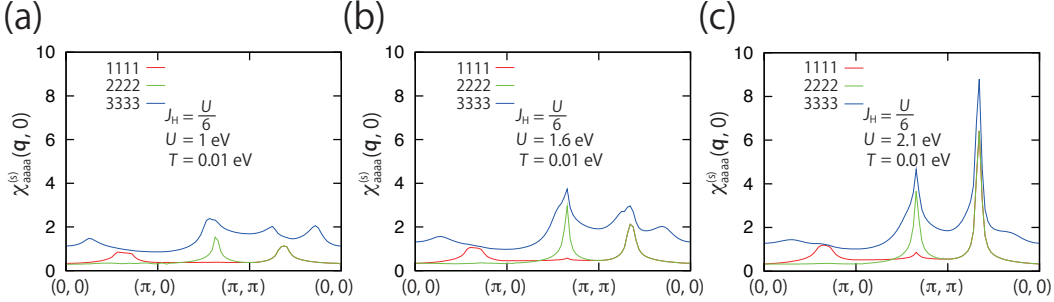


Figure 1.12: Momentum dependence of the static susceptibility in a spin sector at $U = 1, 1.6, 2.1$ eV in the FLEX approximation [2] for a 2D tight-binding model of Sr_2RuO_4 , where the non-interacting FS is the same as that obtained in the LDA [4, 5]. 64×64 meshes and 1024 Matsubara frequencies are used. 1, 2, and 3 denote the d_{xz} , the d_{yz} , and the d_{xy} orbitals, respectively.

the typical form in the FL [16]. In addition to the above QP damping, the authors add the T -linear term, $0.6T$, only for the d_{xy} orbital in the case of the in-plane resistivity, assuming that Sr_2RuO_4 is a nearly FM metal. This assumption is inconsistent with the experiment [20]. However, the similar temperature dependence of the in-plane resistivity will be obtained at low temperatures in the cases without the above T -linear term since the dominant contribution to the in-plane conduction will arise from the $d_{xz/yz}$ orbital, whose QP damping is smaller than that of the d_{xy} orbital.

Although the above phenomenological theory seems to be reasonable, it is necessary to analyze the transport properties beyond the phenomenological theory, i.e. on the basis of a microscopic theory satisfying conservation laws, since the following factors lacking in the phenomenological theory will be important in Ru oxides. As I will explain in §2.3.1, to obtain the thermodynamically consistent result about transport, we should treat conservation laws correctly.

One is the momentum dependence of the self-energy of electrons. The real and the imaginary parts of the self-energy lead to the renormalization of the band velocity and the QP damping.

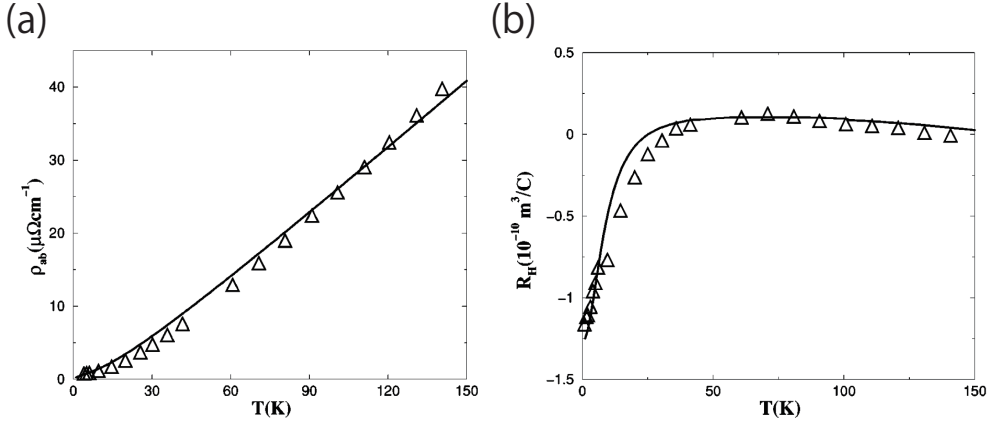


Figure 1.13: Temperature dependence of (a) the in-plane resistivity and (b) the Hall coefficient on the basis of the phenomenological theory in the relaxation time approximation by using a tight-binding model of Sr_2RuO_4 and assuming a typical FL type QP damping. The solid lines in (a) and (b) are the theoretical results, and the triangles in (a) and (b) show experimental data from Ref. [22] and from Ref. [30], respectively. [These experimental data are shown in 1.3 (a) and (b).] Reprinted from Ref. [18], “Copyright 2000 by the American Physical Society”.

In particular, the effect of the momentum dependence of QP damping becomes considerable for a quasi-2D SCES since the van Hove singularity (vHs), which exists in 2D systems [57], gives strong momentum dependence. Actually, it is known that for a single-orbital Hubbard model on a 2D square lattice near the AF QCP [11, 58], the strong momentum dependence of the QP damping gives rise to the non-FL-like temperature dependence of the in-plane resistivity. As I will show in §2.3.1, the resistivity is proportional to the QP damping when only the most divergent contributions with respect to the QP lifetime, which is the inverse of the QP damping, are taken into account. It should be noted that in addition to $\text{Sr}_2\text{Ru}_{1-y}\text{Ti}_y\text{O}_4$ [24] at $y = 0.025$, $\text{Ca}_{2-x}\text{Sr}_x\text{RuO}_4$ [59] around $x = 0.5$ shows the non-FL-like temperature dependence of the in-plane resistivity [Fig. 1.14 (a)], indicating the importance of the momentum dependence of the imaginary part of the self-energy of electrons.

Another factor is the temperature dependence of the electron-hole four-point VF. The electron-hole four-point VF describes the multiple electron-hole scattering [10], which is strongly enhanced and shows unusual temperature dependence near a QCP [39]. Similarly to the momentum dependence of the self-energy of electrons, this plays very important roles in discussing the transport properties of SCES since, as we will see from Eq. (2.47) in §2.3.1, this leads to a correction to the current. In particular, the effect is significantly important in the Hall coefficient compared with the resistivity [11, 15]. As we will see from Eqs. (3.5) in §3.3 and (3.14) in §3.4, this difference arises from the dependence on the correction of the angle for the current, which plays the most important role in discussing the effect of electron correlation on the Hall coefficient. Actually, it is known that for a single-orbital Hubbard model on a 2D square lattice near the AF QCP, the temperature dependence of the electron-hole four-point VF gives rise to the CW-like temperature dependence of the Hall coefficient [11, 15]. The similar temperature dependence has been experimentally observed in $\text{Ca}_{2-x}\text{Sr}_x\text{RuO}_4$ around $x = 0.5$ [23], as shown in Fig. 1.14 (b). Thus, the effect of the temperature dependence of the electron-hole four-point VF is also necessary to be analyzed.

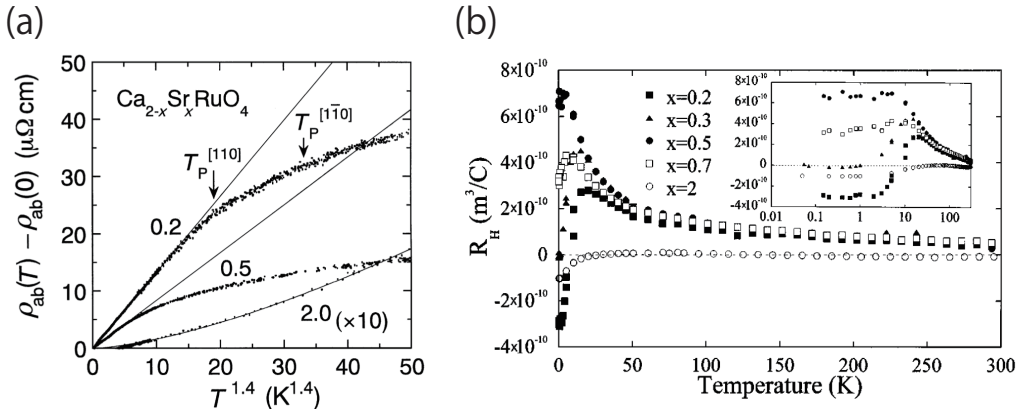


Figure 1.14: Temperature dependence of (a) the in-plane resistivity [59] of $\text{Ca}_{2-x}\text{Sr}_x\text{RuO}_4$ and (b) the Hall coefficient [23] of $\text{Ca}_{2-x}\text{Sr}_x\text{RuO}_4$ in the weak magnetic field. In the measurement of (b), the magnetic field sweeps from -2 to 2 T for $T < 50$ K and from -3 to 3 T for $T > 50$ K. (a) and (b) are reprinted from Ref. [59], “Copyright 2000 by the American Physical Society” and from Ref. [23]., “Copyright 2001 by the American Physical Society”, respectively.

1.4 Motivation

As explained above, the origins of three of five unusual properties of Sr_2RuO_4 have not been clarified yet, and there are two remaining issues.

The aims of the analyses of this thesis are to clarify the origin of unusual transport properties of Ru oxides and to reveal the effects of both the momentum dependence of the self-energy of electrons and the temperature dependence of the electron-hole four-point VF in multi-orbital SCES from a theoretical point of view. In particular, the goals are to clarify the origins of the unusual transport properties of Ru oxides and to understand what are the effects of orbital degrees of freedom on the transport properties of SCESs. However, in this thesis, I do not investigate out-of-plane conduction and the effects of dilute nonmagnetic impurities on the transport properties due to the difficulties of the treatment. In the former case, the difficulties are the treatments of the three-dimensionality and of the incoherent conduction at high temperatures. In the latter case, the difficulty is the treatment of nonmagnetic impurity scattering in the presence of strong electron correlation. Although the studies of these issues are remaining future problems, I believe that the results obtained in this thesis will lead to a deep understanding of the transport properties not only in Ru oxides but also in other multi-orbital SCESs.

In order to clarify the effects of both the momentum dependence of the self-energy of electrons and the temperature dependence of the electron-hole four-point VF, I study an effective model of Sr_2RuO_4 in the FLEX approximation including the MT CVC. For simplicity of the actual calculations, I do not consider the case of $\text{Ca}_{2-x}\text{Sr}_x\text{RuO}_4$ around $x = 0.5$, where the rotation of RuO_6 octahedra leads to a unit cell doubling [38].

The treatment used in this thesis is valid to analyze the transport properties in the regions near a QCP at low temperatures. These regions correspond to red ellipse shown in Fig. 1.15. The reason of this applicability is as follows. The transport coefficients are derived by taking account of the most divergent terms with respect to the QP lifetime. This derivation is valid in the metallic phases except high temperature regions. In addition, I neglect the AL CVCs and consider only the MT CVC, since those are of higher order than the MT CVC. In general,

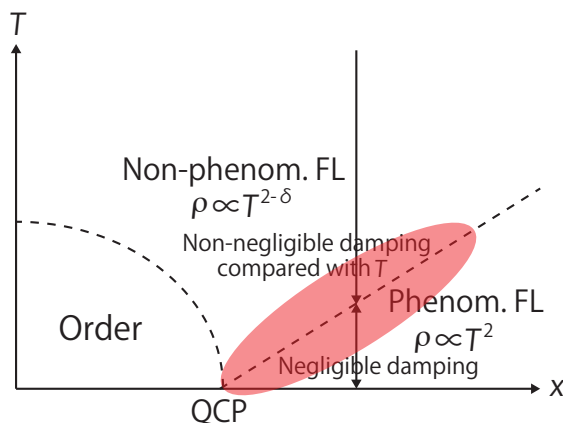


Figure 1.15: One of the typical phase diagrams for SCESs. T is temperature and x is a certain tuning parameter (e.g. pressure). Red ellipse represents the region where the treatment used in this thesis is valid since the contribution of the AL CVCs will be very small compared with the MT CVC in this region.

we should include both the MT and the AL CVCs to obtain the thermodynamically consistent result. However, my approximation to neglect the AL CVCs will be valid to analyze the effects of the two factors neglecting in the phenomenological theory on the transport properties near an AF QCP qualitatively since the contribution of the AL CVCs will be very small compared with that of the MT CVC near the QCP. Actually, for a single-orbital Hubbard model on a 2D square lattice, it is shown that the AL CVCs are negligible compared with the MT CVC near the AF QCP [11, 15]. The similar result will be obtained even for the present multi-orbital Hubbard model. However, the check of the validity is a remaining future problem.

The reason why I use the model of Sr_2RuO_4 is that this model contains not only orbital degrees of freedom but also the vHs, which gives rise to unusual transport properties as the case of single-orbital systems [11, 58]. I think that the model of Sr_2RuO_4 is suitable to investigate the roles of both the momentum dependence of the self-energy of electrons and the temperature dependence of the electron-hole four-point VF in determining the transport properties of multi-orbital SCESs from a theoretical point of view.

Chapter 2

Formalism

In this chapter, I explain the method to analyze the magnetic, the single-particle and the transport properties of Sr_2RuO_4 . In §2.1, I begin with the explanation about an effective model of Sr_2RuO_4 , i.e. the Ru t_{2g} orbital Hubbard model on a 2D square lattice within the next-nearest-neighbor (NNN) hopping, and about how to choose the parameters. Next, in §2.2, I explain the FLEX approximation for multi-orbital systems, which is used to treat effects of electron correlation, following the discussion in Refs. [6, 7]. I also give several remarks on its applicability from a theoretical point of view on the basis of some previous theoretical studies [56, 60] for the single-orbital Hubbard model on a 2D square lattice. Then, §2.3 is devoted to the general derivations of the resistivity and the Hall coefficient for multi-orbital systems on the basis of the microscopic FL theory. In this treatment, only the most divergent contributions with respect to the QP lifetime are considered. As a result, the longitudinal and the transverse conductivities are proportional to the linear and the square terms, respectively. Finally, in §2.4, I give the general derivation of the irreducible electron-hole four-point VF, which is necessary to determine the resistivity and the Hall coefficient, by using the FLEX approximation. Here we call irreducible all diagrams that cannot be split into two parts by removing an electron-hole pair [10]. The derivations shown in §2.3 and §2.4 are just the extensions of those [8, 9, 11] in the single-orbital case.

Hereafter, the following units and notations are used. I set $\hbar = c = \mu_B = k_B = 1$, and choose the coordinates x , y , and z in the directions of the Ru-O bonds [see Fig. 1.1 (a)]. For convenience, the d_{xz} , the d_{yz} and the d_{xy} orbitals are labeled 1, 2 and 3, respectively. In some cases shown below, the spin degree of freedom is not explicitly written since we consider only

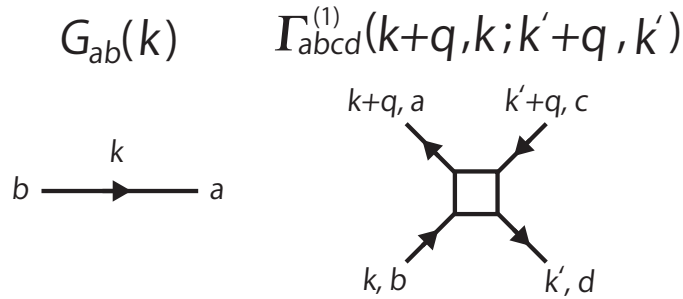


Figure 2.1: Diagrammatic representations of the single-particle Green's function and the electron-hole irreducible four-point VF. The definitions for other electron-hole four-point VFs are the same.

PM states without the SOI. For brevity, the electron-hole four-point VF is called the four-point VF since all the four-point VF we consider below are electron-hole type except a discussion in §2.2.2. I use the abbreviations, k and q , which are $k \equiv (\mathbf{k}, i\omega_m)$ and $q \equiv (\mathbf{q}, i\Omega_n)$ in Matsubara frequency representation or are $k \equiv (\mathbf{k}, \epsilon)$ and $q \equiv (\mathbf{q}, \omega)$ in real frequency representation, where $\mathbf{k} = (k_x, k_y)$ and $\mathbf{q} = (q_x, q_y)$ are wave vectors, ω_m and Ω_n are fermionic and the bosonic Matsubara frequencies, i.e. $\omega_m = \pi T(2m + 1)$ and $\Omega_n = 2\pi Tn$ with integers, m and n , and temperature, T . In the diagrammatic representations shown below, the single-particle Green's function and the four-point VF are defined as those shown in Fig. 2.1. In this definition, the direction of the single-particle Green's function is opposite to that used in a standard textbook [16]: the arrow I use goes from the point where an electron is created to that where an electron is annihilated.

2.1 Effective model of Sr_2RuO_4

In this section, I show an effective model of Sr_2RuO_4 to analyze the magnetic, the single-particle and the transport properties at low temperature, and explain how to choose the parameters. In this effective model, I neglect the SOI, for simplicity, assuming that the effect will be small. (As described in §1.3, the theoretical estimate of the value in the LSDA is 0.167 eV [44], which is small compared with other energy scales.)

In order to analyze the properties of Sr_2RuO_4 , I consider the Ru t_{2g} orbital Hubbard model on a 2D square lattice within the NNN hopping:

$$\hat{H} = \hat{H}_0 + \hat{H}_{\text{int}}, \quad (2.1)$$

$$\hat{H}_0 = \sum_{\mathbf{k}} \sum_{a,b=1}^3 \sum_{s=\uparrow,\downarrow} \epsilon_{ab}(\mathbf{k}) \hat{c}_{\mathbf{k}as}^\dagger \hat{c}_{\mathbf{k}bs}, \quad (2.2)$$

$$\begin{aligned} \hat{H}_{\text{int}} = & U \sum_j \sum_{a=1}^3 \hat{n}_{ja\uparrow} \hat{n}_{ja\downarrow} + U' \sum_j \sum_{a=1}^3 \sum_{b<a} \hat{n}_{ja} \hat{n}_{jb} \\ & - J_{\text{H}} \sum_j \sum_{a=1}^3 \sum_{b<a} (2\hat{\mathbf{s}}_{ja} \cdot \hat{\mathbf{s}}_{jb} + \frac{1}{2} \hat{n}_{ja} \hat{n}_{jb}) + J' \sum_j \sum_{a=1}^3 \sum_{b<a} \hat{c}_{ja\uparrow}^\dagger \hat{c}_{ja\downarrow}^\dagger \hat{c}_{jb\downarrow} \hat{c}_{jb\uparrow}. \end{aligned} \quad (2.3)$$

Here I have introduced several quantities: $\hat{c}_{\mathbf{k}as}^\dagger$ ($\hat{c}_{\mathbf{k}as}$) is the creation (annihilation) operator that creates (annihilates) an electron in a with spin s at \mathbf{k} , $\hat{n}_{ia} = \sum_s \hat{n}_{ias} = \sum_s \hat{c}_{ias}^\dagger \hat{c}_{ias}$, $\hat{\mathbf{s}}_{ia} = (1/2) \sum_{s,s'} \hat{c}_{ias}^\dagger \boldsymbol{\sigma}_{s,s'} \hat{c}_{ias'}$ with $\boldsymbol{\sigma}_{s,s'}$ being the Pauli matrices, and $\epsilon_{ab}(\mathbf{k})$, U , U' , J_{H} , and J' represent the energy dispersions measuring from the chemical potential, μ , the intra-orbital and the inter-orbital Coulomb interactions, the Hund's rule coupling, and the pair hopping, respectively. The chemical potential is determined so that the total occupation number, n_e , satisfies $n_e = 4$:

$$n_e = \frac{2}{N} \sum_{\mathbf{k}} \sum_{\alpha} f(\epsilon_{\alpha}(\mathbf{k})) + \frac{2T}{N} \sum_k \sum_{a=1}^3 [G_{aa}(k) - G_{aa}^{(0)}(k)]. \quad (2.4)$$

Here 2 is the factor of the spin degeneracy, α is the band index, $f(\epsilon)$ is the Fermi-Dirac distribution function,

$$\epsilon_{\alpha}(\mathbf{k}) = \sum_{a,b=1}^3 (U_{\mathbf{k}}^\dagger)_{\alpha;a} \epsilon_{ab}(\mathbf{k}) (U_{\mathbf{k}})_{b;\alpha}, \quad (2.5)$$

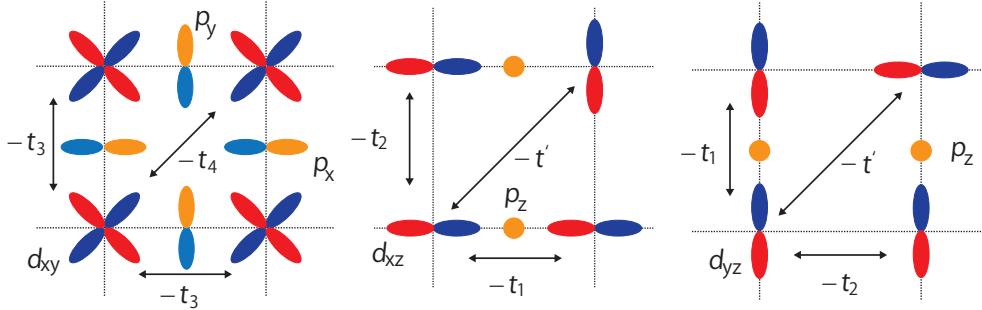


Figure 2.2: Schematic picture of the in-plane hopping processes for the Ru t_{2g} orbitals within the NNN hopping. The difference of a color in each orbital represents that of the sign of the wave function.

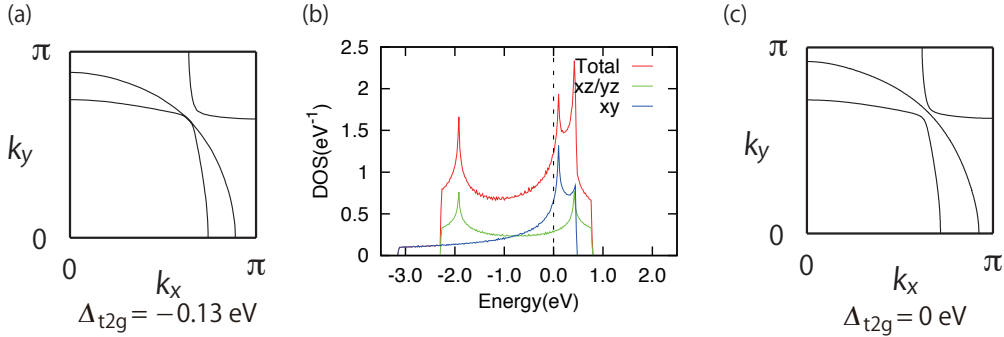


Figure 2.3: (a) FS and (b) DOS of the effective model for $\Delta_{t_{2g}} = -0.13$ eV, where the non-interacting FS is the same as that obtained in the LDA [4, 5], and (c) FS of the effective model for $\Delta_{t_{2g}} = 0$ eV, where the occupation numbers of these orbitals are 1.33.

with $(U_{\mathbf{k}})_{a;\alpha}$ being a unitary matrix to diagonalize \hat{H}_0 , and $G_{ab}^{(0)}(k)$ and $G_{ab}(k)$ are the non-interacting and the interacting single-particle Green's functions, whose chemical potentials are the same. $G_{ab}^{(0)}(k)$ is given by

$$G_{ab}^{(0)}(k) = \sum_{\alpha} (U_{\mathbf{k}})_{a;\alpha} \frac{1}{i\omega_m - \epsilon_{\alpha}(\mathbf{k})} (U_{\mathbf{k}}^{\dagger})_{\alpha;b}, \quad (2.6)$$

and the method to determine $G_{ab}(k)$ is described in §2.2. The reason why Eq. (2.4) is used instead of the equation where only $G_{aa}(k)$ appears is to exclude the ultraviolet divergent term in it.

In order to carry out numerical calculations, I choose the parameters in \hat{H}_0 and \hat{H}_{int} as follows.

For the non-interacting part, \hat{H}_0 , the energy dispersions are given by

$$\epsilon_{11}(\mathbf{k}) = \frac{\Delta_{t_{2g}}}{3} - 2t_1 \cos k_x - 2t_2 \cos k_y - \mu, \quad (2.7)$$

$$\epsilon_{12}(\mathbf{k}) = \epsilon_{21}(\mathbf{k}) = -4t' \sin k_x \sin k_y, \quad (2.8)$$

$$\epsilon_{22}(\mathbf{k}) = \frac{\Delta_{t_{2g}}}{3} - 2t_2 \cos k_x - 2t_1 \cos k_y - \mu, \quad (2.9)$$

$$\epsilon_{33}(\mathbf{k}) = -\frac{2\Delta_{t_{2g}}}{3} - 2t_3(\cos k_x + \cos k_y) - 4t_4 \cos k_x \cos k_y - \mu, \quad (2.10)$$

$$\epsilon_{ab}(\mathbf{k}) = 0 \quad \text{otherwise,} \quad (2.11)$$

and the parameters are chosen so as to reproduce the band structure obtained in the LDA [4, 5]: the hopping integrals within the NNN hopping processes shown in Fig. 2.2 are $(t_1, t_2, t_3, t_4, t') = (0.675, 0.09, 0.45, 0.18, -0.03)$ (eV) and the CEF energy between the d_{xy} and the $d_{xz/yz}$ orbitals are $\Delta_{t_{2g}} = -0.13$ eV [2]. Figure 2.2 shows the schematic pictures of the in-plane hopping processes for the Ru t_{2g} orbitals within the NNN hopping. This choice of the parameters is based on the assumption that the electronic structure obtained in the LDA [4, 5] is a good starting point in order to include correlation effect beyond the mean-field level. In this choice, the total bandwidth is about 4 eV, the occupation numbers of the $d_{xz/yz}$ and the d_{xy} orbitals are 1.38 and 1.25, respectively, the γ -FS is located nearer to the inner FS than in the case of the experiments [21, 25], and the vHs for the d_{xy} orbital is located above the Fermi level. The FS and the DOS of this effective model are shown in Figs. 2.3 (a) and (b), respectively. Note that if we set $\Delta_{t_{2g}} = 0$ eV, the occupation numbers of the Ru t_{2g} orbitals become the experimentally observed values [21], i.e. 1.33. In this case, the obtained FS is in better agreement with the experimentally observed FS [21, 25] than for $\Delta_{t_{2g}} = -0.13$ eV [compare Figs. 2.3 (a) and (c)].

For the interacting part, \hat{H}_{int} , I use the FLEX approximation, which is one of the perturbation theories to take account of effects of electron correlation. The detailed treatment is described in the next section.

2.2 FLEX approximation for multi-orbital systems

In this section, I briefly explain the FLEX approximation for multi-orbital systems, which is used to treat effects of electron correlation, by following the discussion of Refs. [6, 7], and give several remarks on its applicability from a theoretical point of view. These remarks are based on some previous theoretical studies [56, 60] for the single-orbital Hubbard model on a 2D square lattice.

As I will explain below in detail, the FLEX approximation is suitable for describing the electronic and the transport properties at low temperatures with moderately strong electron correlation qualitatively. In particular, the suitability becomes better in analyses of the transport properties such as the resistivity and the Hall coefficient than in those of the electronic structures since the importance of the electronic state near the Fermi level, which can be appropriately treated in the FLEX approximation, is more significant in these transport properties.

2.2.1 General derivation

After explaining what the FLEX approximation is and its merits from a theoretical point of view, I show the self-consistent loop of this approximation, which is used to determine the single-particle quantities and the susceptibilities.

The FLEX approximation is a perturbation theory beyond the RPA on the basis of a conserving approximation [3, 60, 61, 62]. In this approximation, the renormalization of fluctuations due to electron correlation is taken into account within the one-loop order. It is noted that in the conserving approximation, whose discussion is based on a free energy, conservation laws hold automatically [61, 62]. To be precise, in the conserving approximation [61, 62], choosing the form of the Luttinger-Ward functional, $\Phi_{\text{LW}}[G]$, which appears in the free energy, we obtain some quantities by the functional derivations of $\Phi_{\text{LW}}[G]$. It is also noted that the reason of the name of the FLEX approximation is that in this approximation, exchange of collective excitations can be taken into account systematically [3, 60].

There are several merits of the FLEX approximation. One is to satisfy conservation laws for bulk quantities automatically. This is crucial for obtaining a reasonable description of transport. Another merit is to include spatial and local correlation in principle, although the account of local correlation is not appropriate for large values of electron correlation [56]. Another merit is to take account of the mode-mode coupling of fluctuations partially through the self-energy of electrons [3]. This account of the mode-mode coupling leads both to a suppression of the instability obtained in the RPA and to the Curie-Weiss (CW) like temperature dependence of the susceptibilities at several wave vectors. (As I will present in §3, the CW like temperature dependence is obtained in the FLEX approximation for an effective model of Sr_2RuO_4 .)

It should be noted that the terms neglected in the FLEX approximation give rise to a larger mass enhancement, a larger suppression of the instability and a stronger temperature dependence of the susceptibilities in the case of the single-orbital Hubbard model on a 2D square lattice [56, 39]. Even for multi-orbital Hubbard models on the same lattice, we will obtain the similar result.

I go on to show the self-consistent loop of the FLEX approximation, which is used to determine the single-particle quantities, the susceptibilities, and the effective interaction.

For the actual calculations, I use $\Phi_{\text{LW}}[G]$ consisting of bubble and ladder diagrams only for electron-hole scattering processes [6, 7], which become very important near a QCP [39]. Correspondingly, $G_{ab}(k)$, the self-energy of electrons, $\Sigma_{ab}(k)$, and the effective interaction, $V_{abcd}(q)$, are determined by the following set of equations:

$$G_{ab}(k) = G_{ab}(k) + \sum_{c,d} G_{ac}^{(0)}(k) \Sigma_{cd}(k) G_{db}(k), \quad (2.12)$$

$$\chi_{abcd}(q) = -\frac{T}{N} \sum_k G_{db}(k) G_{ac}(k+q), \quad (2.13)$$

$$\chi_{abcd}^{(\text{S})}(q) = \chi_{abcd}(q) + \sum_{\{a'\}} \chi_{aba'b'}(q) \Gamma_{a'b'c'd'}^{\text{S}} \chi_{c'd'cd}^{(\text{S})}(q), \quad (2.14)$$

$$\chi_{abcd}^{(\text{C})}(q) = \chi_{abcd}(q) - \sum_{\{a'\}} \chi_{aba'b'}(q) \Gamma_{a'b'c'd'}^{\text{C}} \chi_{c'd'cd}^{(\text{C})}(q), \quad (2.15)$$

$$\begin{aligned} V_{abcd}(q) &= \frac{3}{2} \sum_{\{a'\}} \Gamma_{aba'b'}^{\text{S}} \chi_{a'b'c'd'}^{(\text{S})}(q) \Gamma_{c'd'cd}^{\text{S}} + \frac{3}{2} \Gamma_{abcd}^{\text{S}} \\ &+ \frac{1}{2} \sum_{\{a'\}} \Gamma_{aba'b'}^{\text{C}} \chi_{a'b'c'd'}^{(\text{C})}(q) \Gamma_{c'd'cd}^{\text{C}} - \frac{1}{2} \Gamma_{abcd}^{\text{C}} \\ &- \sum_{\{a'\}} \frac{1}{2} (\Gamma_{aba'b'}^{\text{S}} + \Gamma_{aba'b'}^{\text{C}}) \chi_{a'b'c'd'}(q) \frac{1}{2} (\Gamma_{c'd'cd}^{\text{S}} + \Gamma_{c'd'cd}^{\text{C}}), \end{aligned} \quad (2.16)$$

$$\Sigma_{ac}(k) = \frac{T}{N} \sum_q \sum_{b,d} V_{abcd}(q) G_{bd}(k-q). \quad (2.17)$$

Here $\sum_{\{a\}} = \sum_{a,b,c,d}$, and $\chi_{abcd}^{(\text{S/C})}(q)$ and $\Gamma_{abcd}^{\text{S/C}}$ are the susceptibility for a spin/charge sector

and the bare interaction vertex for a spin/charge sector, which is given by

$$\Gamma_{abcd}^{S/C} = \begin{cases} U/U & \text{for } a = b = c = d \\ J_H/(2U' - J_H) & \text{for } a = b \neq c = d \\ U'/(-U' + 2J_H) & \text{for } a = c \neq b = d \\ J'/J' & \text{for } a = d \neq b = c \\ 0/0 & \text{otherwise} \end{cases} . \quad (2.18)$$

Note that the set of equations of the FLEX approximation, Eqs. (2.12)–(2.17), is easily derived by calculating the RPA type but renormalized effective interaction consisting of bubble and ladder diagrams for electron-hole scattering processes for \hat{H} and neglecting the VC in the susceptibilities.

Concerning Eqs. (2.12)–(2.17), there are two remarks. One is that $\chi_{abcd}^{(S)}(q)$ and $\chi_{abcd}^{(C)}(q)$ contain information about SF and spin-orbital-combined fluctuation and about charge and orbital fluctuations [17], respectively. Note that spin-orbital-combined fluctuation is characterized by the correlation function for the spin-orbital operator, the product of the irreducible matrices of spin and orbital degrees of freedom [17]. For example, for the t_{2g} -orbital Hubbard model, the operator is the product of the Pauli matrix for a spin degree of freedom and the Gell-Mann matrix for an orbital degree of freedom [17]. The other remark is that the last term in Eq. (2.16) is introduced in order to avoid a double counting of the topologically equivalent diagram in the self-energy of electrons.

2.2.2 Applicability

Before going to the next section, I briefly remark on the applicability of the FLEX approximation from a theoretical point of view. Several remarks are given by the comparisons between the results in the FLEX approximation and others for the single-orbital Hubbard model on a 2D square lattice. Others are the results of quantum Monte Carlo (QMC) simulation [60] and those in the second-order and the fourth-order perturbation theories [56] with respect to U . In these calculations, the NNN hopping integral has been neglected, although in Ref. [60] the value has not been written explicitly.

At a moderately large value of U , the single-particle Green's function obtained in the FLEX approximation is in a qualitatively good agreement with that obtained in QMC simulation, although there are quantitative differences at a certain wave vector [60], as shown in Figs. 2.4 and 2.5. In particular, we see from these figures that the agreement is better for $\langle n \rangle = 1$ than for $\langle n \rangle = 0.875$. This indicates that when a system is located nearer to an AF QCP, the more suitable the FLEX approximation is. Note that parquet approximation, whose results are also compared with the others in Figs. 2.4 and 2.5, is one of the perturbation theories, where the three kinds of the irreducible four-point VFs, i.e. longitudinal and transverse electron-hole types and electron-electron type, are self-consistently determined by the (parquet type) Bethe-Salpeter (BS) equations. Namely, the FLEX approximation corresponds to the first step in an iterative solution of this parquet approximation.

On the other hand, when the value of U is very large, the FLEX approximation becomes unsuitable for describing the electronic structures. This unsuitability arises from the inappropriate treatment of local correlation since local correlation becomes important for large values of U [52, 64]. Actually, in the FLEX approximation, the incoherent peak in electronic spectrum,

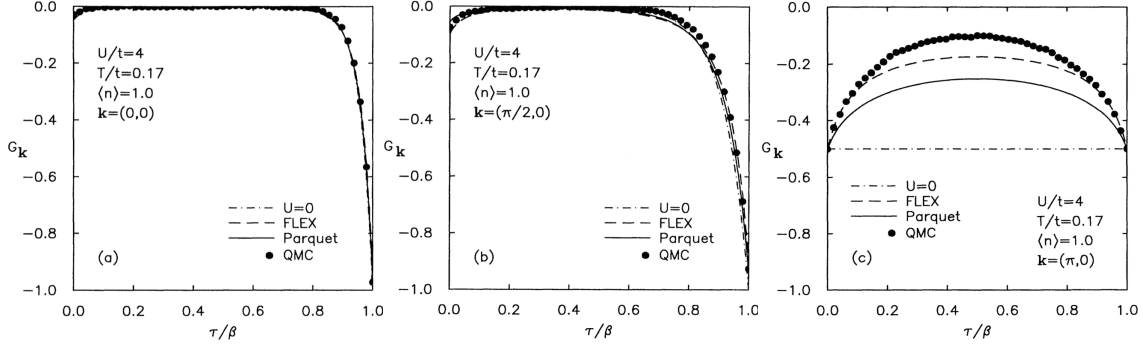


Figure 2.4: Single-particle Green's function obtained in several methods for the single-orbital Hubbard model. 8×8 meshes are used and $\langle n \rangle$ is fixed at 1. We see the better agreement between the results of the QMC simulation and the FLEX approximation than the agreement between those of the QMC simulation and the parquet approximation. The situation becomes opposite for $\langle n \rangle = 0.875$, i.e. away from half-filling. Reprinted from Ref. [60], “Copyright 1991 by the American Physical Society”.

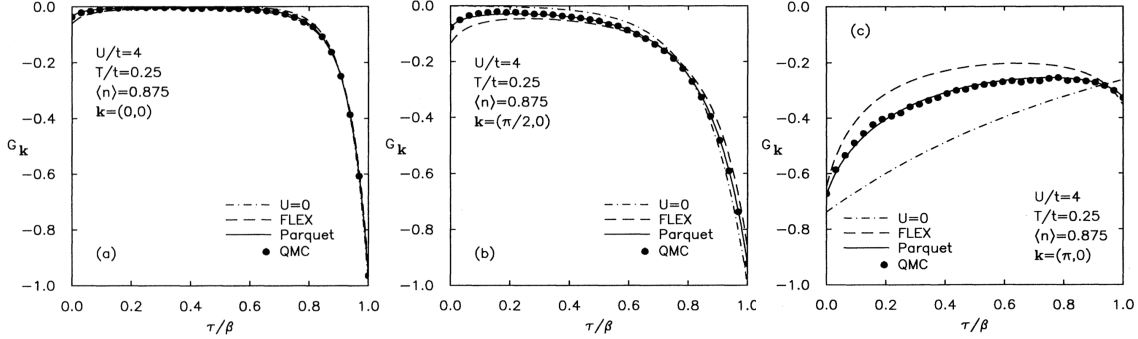


Figure 2.5: Single-particle Green's function obtained in some methods for the single-orbital Hubbard model. 8×8 meshes are used and $\langle n \rangle$ is fixed at 0.875. We see the worse agreement between the results of the QMC simulation and the FLEX approximation than the agreement between those of the QMC simulation and the parquet approximation. The situation becomes opposite for $\langle n \rangle = 1$, i.e. half-filling. Reprinted from Ref. [60], “Copyright 1991 by the American Physical Society”.

which arises from local correlation, is smeared out for large values of U at half-filling [Figs. 2.6 (b)], although in the second-order and the fourth-order perturbation theories, the incoherent peak appears [compare Figs. 2.6 (a) and (c)] [56].

However, the FLEX approximation can capture the pseudo-gap behavior near the Fermi level due the momentum dependence of the QP damping, which is induced by the enhanced AF SF; the similar pseudo-gap behavior is obtained in the fourth-order perturbation theory [Fig. 2.6 (c)], although the second-order perturbation theory is insufficient to capture this behavior [Fig. 2.6 (a)].

From these comparisons, it is deduced that the FLEX approximation can appropriately describe only the coherent part of electronic spectrum and cannot appropriately describe the incoherent part due to local correlation. In particular, the FLEX approximation can capture the pseudo-gap behavior near the Fermi level [56, 63], which is one of the unusual electronic behaviors in SCESs. However, this approximation cannot capture the Mott transition due to local correlation [64, 65, 66].

It should be noted that it is better to describe the transport properties such as the resistivity

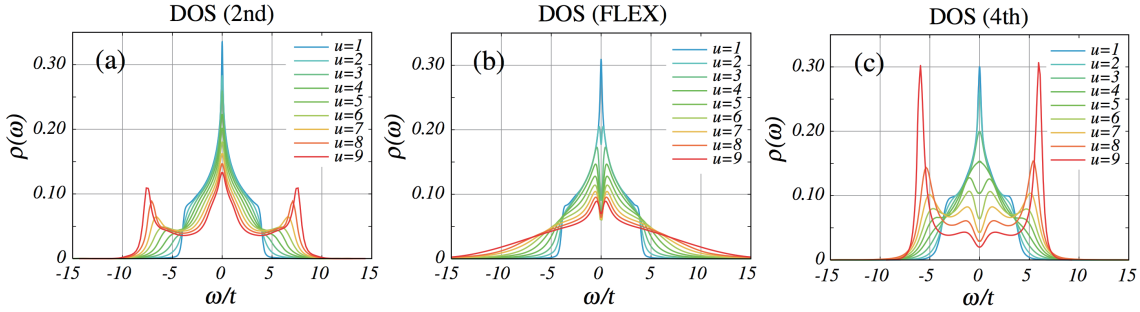


Figure 2.6: DOS obtained in (a) the second-order perturbation theory, (b) the FLEX approximation, and (c) the fourth-order perturbation theory for some values of $u = U/t$ by using the Padé approximation. 64×64 meshes and 1024 Matsubara frequencies are used. There are two remarks to be drawn. One is that the pseudo-gap behavior near the Fermi level is obtained in the fourth-order perturbation theory and the FLEX approximation, while the second-order perturbation theory is insufficient to describe this. The other remark is that the incoherent peak appears in the second-order and the fourth-order perturbation theories, although at the same value of u the incoherent part is smeared out in the FLEX approximation. Reprinted from Ref. [56], “Copyright 2008 by Physical Society of Japan”.

and the Hall coefficient by the FLEX approximation than the electronic structures since the importance of the coherent part of electronic spectrum, which can be well treated in the FLEX approximation, becomes more significant for these transport properties in metallic phases.

Since the similar result with the results described above will be obtained even in multi-orbital Hubbard models on a 2D square lattice, I conclude that the FLEX approximation is suitable for describing the electronic properties and the transport properties at low temperatures with moderately strong electron correlation qualitatively.

Note that the single-particle Green’s function obtained in the FLEX approximation is not perfectly the same as that for the standard FL theory [10, 16], where the momentum dependence of the QP damping is neglected. This is the reason why I use the word of the microscopic FL theory instead of the FL theory in the formulations of the resistivity and the Hall coefficient. As I will show in §2.3, I assume that the main contribution of the single-particle Green’s function arises from the coherent part of the electronic spectrum, which is not perfectly the same as the standard FL theory but has the similar singularity in ω -limit or \mathbf{q} -limit, and derive the transport coefficients.

2.3 Transport coefficients on the basis of the microscopic FL theory

In this section, I give the general derivations of the resistivity and the Hall coefficient in the weak-field limit for multi-orbital systems on the basis of the microscopic FL theory. These derivations are just the extension of those [8, 9] in the single-orbital case.

In the following, let us consider the in-plane current and a short-ranged interacting system with orbital degrees of freedom. In the case of a short-ranged interacting system, the singularity of the two-particle Green’s function, which appears in the conductivities, in \mathbf{q} -limit or ω -limit arises from the product of the single-particle Green’s functions whose poles coincide [10, 16]. In the case of a long-ranged interacting system, the singularity arises not only from that product

but also the direct term of interaction. The change of the treatment from the formulation presented below is just the replacement of the kind of the unit of the summation of the four-point VF from irreducible to proper irreducible [10]. Here we call proper all diagrams that cannot be split into two parts by removing a single interaction line [10].

2.3.1 Resistivity

I begin with the general derivation of the resistivity for multi-orbital systems by extending that for single-orbital systems, given by G. M. Éliashberg [8].

The outline of the derivation is as follows. Since the resistivity is the inverse of the static longitudinal conductivity, we consider the longitudinal conductivity on the basis of the Kubo formula [67]. After carrying out the analytic continuations of the terms appearing in the longitudinal conductivity, the exact expression is obtained. In particular, the expression can be written in a more compact form by using the three-point vector VF, which is the current including all the corrections due to electron correlation, instead of the irreducible four-point VF. Since the exact expression is difficult to solve, we consider a simplified case: only the most divergent terms with respect to the QP lifetime are taken into account. This procedure is based on the microscopic FL theory, and is correct in the coherent limit, i.e. the QP dampings at all the wave vectors are small compared with temperature considered. In addition, this procedure remains approximately correct, even when QP dampings at some wave vectors are not small compared with temperature considered. The reason is that in that case the QP dampings at the others are small and electrons at these wave vectors lead to the dominant contributions to the transport properties such as the resistivity. In this treatment, the longitudinal conductivity is given by the terms related to the retarded-advanced pair of the single-particle Green's function since that pair is proportional to the QP lifetime and the other pairs (i.e. retarded-retarded and advanced-advanced types) are of higher order. Thus, the longitudinal conductivity is proportional to the linear term with respect to the QP lifetime in this treatment.

From the Kubo formula [67], the longitudinal conductivity is given by

$$\sigma_{xx} = 2e^2 \sum_{\mathbf{k}, \mathbf{k}'} \sum_{\{a\}} (v_{\mathbf{k}x})_{ba} (v_{\mathbf{k}'x})_{cd} \lim_{\omega \rightarrow 0} \frac{\tilde{K}_{abcd}^{(R)}(\mathbf{k}, \mathbf{k}'; \omega) - \tilde{K}_{abcd}^{(R)}(\mathbf{k}, \mathbf{k}'; 0)}{i\omega}, \quad (2.19)$$

Here 2 is the factor of the spin degeneracy, $(v_{\mathbf{k}x})_{ba}$ is

$$(v_{\mathbf{k}x})_{ba} = \sum_{\alpha} (U_{\mathbf{k}})_{b;\alpha} \frac{\partial \epsilon_{\alpha}(\mathbf{k})}{\partial k_x} (U_{\mathbf{k}}^{\dagger})_{\alpha;a}, \quad (2.20)$$

and $\tilde{K}_{abcd}^{(R)}(\mathbf{k}, \mathbf{k}'; \omega)$ is obtained by the analytic continuation of $\tilde{K}_{abcd}(\mathbf{k}, \mathbf{k}'; i\Omega_n)$, which is

$$\begin{aligned} \tilde{K}_{abcd}(\mathbf{k}, \mathbf{k}'; i\Omega_n) &= \frac{1}{N} \int_0^{\beta} d\tau e^{i\Omega_n \tau} \langle T_{\tau} \hat{c}_{\mathbf{k}b}^{\dagger}(\tau) \hat{c}_{\mathbf{k}a}(\tau) \hat{c}_{\mathbf{k}'c}^{\dagger} \hat{c}_{\mathbf{k}'d} \rangle \\ &= -\delta_{\mathbf{k}, \mathbf{k}'} \frac{T}{N} \sum_m G_{ac}(\mathbf{k}, i\epsilon_m + i\Omega_n) G_{db}(\mathbf{k}, i\epsilon_m) \\ &\quad - \frac{T^2}{N} \sum_{m, m'} \sum_{\{A\}} G_{aA}(\mathbf{k}, i\epsilon_m + i\Omega_n) G_{dD}(\mathbf{k}', i\epsilon_{m'}) \Gamma_{\{A\}}(\mathbf{k}, \mathbf{k}'; i\Omega_n) \\ &\quad \times G_{Bb}(\mathbf{k}, i\epsilon_m) G_{Cc}(\mathbf{k}', i\epsilon_{m'} + i\Omega_n). \end{aligned} \quad (2.21)$$

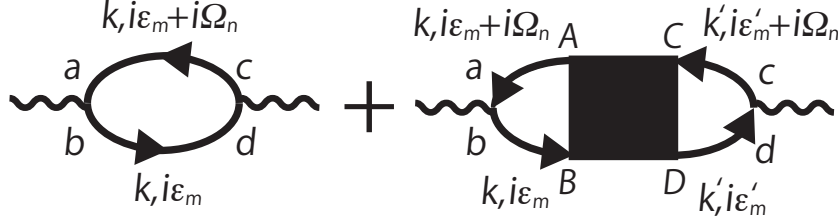


Figure 2.7: Dyson's equation of Eq. (2.21).

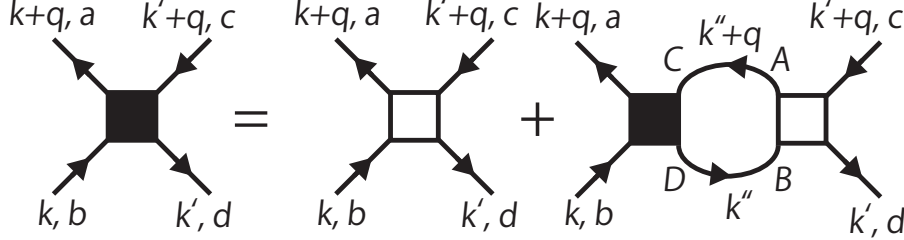


Figure 2.8: Relation between the reducible and the irreducible four-point VF. Black (white) square represents the reducible (irreducible) four-point VF.

The corresponding diagrammatic representation is given in Fig. 2.7. Here $\Gamma_{\{A\}}(k, k'; i\Omega_n)$ is the reducible four-point VF, which is related to the irreducible four-point VF by the BS equation, as shown in Fig. 2.8, and I have used the following abbreviation:

$$\Gamma_{\{A\}}(k, k'; i\Omega_n) \equiv \Gamma_{ABCD}(\mathbf{k}, i\epsilon_m + i\Omega_n, \mathbf{k}, i\epsilon_m; \mathbf{k}', i\epsilon'_m + i\Omega_n, \mathbf{k}', i\epsilon'_m). \quad (2.22)$$

Thus, in order to obtain the longitudinal conductivity, we have to carry out the analytic continuation of $\tilde{K}_{abcd}(k, k'; i\Omega_n)$ with respect to Matsubara frequencies to real frequency plane. It should be noted that $i\Omega_n \rightarrow \omega + i0+$ is carried out after taking the summation with respect to Matsubara frequencies. (Simple cases of the analytic continuation are explained in a standard textbook [16].)

For the first term of Eq. (2.21), the analytic continuation is simple, and the result is

$$\begin{aligned} & -\delta_{\mathbf{k}, \mathbf{k}'} \frac{T}{N} \sum_m G_{ac}(\mathbf{k}, i\epsilon_m + i\Omega_n) G_{db}(\mathbf{k}, i\epsilon_m) \\ &= -\delta_{\mathbf{k}, \mathbf{k}'} \frac{1}{N} \int_C \frac{d\epsilon}{4\pi i} \tanh \frac{\epsilon}{2T} G_{ac}(\mathbf{k}, \epsilon + i\Omega_n) G_{db}(\mathbf{k}, \epsilon) \\ &= -\delta_{\mathbf{k}, \mathbf{k}'} \frac{1}{N} \int_{-\infty}^{\infty} \frac{d\epsilon}{4\pi i} \left[\tanh \frac{\epsilon}{2T} G_{ac}^{(R)}(\mathbf{k}, \epsilon + i\Omega_n) \left(G_{db}^{(R)}(\mathbf{k}, \epsilon) - G_{db}^{(A)}(\mathbf{k}, \epsilon) \right) \right. \\ & \quad \left. + \tanh \frac{\epsilon}{2T} \left(G_{ac}^{(R)}(\mathbf{k}, \epsilon) - G_{ac}^{(A)}(\mathbf{k}, \epsilon) \right) G_{db}^{(A)}(\mathbf{k}, \epsilon - i\Omega_n) \right] \\ & \rightarrow -\delta_{\mathbf{k}, \mathbf{k}'} \frac{1}{N} \int_{-\infty}^{\infty} \frac{d\epsilon}{4\pi i} \left[\tanh \frac{\epsilon}{2T} g_{1;acdb}(k; \omega) + \left(\tanh \frac{\epsilon + \omega}{2T} - \tanh \frac{\epsilon}{2T} \right) g_{2;acdb}(k; \omega) \right. \\ & \quad \left. - \tanh \frac{\epsilon + \omega}{2T} g_{3;acdb}(k; \omega) \right], \end{aligned} \quad (2.23)$$

where the contour C is shown in Fig. 2.9 (a), \rightarrow represents $i\Omega_n \rightarrow \omega + i0+$, and

$$g_{1;acdb}(k; \omega) = G_{ac}^{(R)}(\mathbf{k}, \epsilon + \omega) G_{db}^{(R)}(\mathbf{k}, \epsilon), \quad (2.24)$$

$$g_{2;acdb}(k; \omega) = G_{ac}^{(R)}(\mathbf{k}, \epsilon + \omega) G_{db}^{(A)}(\mathbf{k}, \epsilon), \quad (2.25)$$

$$g_{3;acdb}(k; \omega) = G_{ac}^{(A)}(\mathbf{k}, \epsilon + \omega) G_{db}^{(A)}(\mathbf{k}, \epsilon). \quad (2.26)$$

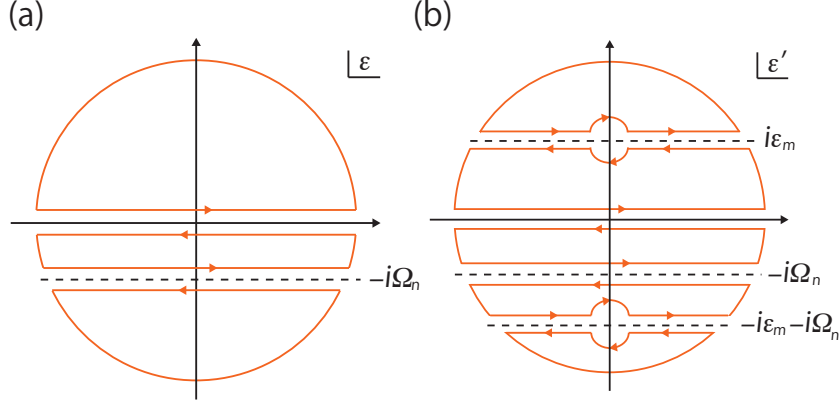


Figure 2.9: Contours (a) C and (b) C' used for the analytic continuations of the first and the second terms of Eq. (2.21). Note that (b) is one of the orderings of the locations of the poles, and there are the other orderings (see Fig. 2.10).

As I will explain below, $g_{2;acdb}(k; \omega)$, which is proportional to the linear term of the QP lifetime, is most important when we consider the most divergent contributions with respect to the QP lifetime to the conductivities.

For the second term of Eq. (2.21), the analytic continuation is complicated but can be carried out by paying careful attention to several points explained below.

In order to carry out the analytic continuation of the second term of Eq. (2.21), it is necessary to elucidate the analytic properties of the four-point VF.

For this purpose, it is sufficient to elucidate the analytic properties of the two-particle Green's function since that is connected with the four-point VF by the BS equation [10]. The analytic properties of the two-particle Green's function, $K(\epsilon, \epsilon'; \omega)$ with the complex variables, ϵ , ϵ' , and ω , are elucidated by the Lehmann representation. [For brevity, parameters of $K(\epsilon, \epsilon'; \omega)$ except the Matsubara frequencies are discarded here.] Note that the Lehmann representation is given by

$$\begin{aligned}
& K(\epsilon, \epsilon'; \omega) \\
&= \frac{1}{Z} \frac{1}{T} \sum_{\alpha_1, \alpha_2, \alpha_3, \alpha_4} A(\alpha_1, \alpha_2, \alpha_3, \alpha_4) \\
&\quad \times \left[\frac{e^{-E_1/T} \prod_{j \neq 1} (e^{\Delta E_{1j}/T} + 1)}{(\Delta E_{21} - \epsilon - \omega)(\Delta E_{31} - \epsilon - \epsilon' - \omega)(\Delta E_{41} - \epsilon)} - \frac{e^{-E_2/T} \prod_{j \neq 2} (e^{\Delta E_{2j}/T} + 1)}{(\Delta E_{12} + \epsilon + \omega)(\Delta E_{32} - \epsilon')(\Delta E_{42} + \omega)} \right. \\
&\quad \left. + \frac{e^{-E_3/T} \prod_{j \neq 3} (e^{\Delta E_{3j}/T} + 1)}{(\Delta E_{13} + \epsilon + \epsilon' + \omega)(\Delta E_{23} + \epsilon')(\Delta E_{43} + \epsilon' + \omega)} - \frac{e^{-E_4/T} \prod_{j \neq 4} (e^{\Delta E_{4j}/T} + 1)}{(\Delta E_{14} + \epsilon)(\Delta E_{24} - \omega)(\Delta E_{34} - \epsilon')} \right], \tag{2.27}
\end{aligned}$$

where Z is the grand partition function, $\Delta E_{ij} = E_i - E_j$, and $A(\alpha_1, \alpha_2, \alpha_3, \alpha_4)$ represents the product of the matrix elements of the annihilation and the creation operators.

Since the important points for the discussions about the analytic properties are the denominators of Eq. (2.27), we find that the two-particle Green's function has singularities when

$$\begin{aligned}
& \text{Im}\epsilon = 0, \quad (\text{Im}\epsilon + \text{Im}\omega) = 0, \quad \text{Im}\epsilon' = 0, \quad (\text{Im}\epsilon' + \text{Im}\omega) = 0, \\
& (\text{Im}\epsilon + \text{Im}\epsilon' + \text{Im}\omega) = 0, \quad (\text{Im}\epsilon - \text{Im}\epsilon') = 0. \tag{2.28}
\end{aligned}$$

Thus, the whole space of the variables ϵ , ϵ' , and ω is divided into several regions, shown in Fig. 2.10. As I will show below, the contributions from the regions 22-II, 22-III, and 22-IV are very

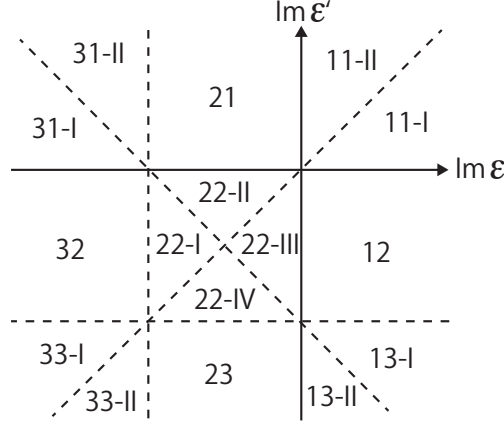


Figure 2.10: Several regions dividing the whole space of the complex variables ϵ , ϵ' , and ω of $K(\epsilon, \epsilon'; \omega)$.

important since these connect with the retarded-advanced pair of the single-particle Green's function, which gives the dominant contributions.

Using these analytic properties and paying careful attention to the inequalities that the three complex variables satisfy, we can carry out the analytic continuations of the second term of Eq. (2.21):

$$\begin{aligned}
& -\frac{T^2}{N} \sum_{m,m'} \sum_{\{A\}} G_{aA}(\mathbf{k}, i\epsilon_m + i\Omega_n) G_{dD}(\mathbf{k}', i\epsilon_{m'}) \Gamma_{\{A\}}(k, k'; i\Omega_n) G_{Bb}(\mathbf{k}, i\epsilon_m) G_{Cc}(\mathbf{k}', i\epsilon_{m'} + i\Omega_n) \\
= & -\frac{1}{N} \int_C \frac{d\epsilon}{4\pi i} \tanh \frac{\epsilon}{2T} \sum_{\{A\}} G_{aA}(\mathbf{k}, \epsilon + i\Omega_n) G_{Bb}(\mathbf{k}, \epsilon) \\
& \times \left[\int_{C'} \frac{d\epsilon'}{4\pi i} \tanh \frac{\epsilon'}{2T} G_{dD}(\mathbf{k}', \epsilon') \Gamma_{\{A\}}(\mathbf{k}, \epsilon + i\Omega_n, \mathbf{k}, \epsilon; \mathbf{k}', \epsilon' + i\Omega_n, \mathbf{k}', \epsilon') G_{Cc}(\mathbf{k}', \epsilon' + i\Omega_n) \right. \\
& + T G_{dD}(\mathbf{k}', \epsilon) \Gamma_{\{A\}}(\mathbf{k}, \epsilon + i\Omega_n, \mathbf{k}, \epsilon; \mathbf{k}', \epsilon + i\Omega_n, \mathbf{k}', \epsilon) G_{Cc}(\mathbf{k}', \epsilon + i\Omega_n) \\
& \left. + T G_{dD}(\mathbf{k}', -\epsilon - i\Omega_n) \Gamma_{\{A\}}(\mathbf{k}, \epsilon + i\Omega_n, \mathbf{k}, \epsilon; \mathbf{k}', -\epsilon, \mathbf{k}', -\epsilon - i\Omega_n) G_{Cc}(\mathbf{k}', -\epsilon) \right] \\
\rightarrow & -\frac{1}{N} \int_{-\infty}^{\infty} \frac{d\epsilon}{4\pi i} \left[\tanh \frac{\epsilon}{2T} \sum_{\{A\}} g_{1;aAbb}(k; \omega) \int_{-\infty}^{\infty} \frac{d\epsilon'}{4\pi i} \sum_{l=1}^3 \mathcal{J}_{1l;\{A\}}(k, k'; \omega) g_{l;CcdD}(k'; \omega) \right. \\
& + \left(\tanh \frac{\epsilon + \omega}{2T} - \tanh \frac{\epsilon}{2T} \right) \sum_{\{A\}} g_{2;aAbb}(k; \omega) \int_{-\infty}^{\infty} \frac{d\epsilon'}{4\pi i} \sum_{l=1}^3 \mathcal{J}_{2l;\{A\}}(k, k'; \omega) g_{l;CcdD}(k'; \omega) \\
& \left. - \tanh \frac{\epsilon + \omega}{2T} \sum_{\{A\}} g_{3;aAbb}(k; \omega) \int_{-\infty}^{\infty} \frac{d\epsilon'}{4\pi i} \sum_{l=1}^3 \mathcal{J}_{3l;\{A\}}(k, k'; \omega) g_{l;CcdD}(k'; \omega) \right], \quad (2.29)
\end{aligned}$$

where the contours C and C' are shown in Figs. 2.9 (a) and (b), and $\mathcal{J}_{ll';\{A\}}(k, k'; \omega)$ is

$$\begin{aligned} \mathcal{J}_{11;\{A\}}(k, k'; \omega) &= \tanh \frac{\epsilon'}{2T} \Gamma_{11;\{A\}}^I(k, k'; \omega) \\ &\quad + \coth \frac{\epsilon' - \epsilon}{2T} \left[\Gamma_{11;\{A\}}^{\text{II}}(k, k'; \omega) - \Gamma_{11;\{A\}}^I(k, k'; \omega) \right], \end{aligned} \quad (2.30)$$

$$\mathcal{J}_{12;\{A\}}(k, k'; \omega) = \left(\tanh \frac{\epsilon' + \omega}{2T} - \tanh \frac{\epsilon'}{2T} \right) \Gamma_{12;\{A\}}(k, k'; \omega), \quad (2.31)$$

$$\begin{aligned} \mathcal{J}_{13;\{A\}}(k, k'; \omega) &= - \tanh \frac{\epsilon' + \omega}{2T} \Gamma_{13;\{A\}}^I(k, k'; \omega) \\ &\quad - \coth \frac{\epsilon + \epsilon' + \omega}{2T} \left[\Gamma_{13;\{A\}}^{\text{II}}(k, k'; \omega) - \Gamma_{13;\{A\}}^I(k, k'; \omega) \right], \end{aligned} \quad (2.32)$$

$$\mathcal{J}_{21;\{A\}}(k, k'; \omega) = \tanh \frac{\epsilon'}{2T} \Gamma_{21;\{A\}}(k, k'; \omega), \quad (2.33)$$

$$\begin{aligned} \mathcal{J}_{22;\{A\}}(k, k'; \omega) &= \coth \frac{\epsilon' - \epsilon}{2T} \left[\Gamma_{22;\{A\}}^{\text{II}}(k, k'; \omega) - \Gamma_{22;\{A\}}^{\text{III}}(k, k'; \omega) \right] \\ &\quad + \coth \frac{\epsilon' + \epsilon + \omega}{2T} \left[\Gamma_{22;\{A\}}^{\text{III}}(k, k'; \omega) - \Gamma_{22;\{A\}}^{\text{IV}}(k, k'; \omega) \right] \\ &\quad - \tanh \frac{\epsilon'}{2T} \left[\Gamma_{22;\{A\}}^{\text{II}}(k, k'; \omega) - \Gamma_{22;\{A\}}^{\text{IV}}(k, k'; \omega) \right], \end{aligned} \quad (2.34)$$

$$\mathcal{J}_{23;\{A\}}(k, k'; \omega) = - \tanh \frac{\epsilon' + \omega}{2T} \Gamma_{23;\{A\}}(k, k'; \omega), \quad (2.35)$$

$$\begin{aligned} \mathcal{J}_{31;\{A\}}(k, k'; \omega) &= \tanh \frac{\epsilon'}{2T} \Gamma_{31;\{A\}}^I(k, k'; \omega) \\ &\quad + \coth \frac{\epsilon + \epsilon' + \omega}{2T} \left[\Gamma_{31;\{A\}}^{\text{II}}(k, k'; \omega) - \Gamma_{31;\{A\}}^I(k, k'; \omega) \right], \end{aligned} \quad (2.36)$$

$$\mathcal{J}_{32;\{A\}}(k, k'; \omega) = \left(\tanh \frac{\epsilon' + \omega}{2T} - \tanh \frac{\epsilon'}{2T} \right) \Gamma_{32;\{A\}}(k, k'; \omega), \quad (2.37)$$

$$\begin{aligned} \mathcal{J}_{33;\{A\}}(k, k'; \omega) &= - \tanh \frac{\epsilon' + \omega}{2T} \Gamma_{33;\{A\}}^I(k, k'; \omega) \\ &\quad - \coth \frac{\epsilon' - \epsilon}{2T} \left[\Gamma_{33;\{A\}}^{\text{II}}(k, k'; \omega) - \Gamma_{33;\{A\}}^I(k, k'; \omega) \right]. \end{aligned} \quad (2.38)$$

Note that the contributions from the poles of $\epsilon' = i\epsilon_m$, 0 , $-i\Omega_n$, and $-i\epsilon_m - i\Omega_n$ to the second term of Eq. (2.21) are given by

$$\begin{aligned} -\frac{1}{N} \sum_{\{A\}} \int_{-\infty}^{\infty} \frac{d\epsilon}{4\pi i} \int_{-\infty}^{\infty} \frac{d\epsilon'}{4\pi i} \coth \frac{\epsilon' - \epsilon}{2T} \left\{ \left(\tanh \frac{\epsilon + \omega}{2T} - \tanh \frac{\epsilon}{2T} \right) g_{2;aABb}(k; \omega) \right. \\ \times \left[\Gamma_{22;\{A\}}^{\text{II}}(k, k'; \omega) - \Gamma_{22;\{A\}}^{\text{III}}(k, k'; \omega) \right] g_{2;CcdD}(k'; \omega) \\ - \tanh \frac{\epsilon + \omega}{2T} g_{3;aABb}(k; \omega) \left[\Gamma_{33;\{A\}}^I(k, k'; \omega) - \Gamma_{33;\{A\}}^{\text{II}}(k, k'; \omega) \right] \\ \times g_{3;CcdD}(k'; \omega) \\ + \tanh \frac{\epsilon}{2T} g_{1;aABb}(k; \omega) \left[\Gamma_{11;\{A\}}^{\text{II}}(k, k'; \omega) - \Gamma_{11;\{A\}}^I(k, k'; \omega) \right] \\ \left. \times g_{1;CcdD}(k'; \omega) \right\}, \end{aligned} \quad (2.39)$$

$$\begin{aligned}
& -\frac{1}{N} \sum_{\{A\}} \int_{-\infty}^{\infty} \frac{d\epsilon}{4\pi i} \int_{-\infty}^{\infty} \frac{d\epsilon'}{4\pi i} \tanh \frac{\epsilon'}{2T} \left\{ \left(\tanh \frac{\epsilon + \omega}{2T} - \tanh \frac{\epsilon}{2T} \right) g_{2;aABb}(k; \omega) \right. \\
& \quad \times \left[\Gamma_{21;\{A\}}(k, k'; \omega) g_{1;CcdD}(k'; \omega) \right. \\
& \quad \quad \left. - \Gamma_{22;\{A\}}^{\text{II}}(k, k'; \omega) g_{2;CcdD}(k'; \omega) \right] \\
& \quad - \tanh \frac{\epsilon + \omega}{2T} g_{3;aABb}(k; \omega) \left[\Gamma_{31;\{A\}}^{\text{I}}(k, k'; \omega) g_{1;CcdD}(k'; \omega) \right. \\
& \quad \quad \left. - \Gamma_{32;\{A\}}(k, k'; \omega) g_{2;CcdD}(k'; \omega) \right] \\
& \quad + \tanh \frac{\epsilon}{2T} g_{1;aABb}(k; \omega) \left[\Gamma_{11;\{A\}}^{\text{I}}(k, k'; \omega) g_{1;CcdD}(k'; \omega) \right. \\
& \quad \quad \left. - \Gamma_{12;\{A\}}(k, k'; \omega) g_{2;CcdD}(k'; \omega) \right] \left. \right\}, \tag{2.40}
\end{aligned}$$

$$\begin{aligned}
& -\frac{1}{N} \sum_{\{A\}} \int_{-\infty}^{\infty} \frac{d\epsilon}{4\pi i} \int_{-\infty}^{\infty} \frac{d\epsilon'}{4\pi i} \tanh \frac{\epsilon' + \omega}{2T} \left\{ \left(\tanh \frac{\epsilon + \omega}{2T} - \tanh \frac{\epsilon}{2T} \right) g_{2;aABb}(k; \omega) \right. \\
& \quad \times \left[\Gamma_{22;\{A\}}^{\text{IV}}(k, k'; \omega) g_{2;CcdD}(k'; \omega) \right. \\
& \quad \quad \left. - \Gamma_{23;\{A\}}(k, k'; \omega) g_{3;CcdD}(k'; \omega) \right] \\
& \quad - \tanh \frac{\epsilon + \omega}{2T} g_{3;aABb}(k; \omega) \left[\Gamma_{32;\{A\}}(k, k'; \omega) g_{2;CcdD}(k'; \omega) \right. \\
& \quad \quad \left. - \Gamma_{33;\{A\}}^{\text{I}}(k, k'; \omega) g_{3;CcdD}(k'; \omega) \right] \\
& \quad + \tanh \frac{\epsilon}{2T} g_{1;aABb}(k; \omega) \left[\Gamma_{12;\{A\}}(k, k'; \omega) g_{2;CcdD}(k'; \omega) \right. \\
& \quad \quad \left. - \Gamma_{13;\{A\}}^{\text{I}}(k, k'; \omega) g_{3;CcdD}(k'; \omega) \right] \left. \right\}, \tag{2.41}
\end{aligned}$$

and

$$\begin{aligned}
& -\frac{1}{N} \sum_{\{A\}} \int_{-\infty}^{\infty} \frac{d\epsilon}{4\pi i} \int_{-\infty}^{\infty} \frac{d\epsilon'}{4\pi i} \coth \frac{\epsilon' + \epsilon + \omega}{2T} \left\{ \left(\tanh \frac{\epsilon + \omega}{2T} - \tanh \frac{\epsilon}{2T} \right) g_{2;aABb}(k; \omega) \right. \\
& \quad \times \left[\Gamma_{22;\{A\}}^{\text{III}}(k, k'; \omega) - \Gamma_{22;\{A\}}^{\text{IV}}(k, k'; \omega) \right] g_{2;CcdD}(k'; \omega) \\
& \quad - \tanh \frac{\epsilon + \omega}{2T} g_{3;aABb}(k; \omega) \left[\Gamma_{31;\{A\}}^{\text{II}}(k, k'; \omega) - \Gamma_{31;\{A\}}^{\text{I}}(k, k'; \omega) \right] \\
& \quad \times g_{1;CcdD}(k'; \omega) \\
& \quad + \tanh \frac{\epsilon}{2T} g_{1;aABb}(k; \omega) \left[\Gamma_{13;\{A\}}^{\text{I}}(k, k'; \omega) - \Gamma_{13;\{A\}}^{\text{II}}(k, k'; \omega) \right] \\
& \quad \times g_{3;CcdD}(k'; \omega) \left. \right\}, \tag{2.42}
\end{aligned}$$

respectively.

There are two remarks about quantities in Eq. (2.29). One is that in Eq. (2.29), I do not explicitly write whether the integral with respect to ϵ' is the principal integral or not for brevity: the integral is the principal integral when the \coth terms in $\mathcal{J}_{ij;\{A\}}(k, k'; \omega)$ are calculated. (The

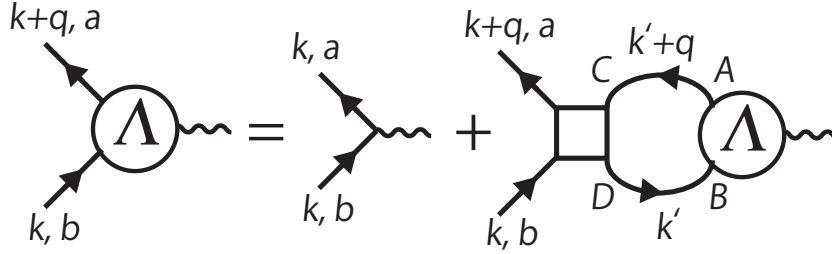


Figure 2.11: Relation between the irreducible four-point VF and the three-point vector VF. The first term of the right-hand side represents $(v_{\mathbf{k}\mu})_{ab}$.

numerical treatment of such principal integral will be explained in §3.) The other is that for the analytic continuation with respect to $i\epsilon_{m'}$, the additional terms appear since C' does not contain the poles of $\epsilon' = \epsilon$ and $\epsilon' = -\epsilon - i\Omega_n$. These additional terms are canceled out with the contributions from the integrals around the points $\epsilon' = \epsilon$ and $\epsilon' = -\epsilon - i\Omega_n$, and the remaining terms about the upper and the lower lines along $\epsilon' = \epsilon$ and $\epsilon' = -\epsilon - i\Omega_n$ become the principal integrals.

Combining Eq. (2.29) with Eq. (2.23), we find

$$\begin{aligned}
\tilde{K}_{abcd}^{(R)}(\mathbf{k}, \mathbf{k}'; \omega) = & -\frac{1}{N} \int_{-\infty}^{\infty} \frac{d\epsilon}{4\pi i} \left[\tanh \frac{\epsilon}{2T} \sum_{A,B} g_{1;aABb}(k; \omega) \right. \\
& \times \left(\delta_{\mathbf{k}, \mathbf{k}'} \delta_{c,A} \delta_{d,B} + \int_{-\infty}^{\infty} \frac{d\epsilon'}{4\pi i} \sum_{C,D} \sum_{l=1}^3 \mathcal{J}_{1l;\{A\}}(k, k'; \omega) g_{l;CcdD}(k'; \omega) \right) \\
& + \left(\tanh \frac{\epsilon + \omega}{2T} - \tanh \frac{\epsilon}{2T} \right) \sum_{A,B} g_{2;aABb}(k; \omega) \\
& \times \left(\delta_{\mathbf{k}, \mathbf{k}'} \delta_{c,A} \delta_{d,B} + \int_{-\infty}^{\infty} \frac{d\epsilon'}{4\pi i} \sum_{C,D} \sum_{l=1}^3 \mathcal{J}_{2l;\{A\}}(k, k'; \omega) g_{l;CcdD}(k'; \omega) \right) \\
& - \tanh \frac{\epsilon + \omega}{2T} \sum_{A,B} g_{3;aABb}(k; \omega) \\
& \left. \times \left(\delta_{\mathbf{k}, \mathbf{k}'} \delta_{c,A} \delta_{d,B} + \int_{-\infty}^{\infty} \frac{d\epsilon'}{4\pi i} \sum_{C,D} \sum_{l=1}^3 \mathcal{J}_{3l;\{A\}}(k, k'; \omega) g_{l;CcdD}(k'; \omega) \right) \right]. \tag{2.43}
\end{aligned}$$

Then, in order to write the longitudinal conductivity in a more compact form, let us introduce the three-point vector VF ($\mu = x, y$), which is the current including all the corrections due to electron correlation,

$$\begin{aligned}
\Lambda_{\mu;ab}(k; q) &= \Lambda_{\mu;ab}(\mathbf{k} + \mathbf{q}, i\epsilon_m + i\Omega_n, \mathbf{k}, i\epsilon_m) \\
&= (v_{\mathbf{k}\mu})_{ab} + \frac{T}{N} \sum_{k'} \sum_{\{A\}} \Gamma_{abCD}(k, k'; q) G_{BD}(k') G_{CA}(k' + q) (v_{\mathbf{k}'\mu})_{AB} \tag{2.44}
\end{aligned}$$

$$= (v_{\mathbf{k}\mu})_{ab} + \frac{T}{N} \sum_{k'} \sum_{\{A\}} \Gamma_{abCD}^{(1)}(k, k'; q) G_{BD}(k') G_{CA}(k' + q) \Lambda_{\mu;AB}(k'; q), \tag{2.45}$$

where we have used the relation between $\Gamma_{abCD}(k, k', q)$ and $\Gamma_{abCD}^{(1)}(k, k', q)$, shown in Fig. 2.8. The corresponding diagrammatic representation of Eq. (2.45) is shown in Fig. 2.11. It is noted that the second term of Eq. (2.45) is called the CVC since this term represents the correction

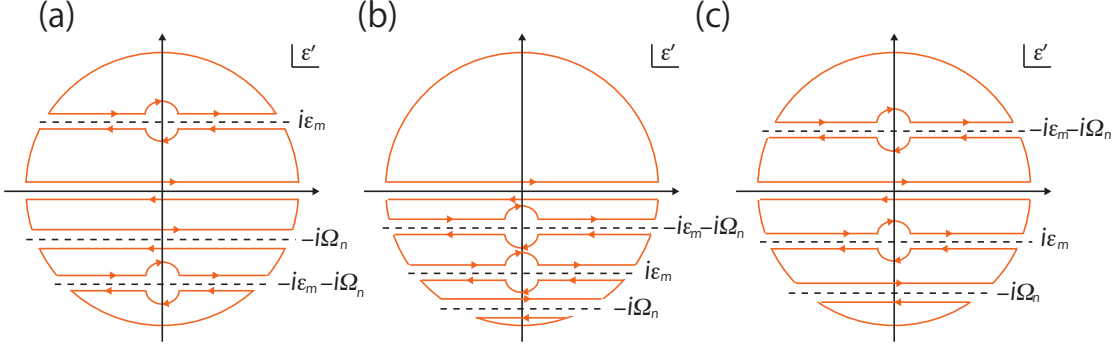


Figure 2.12: Contours used for the analytic continuations of the three-point vector VF. There are three possibilities of the three-point vector VF in real frequency representation, which is characterized by the inequalities of the Matsubara frequencies of the outgoing and the incoming lines: $i\epsilon_m > 0$ and $i\epsilon_m + i\Omega_n > 0$ in (a), $i\epsilon_m < 0$ and $i\epsilon_m + i\Omega_n > 0$ in (b), and $i\epsilon_m < 0$ and $i\epsilon_m + i\Omega_n < 0$ in (c), respectively.

term to the current due to the four-point VF. It is also noted that by using Eqs. (2.21) and (2.45), we have

$$\begin{aligned}
 & \sum_{\mathbf{k}, \mathbf{k}' \{a\}} (v_{\mathbf{k}x})_{ba} (v_{\mathbf{k}'x})_{cd} \tilde{K}_{abcd}(\mathbf{k}, \mathbf{k}'; i\Omega_n) \\
 &= -\frac{T}{N} \sum_k \sum_{\{a\}} (v_{\mathbf{k}x})_{ba} G_{ac}(\mathbf{k}, i\epsilon_m + i\Omega_n) G_{db}(\mathbf{k}, i\epsilon_m) \Lambda_{x;cd}(k; \mathbf{q} = \mathbf{0}, i\Omega_n). \quad (2.46)
 \end{aligned}$$

Before going to the analytic continuation of the three-point vector VF, I remark that the CVC plays very important roles in discussing the transport properties. In particular, this CVC is necessary to obtain the thermodynamically consistent results about transport. Note that the thermodynamically consistent result means the correct result, where conservation laws satisfy. One of the examples of the importance is the absence of the resistivity in the continuum, where there is no Umklapp process [68]. Namely, the physically correct conductivity is obtained only when the CVC, which is neglected in the relaxation time approximation [57], is correctly taken into account. Such treatment also plays an important role in discussing the Drude weight: the renormalization of the Drude weight is absent in the continuum, and the renormalization arises from the Umklapp process [69]. Furthermore, the absence of the renormalization of the electron cyclotron frequency in the continuum, i.e. Kohn's theorem, results from the conservation law [70, 71].

The analytic continuation of the three-point vector VF is easily carried out by using the three kinds of contours shown in Figs. 2.12 (a)–(c). These kinds are originated from the time orderings of the outgoing and the incoming lines: $i\epsilon_m > 0$ and $i\epsilon_m + i\Omega_n > 0$, $i\epsilon_m < 0$ and $i\epsilon_m + i\Omega_n > 0$, and $i\epsilon_m < 0$ and $i\epsilon_m + i\Omega_n < 0$. Since the second term of Eq. (2.45) can be

rewritten as

$$\begin{aligned}
& \frac{T}{N} \sum_{\mathbf{k}'} \sum_{\{A\}} \Gamma_{abCD}(k, \mathbf{k}'; q) G_{BD}(\mathbf{k}') G_{CA}(\mathbf{k}' + q) (v_{\mathbf{k}'\mu})_{AB} \\
&= \frac{1}{N} \sum_{\mathbf{k}'} \sum_{\{A\}} \left[\int_{-\infty}^{\infty} \frac{d\epsilon'}{4\pi i} \tanh \frac{\epsilon'}{2T} \Gamma_{abCD}(\mathbf{k}, i\epsilon_m, \mathbf{k}', \epsilon'; \mathbf{q}, i\Omega_n) G_{BD}(\mathbf{k}', \epsilon') G_{CA}(\mathbf{k}' + \mathbf{q}, \epsilon' + i\Omega_n) \right. \\
&\quad + T \Gamma_{abCD}(\mathbf{k}, i\epsilon_m, \mathbf{k}', i\epsilon_m; \mathbf{q}, i\Omega_n) G_{BD}(\mathbf{k}', i\epsilon_m) G_{CA}(\mathbf{k}' + \mathbf{q}, i\epsilon_m + i\Omega_n) \\
&\quad \left. + T \Gamma_{abCD}(\mathbf{k}, i\epsilon_m, \mathbf{k}', -i\epsilon_m - i\Omega_n; \mathbf{q}, i\Omega_n) G_{BD}(\mathbf{k}', -i\epsilon_m - i\Omega_n) G_{CA}(\mathbf{k}' + \mathbf{q}, -i\epsilon_m) \right] (v_{\mathbf{k}'\mu})_{AB}, \tag{2.47}
\end{aligned}$$

the three-point vector VF in real frequency representation is

$$\begin{aligned}
\Lambda_{\mu;j;ab}(k; q) &= (v_{\mathbf{k}\mu})_{ab} + \frac{1}{N} \sum_{\mathbf{k}'} \sum_{\{A\}} \sum_{l=1}^3 \int_{-\infty}^{\infty} \frac{d\epsilon}{4\pi i} \mathcal{J}_{jl;abCD}(k, \mathbf{k}'; q) g_{l;CABD}(\mathbf{k}'; q) (v_{\mathbf{k}\mu})_{AB} \tag{2.48} \\
&= (v_{\mathbf{k}\mu})_{ab} + \frac{1}{N} \sum_{\mathbf{k}'} \sum_{\{A\}} \sum_{l=1}^3 \int_{-\infty}^{\infty} \frac{d\epsilon}{4\pi i} \mathcal{J}_{jl;abCD}^{(1)}(k, \mathbf{k}'; q) g_{l;CABD}(\mathbf{k}'; q) \Lambda_{\mu;l;AB}(k; q), \tag{2.49}
\end{aligned}$$

where $j = 1, 2, 3$ of $\Lambda_{\mu;j;ab}(k; q)$ correspond to Figs. 2.12 (a), (b), (c), respectively. Similarly to case of the analytic continuation of the second term of Eq. (2.21), I do not explicitly write whether the integral with respect to ϵ' is the principal integral or not, for brevity: the integral is the principal integral when the coth terms in $\mathcal{J}_{ij;\{A\}}(k, \mathbf{k}'; \omega)$ are calculated. In addition, the reason why the additional terms appear in Eq. (2.47) is the same as the case of the analytic continuation of the second term of Eq. (2.21): the contour, C' , does not contain the poles of $\epsilon' = i\epsilon_m$ and $\epsilon' = -i\epsilon_m - i\Omega_n$.

Using this three-point vector VF, we have

$$\begin{aligned}
& \sum_{\mathbf{k}} \sum_{\{a\}} (v_{\mathbf{k}x})_{ba} (v_{\mathbf{k}x})_{cd} \tilde{K}_{abcd}^{(R)}(\mathbf{k}, \mathbf{k}'; \omega) \\
&= -\frac{1}{N} \sum_{\mathbf{k}} \sum_{\{a\}} (v_{\mathbf{k}x})_{ba} \int_{-\infty}^{\infty} \frac{d\epsilon}{4\pi i} \left[\tanh \frac{\epsilon}{2T} g_{1;acdb}(k; \omega) \Lambda_{x;1;cd}(k; \omega) \right. \\
&\quad + \left(\tanh \frac{\epsilon + \omega}{2T} - \tanh \frac{\epsilon}{2T} \right) g_{2;acdb}(k; \omega) \Lambda_{x;2;cd}(k; \omega) \\
&\quad \left. - \tanh \frac{\epsilon + \omega}{2T} g_{3;acdb}(k; \omega) \Lambda_{x;3;cd}(k; \omega) \right]. \tag{2.50}
\end{aligned}$$

Although this expression is exact, it is difficult to solve. Thus, a simplified treatment is necessary.

In order to proceed with the calculation, let us consider only the most divergent terms with respect to the QP lifetime. In this case, the leading contributions arise from only $g_{2;\{a\}}(k; \omega)$ terms since the singularity appears only when the poles of the factors of the Green's function coincide [10, 16]. We recall that only for the retarded-advanced pair, $g_{2;\{a\}}(k; \omega)$, the pair of the single-particle Green's functions has the term such as $2\pi z_{\mathbf{k}}^2 \delta(\epsilon - \xi^*(\mathbf{k})) / (-i\omega - 2z_{\mathbf{k}} \text{Im}\Sigma^{(R)}(\mathbf{k}, \epsilon))$, the linear term of the QP lifetime (in case of multi-orbital systems, the indices of the QP bands are added) [10, 16], and that for the other pairs, the QP lifetime dependence is negligible within the linear order. Although this expression is the result in the standard FL theory [10, 16], the

similar QP lifetime dependence will be realized even in microscopic perturbation theories, in which the single-particle Green's function obtained is not the same as that in the standard FL theory.

Since the leading contributions arise from only $g_{2;\{a\}}(k; \omega)$ terms, we introduce the quantities, $\mathcal{J}_{ij;\{a\}}^{(0)}(k, k'; \omega)$ and $\Lambda_{\mu;i;ab}^{(0)}(k; \omega)$, which do not contain $g_{2;\{a\}}(k; \omega)$:

$$\begin{aligned} \mathcal{J}_{ij;\{a\}}^{(0)}(k, k'; \omega) &= \mathcal{J}_{ij;\{a\}}^{(1)}(k, k'; \omega) + \sum_{l \neq 2} \frac{1}{N} \sum_{\mathbf{k}''} \sum_{\{A\}} \int_{-\infty}^{\infty} \frac{d\epsilon''}{4\pi i} \mathcal{J}_{il;abCD}^{(0)}(k, k''; \omega) \\ &\quad \times g_{l;CABD}(k''; \omega) \mathcal{J}_{lj;ABcd}^{(1)}(k'', k'; \omega), \end{aligned} \quad (2.51)$$

$$\begin{aligned} \Lambda_{\mu;i;ab}^{(0)}(k; \omega) &= (v_{\mathbf{k}\mu})_{ab} + \sum_{\{A\}} \sum_{j \neq 2} \frac{1}{N} \sum_{\mathbf{k}'} \int_{-\infty}^{\infty} \frac{d\epsilon'}{4\pi i} \mathcal{J}_{ij;abCD}^{(0)}(k, k'; \omega) g_{j;CABD}(k'; \omega) (v_{\mathbf{k}'\mu})_{AB}. \end{aligned} \quad (2.52)$$

Note that $\Lambda_{\mu;i;ab}^{(0)}(k; \omega)$ can be regarded as irreducible with respect to retarded-advanced pairs. By using these quantities, we obtain

$$\begin{aligned} &\sum_{\mathbf{k}} \sum_{\{a\}} (v_{\mathbf{k}x})_{ba} (v_{\mathbf{k}x})_{cd} \tilde{K}_{abcd}^{(R)}(\mathbf{k}, \mathbf{k}'; \omega) \\ &= -\frac{1}{N} \sum_{\mathbf{k}} \sum_{\{a\}} (v_{\mathbf{k}x})_{ba} \int_{-\infty}^{\infty} \frac{d\epsilon}{4\pi i} \left[\tanh \frac{\epsilon}{2T} g_{1;acdb}(k; \omega) \Lambda_{x;1;cd}^{(0)}(k; \omega) \right. \\ &\quad \left. - \tanh \frac{\epsilon + \omega}{2T} g_{3;acdb}(k; \omega) \Lambda_{x;3;cd}^{(0)}(k; \omega) \right] \\ &\quad - \frac{1}{N} \sum_{\mathbf{k}} \sum_{\{a\}} \Lambda_{x;2;ba}^{(0)}(k; \omega) \int_{-\infty}^{\infty} \frac{d\epsilon}{4\pi i} \left(\tanh \frac{\epsilon + \omega}{2T} - \tanh \frac{\epsilon}{2T} \right) g_{2;acdb}(k; \omega) \Lambda_{x;2;cd}(k; \omega). \end{aligned} \quad (2.53)$$

Note that at this form, the longitudinal conductivity is exactly calculated. Here I have used the exchange symmetry of the four-point VF in Matsubara frequency representation, e.g. $\Gamma(1234) = \Gamma(3412)$, and the equations for $\mathcal{J}_{ll';\{A\}}^{(0)}(k, k'; \omega)$, which are the replaced versions of Eqs. (2.31) and (2.33) and Eqs. (2.32), (2.36). To be precise, these are used to rewrite the second terms of $\Lambda_{x;1;ba}^{(0)}$ and $\Lambda_{x;3;ba}^{(0)}$ in Eq. (2.52) since the following relations are obtained by using these:

$$\begin{aligned} &-\frac{1}{N} \sum_{\mathbf{k}} \sum_{\{a\}} \int_{-\infty}^{\infty} \frac{d\epsilon}{4\pi i} (v_{\mathbf{k}x})_{ba} \tanh \frac{\epsilon}{2T} g_{1;acdb}(k; \omega) \\ &\quad \times \frac{1}{N} \sum_{\mathbf{k}'} \sum_{\{A\}} \int_{-\infty}^{\infty} \frac{d\epsilon'}{4\pi i} \mathcal{J}_{12;cdCD}^{(0)}(k, k'; \omega) g_{2;CABD}(k'; \omega) \Lambda_{x;2;AB}(k'; \omega) \\ &= -\frac{1}{N} \sum_{\mathbf{k}} \sum_{\{a\}} \int_{-\infty}^{\infty} \frac{d\epsilon}{4\pi i} \left[\frac{1}{N} \sum_{\mathbf{k}'} \sum_{\{A\}} \int_{-\infty}^{\infty} \frac{d\epsilon'}{4\pi i} \mathcal{J}_{21;baBA}^{(0)}(k, k'; \omega) g_{1;BDCA}(k'; \omega) (v_{\mathbf{k}'x})_{DC} \right] \\ &\quad \times \left(\tanh \frac{\epsilon + \omega}{2T} - \tanh \frac{\epsilon}{2T} \right) g_{2;acdb}(k; \omega) \Lambda_{x;2;AB}(k; \omega), \end{aligned} \quad (2.54)$$

and

$$\begin{aligned}
& -\frac{1}{N} \sum_{\mathbf{k}} \sum_{\{a\}} \int_{-\infty}^{\infty} \frac{d\epsilon}{4\pi i} (v_{\mathbf{k}x})_{ba} \left(-\tanh \frac{\epsilon+\omega}{2T} \right) g_{3;acdb}(k; \omega) \\
& \times \frac{1}{N} \sum_{\mathbf{k}'} \sum_{\{A\}} \int_{-\infty}^{\infty} \frac{d\epsilon'}{4\pi i} \mathcal{J}_{32;cdCD}^{(0)}(k, k'; \omega) g_{2;CABD}(k'; \omega) \Lambda_{x;2;AB}(k'; \omega) \\
& = -\frac{1}{N} \sum_{\mathbf{k}} \sum_{\{a\}} \int_{-\infty}^{\infty} \frac{d\epsilon}{4\pi i} \left[\frac{1}{N} \sum_{\mathbf{k}'} \sum_{\{A\}} \int_{-\infty}^{\infty} \frac{d\epsilon'}{4\pi i} \mathcal{J}_{23;baBA}^{(0)}(k, k'; \omega) g_{3;BDCA}(k'; \omega) (v_{\mathbf{k}'x})_{DC} \right] \\
& \times \left(\tanh \frac{\epsilon+\omega}{2T} - \tanh \frac{\epsilon}{2T} \right) g_{2;acdb}(k; \omega) \Lambda_{x;2;AB}(k; \omega). \tag{2.55}
\end{aligned}$$

Since the dominant contributions arise from the second term of Eq. (2.53), we get finally

$$\sigma_{xx} = \frac{2e^2}{N} \sum_{\mathbf{k}} \sum_{\{a\}} \int_{-\infty}^{\infty} \frac{d\epsilon}{2\pi} \Lambda_{x;2;ba}^{(0)}(k; 0) g_{2;acdb}(k; 0) \Lambda_{x;2;cd}(k; 0) \left(-\frac{\partial f(\epsilon)}{\partial \epsilon} \right). \tag{2.56}$$

where

$$\Lambda_{x;2;cd}(k; 0) = \Lambda_{x;2;cd}^{(0)}(k; 0) + \frac{1}{N} \sum_{\mathbf{k}'} \sum_{\{A\}} \int_{-\infty}^{\infty} \frac{d\epsilon'}{4\pi i} \mathcal{J}_{22;cdCD}^{(0)}(k, k'; 0) g_{2;CABD}(k'; 0) \Lambda_{\mu;2;AB}(k; 0), \tag{2.57}$$

and

$$\Lambda_{\mu;2;ba}^{(0)}(k; 0) = (v_{\mathbf{k}\mu})_{ba} + \frac{\partial}{\partial k_{\mu}} \text{Re}\Sigma_{ba}^{(R)}(k), \tag{2.58}$$

which is one of the Ward identities [10, 72]. In deriving Eq. (2.56), I have used

$$\tanh \frac{\epsilon+\omega}{2T} - \tanh \frac{\epsilon}{2T} = 2\omega \left(-\frac{\partial f(\epsilon)}{\partial \epsilon} \right) + O\left(\left(\frac{\omega}{T} \right)^2 \right). \tag{2.59}$$

We see from Eq. (2.56) that the longitudinal conductivity is proportional to the linear term with respect to the QP lifetime since the retarded-advanced pair, $g_{2;CABD}(k'; 0)$, gives the linear term. Also, we see from Eqs. (2.57), and (2.58) that electron correlation gives rise to both the renormalization of the band velocity through the real part of the self-energy of electrons and the correction to the current through the four-point VF. Namely, these are the modifications from the result in the relaxation time approximation [57], where $\Lambda_{x;2;ba}^{(0)}(k; 0)$ and $\Lambda_{x;2;cd}(k; 0)$ replace by $(v_{\mathbf{k}x})_{ba}$ and $(v_{\mathbf{k}x})_{cd}$ in Eq. (2.56), due to electron correlation.

To sum up, we can calculate the longitudinal conductivity by Eqs. (2.56), (2.57), and (2.58) if we give the form of $\mathcal{J}_{22;abcd}^{(0)}(k, k'; 0)$, whose derivation in the FLEX approximation will be explained in §2.4.

2.3.2 Hall coefficient in the weak-field limit

I go on to give the general derivation of the Hall coefficient for multi-orbital systems in the weak-field limit (i.e. $\omega_c \tau \ll 1$) [57] by extending the formulation for single-orbital systems, given by H. Kohno and K. Yamada [9]; τ and ω_c are the mean free time of electrons and the cyclotron frequency. Note that the formulation in the continuum has been given by H.

Fukuyama *et al.* [73]. For simplicity, let us assume that the system has both the mirror planes with respect to the xz - and yz -planes and the equivalence between the x - and the y -directions. These assumptions are valid for Sr_2RuO_4 .

The outline of the derivation is as follows. In order to calculate the Hall coefficient in the weak-field limit, we consider uniform static weak magnetic field, H , applied along the z -direction, and derive the expression of the transverse conductivity being proportional to H on the basis of the Kubo formula [67]. For the actual formulation, the vector potential is used instead of H . Before carrying out the analytic continuations, we calculate \mathbf{q} -linear terms of the transverse conductivity, which are the coefficients of the vector potential. In particular, we consider a simplified case, which is similar to the case of the longitudinal conductivity, on the basis of the microscopic FL theory: only the most divergent terms with respect to the QP lifetime are taken into account. In this treatment, we can neglect the \mathbf{q} -linear terms due to the four-point and the six-point VFs, which are the next-leading terms compared with the remaining terms. After calculating the \mathbf{q} -linear terms, we carry out the analytic continuations in a similar way to the case of the longitudinal conductivity. Taking $\lim_{\omega \rightarrow 0} \lim_{\mathbf{q} \rightarrow 0}$, we obtain the transverse conductivity in the weak-field limit. In this treatment, the transverse conductivity being proportional to H is proportional to the square term with respect to the QP lifetime, while, as described in §2.3.1, the longitudinal conductivity without H is proportional to the linear term. Combining the transverse conductivity formulated with the longitudinal conductivity derived in §2.3.1, we obtain the Hall coefficient in the weak-field limit, which is independent of the QP lifetime in the coherent limit.

Let us consider uniform static weak magnetic field, which is given by

$$\mathbf{H} = \nabla \times \mathbf{A}(\mathbf{r}) = (0, 0, H). \quad (2.60)$$

In particular, the effect is taken into account within the linear response. In this treatment, it is sufficient to consider

$$\mathbf{A}(\mathbf{r}) = \mathbf{A}(\mathbf{q})e^{i\mathbf{q}\cdot\mathbf{r}}, \quad (2.61)$$

and the corrections of H to the Hamiltonian and the current operator are

$$\begin{aligned} \hat{H}_{\text{ext}} &= - \int d\mathbf{r} \hat{\mathbf{J}}(\mathbf{r}) \cdot \mathbf{A}(\mathbf{r}) \\ &= - \hat{\mathbf{J}}(-\mathbf{q}) \cdot \mathbf{A}(\mathbf{q}) \\ &= - e \sum_{\mathbf{k}} \sum_{a,b} (\mathbf{v}_{\mathbf{k}})_{ba} \cdot \mathbf{A}(\mathbf{q}) \hat{c}_{\mathbf{k}+\frac{\mathbf{q}}{2}b}^\dagger \hat{c}_{\mathbf{k}-\frac{\mathbf{q}}{2}a}, \end{aligned} \quad (2.62)$$

and

$$\hat{J}^{\text{H}}(\mathbf{q}) - \hat{J}(\mathbf{q}) = -e^2 \sum_{\mathbf{k}} \sum_{a,b} \mathbf{A}(\mathbf{q}) \cdot \nabla_{\mathbf{k}} (\mathbf{v}_{\mathbf{k}})_{ba} \hat{c}_{\mathbf{k}b}^\dagger \hat{c}_{\mathbf{k}a}, \quad (2.63)$$

respectively. In other words, when we consider uniform static magnetic field within the linear response, the total Hamiltonian and the current operator become

$$\hat{H}_0 + \hat{H}_{\text{int}} + \hat{H}_{\text{ext}}, \quad (2.64)$$

and

$$\hat{J}^{\text{H}}(-\mathbf{q}) = e \sum_{\mathbf{k}} \sum_{a,b} (\mathbf{v}_{\mathbf{k}})_{ba} \hat{c}_{\mathbf{k}+\frac{q}{2}\mathbf{b}}^\dagger \hat{c}_{\mathbf{k}-\frac{q}{2}\mathbf{a}} - e^2 \sum_{\mathbf{k}} \sum_{a,b} \mathbf{A}(-\mathbf{q}) \cdot \nabla_{\mathbf{k}} (\mathbf{v}_{\mathbf{k}})_{ba} \hat{c}_{\mathbf{k}b}^\dagger \hat{c}_{\mathbf{k}a}, \quad (2.65)$$

respectively. As describe in §2.1, $\hat{H}_0 + \hat{H}_{\text{int}}$ is given by Eq. (2.3).

In the weak-field limit, the Hall coefficient, R_{H} , is given by

$$R_{\text{H}} = \lim_{H \rightarrow 0} \frac{\sigma_{xy}^{(1)}}{\sigma_{xx}^2} \frac{1}{H}, \quad (2.66)$$

where σ_{xx} is the longitudinal conductivity without H , and $\sigma_{xy}^{(1)}$ is the transverse conductivity being proportional to H . Here we have used the equivalence between the x - and the y -directions, which is one of the assumptions. Note that due to the assumptions about symmetry (i.e., two mirror planes and the rotation axis) the Hall coefficient under the magnetic field along the z -direction becomes scalar, although in general the Hall coefficient is a third-rank axial tensor.

Since we have derived the longitudinal conductivity without H in §2.3.1, the remaining thing is to calculate $\sigma_{xy}^{(1)}$. Similarly to the case of the longitudinal conductivity, let us consider a simplified case on the basis of the microscopic FL theory: only the most divergent contributions with respect to the QP lifetime are taken into account.

I begin with the explanation about a calculation of the \mathbf{q} -liner terms of the transverse conductivity since H is related to the vector potential through the equation,

$$\mathbf{H} = i\mathbf{q} \times \mathbf{A}(\mathbf{q}) e^{i\mathbf{q}\cdot\mathbf{r}} = (0, 0, iq_x A_y(\mathbf{q}) - iq_y A_x(\mathbf{q})) e^{i\mathbf{q}\cdot\mathbf{r}}. \quad (2.67)$$

Note that $\lim_{H \rightarrow 0}$ is equivalent to $\lim_{\mathbf{q} \rightarrow 0}$.

From the Kubo formula [67] for the transverse conductivity within the linear response of H , $\sigma_{xy}^{(1)}/H$ is obtained by

$$\lim_{H \rightarrow 0} \frac{\sigma_{xy}^{(1)}}{H} = \lim_{\omega \rightarrow 0} \lim_{\mathbf{q} \rightarrow 0} \frac{\sigma_{xy}(\mathbf{q}, \omega)}{iq_x A_y(\mathbf{q}) - iq_y A_x(\mathbf{q})} e^{-i\mathbf{q}\cdot\mathbf{r}}. \quad (2.68)$$

Note that it is known that the order of the limits in the right-hand side of Eq. (2.68) is very important since the dynamic and uniform field (i.e. $\lim_{\omega \rightarrow 0} \lim_{\mathbf{q} \rightarrow 0}$) is necessary to obtain finite currents; on the other hand, the static and non-uniform field (i.e. $\lim_{\mathbf{q} \rightarrow 0} \lim_{\omega \rightarrow 0}$) does not give rise to currents due the screening induced by the modulations of the charge distribution [57, 74]. Here,

$$\sigma_{xy}(\mathbf{q}, \omega) = 2e^3 \sum_{\alpha=x,y} \frac{\Phi_{xy\alpha}^{(\text{R})}(\mathbf{q}, \omega) - \Phi_{xy\alpha}^{(\text{R})}(\mathbf{q}, 0)}{i\omega} A_{\alpha}(\mathbf{q}), \quad (2.69)$$

and $\Phi_{xy\alpha}^{(\text{R})}(\mathbf{q}; \omega)$ is obtained by the analytic continuation of $\Phi_{xy\alpha}(q)$, which is

$$\begin{aligned} \Phi_{xy\alpha}(q) &= \frac{1}{e^3} \frac{T}{N} \int_0^\beta d\tau \int_0^\beta d\tau' e^{i\Omega_n(\tau-\tau')} \langle \text{T}_\tau \hat{J}_x^{\text{H}}(\mathbf{q}, \tau) \hat{J}_y^{\text{H}}(\mathbf{0}, \tau') \rangle \\ &= -\delta_{\alpha,y} \frac{1}{e} \frac{T}{N} \int_0^\beta d\tau \int_0^\beta d\tau' e^{i\Omega_n(\tau-\tau')} \langle \text{T}_\tau \hat{J}_x(\mathbf{q}, \tau) \sum_{\mathbf{k}} \sum_{a,b} \frac{\partial (v_{\mathbf{k}y})_{ba}}{\partial k_\alpha} \hat{c}_{\mathbf{k}b}^\dagger(\tau') \hat{c}_{\mathbf{k}a}(\tau') \rangle \\ &\quad + \frac{1}{e^3} \frac{T}{N} \int_0^\beta d\tau \int_0^\beta d\tau' \int_0^\beta d\tau'' e^{i\Omega_n(\tau-\tau')} \langle \text{T}_\tau \hat{J}_x(\mathbf{q}, \tau) \hat{J}_y(\mathbf{0}, \tau') \hat{J}_\alpha(-\mathbf{q}, \tau'') \rangle. \end{aligned} \quad (2.70)$$

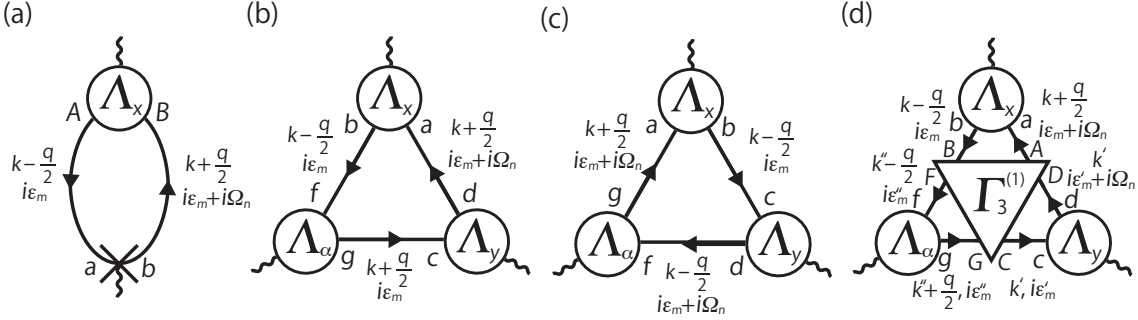


Figure 2.13: Diagrammatic representation of each term of Eq. (2.71); the first, the second, the third, and the fourth terms correspond to (a), (b), (c), and (d), respectively. \times in (a) represents momentum derivative.

In deriving Eq. (2.70), I neglect the other \mathbf{A} -linear term originated from $\hat{J}_x^H(\mathbf{q}, \tau)$ since this does not lead to a \mathbf{q} -linear term, i.e. this term is \mathbf{q} -independent. Thus, what we have to do are to exclude the \mathbf{q} -linear term of $\Phi_{xy\alpha}(\mathbf{q}; i\Omega_n)$ and to carry out the analytic continuation of that.

Using the three-point vector VF, we can rewrite Eq. (2.70) as follows:

$$\begin{aligned}
\Phi_{xy\alpha}(q) &= \delta_{\alpha,y} \frac{T}{N} \sum_{\mathbf{k}} \sum_{a,b,A,B} \frac{\partial(v_{\mathbf{k}y})_{ba}}{\partial k_{\alpha}} G_{aA}(\mathbf{k}_-, i\epsilon_m) \Lambda_{x;AB}(\mathbf{k}_-, i\epsilon_m, \mathbf{k}_+, i\epsilon_{m+n}) G_{Bb}(\mathbf{k}_+, i\epsilon_{m+n}) \\
&+ \frac{T}{N} \sum_{\mathbf{k}} \sum_{\{a\},f,g} G_{fb}(\mathbf{k}_-, i\epsilon_m) \Lambda_{x;ba}(\mathbf{k}_-, i\epsilon_m, \mathbf{k}_+, i\epsilon_{m+n}) G_{ad}(\mathbf{k}_+, i\epsilon_{m+n}) \\
&\quad \times \Lambda_{\alpha;gf}(\mathbf{k}_+, i\epsilon_m, \mathbf{k}_-, i\epsilon_m) G_{cg}(\mathbf{k}_+, i\epsilon_m) \Lambda_{y;dc}(\mathbf{k}_+, i\epsilon_{m+n}, \mathbf{k}_+, i\epsilon_m) \\
&+ \frac{T}{N} \sum_{\mathbf{k}} \sum_{\{a\},f,g} G_{ag}(\mathbf{k}_+, i\epsilon_{m+n}) \Lambda_{x;ba}(\mathbf{k}_-, i\epsilon_m, \mathbf{k}_+, i\epsilon_{m+n}) G_{cb}(\mathbf{k}_-, i\epsilon_m) \\
&\quad \times \Lambda_{\alpha;gf}(\mathbf{k}_+, i\epsilon_{m+n}, \mathbf{k}_-, i\epsilon_{m+n}) G_{fd}(\mathbf{k}_-, i\epsilon_{m+n}) \Lambda_{y;dc}(\mathbf{k}_-, i\epsilon_{m+n}, \mathbf{k}_-, i\epsilon_m) \\
&+ \left(\frac{T}{N}\right)^3 \sum_{\mathbf{k}, \mathbf{k}', \mathbf{k}''} \sum_{\{a\},f,g} \sum_{\{A\},F,G} G_{Bb}(\mathbf{k}_-, i\epsilon_m) \Lambda_{x;ba}(\mathbf{k}_-, i\epsilon_m, \mathbf{k}_+, i\epsilon_{m+n}) G_{aA}(\mathbf{k}_+, i\epsilon_{m+n}) \\
&\quad \times G_{Gg}(\mathbf{k}_+, i\epsilon_{m''}) \Lambda_{\alpha;gf}(\mathbf{k}_+, i\epsilon_{m''}, \mathbf{k}_-, i\epsilon_{m''}) G_{fF}(\mathbf{k}_-, i\epsilon_{m''}) \\
&\quad \times G_{Dd}(\mathbf{k}', i\epsilon_{m'+n}) \Lambda_{y;dc}(\mathbf{k}', i\epsilon_{m'+n}, \mathbf{k}', i\epsilon_{m'}) G_{cC}(\mathbf{k}', i\epsilon_{m'}) \\
&\quad \times \Gamma_{3;ABCDFG}^{(1)}(\mathbf{k}_+, i\epsilon_{m+n}, \mathbf{k}_-, i\epsilon_m; \mathbf{k}', i\epsilon_{m'}, \mathbf{k}', i\epsilon_{m'+n}; \mathbf{k}_-, i\epsilon_{m''}, \mathbf{k}_+, i\epsilon_{m''}), \quad (2.71)
\end{aligned}$$

where $\Gamma_{3;ABCDFG}^{(1)}(\mathbf{k}_+, i\epsilon_{m+n}, \mathbf{k}_-, i\epsilon_m; \mathbf{k}', i\epsilon_{m'}, \mathbf{k}', i\epsilon_{m'+n}; \mathbf{k}_-, i\epsilon_{m''}, \mathbf{k}_+, i\epsilon_{m''})$ is the irreducible six-point VF, $\mathbf{k}_{\pm} = \mathbf{k} \pm \frac{\mathbf{q}}{2}$, and $\epsilon_{m+n} = \epsilon_m + \Omega_n$. The diagrammatic representations of each term of Eq. (2.71) is shown in Fig. 2.13.

In order to exclude the \mathbf{q} -linear terms of Eq. (2.71), let us consider the contributions from each term. For the pair of the single-particle Green's functions, we have

$$\begin{aligned}
G_{aA}(\mathbf{k}_-, i\epsilon_m) G_{Bb}(\mathbf{k}_+, i\epsilon_{m+n}) &= G_{aA}(\mathbf{k}, i\epsilon_m) G_{Bb}(\mathbf{k}, i\epsilon_{m+n}) \\
&+ \sum_{\eta=x,y} \frac{q_{\eta}}{2} \left[G_{aA}(\mathbf{k}, i\epsilon_m) \frac{\overleftarrow{\partial}}{\partial k_{\eta}} G_{Bb}(\mathbf{k}, i\epsilon_{m+n}) \right], \quad (2.72)
\end{aligned}$$

where

$$\left[G_{aA}(\mathbf{k}, i\epsilon_m) \overleftrightarrow{\frac{\partial}{\partial k_\eta}} G_{Bb}(\mathbf{k}, i\epsilon_{m+n}) \right] \equiv G_{aA}(\mathbf{k}, i\epsilon_m) \frac{\partial G_{Bb}(\mathbf{k}, i\epsilon_{m+n})}{\partial k_\eta} - \frac{\partial G_{aA}(\mathbf{k}, i\epsilon_m)}{\partial k_\eta} G_{Bb}(\mathbf{k}, i\epsilon_{m+n}). \quad (2.73)$$

For the three-point vector VF for the y component, we have

$$\Lambda_{y;dc}(\mathbf{k}_\pm, i\epsilon_{m+n}, \mathbf{k}_\pm, i\epsilon_m) = \Lambda_{y;dc}(\mathbf{k}, i\epsilon_{m+n}, \mathbf{k}, i\epsilon_m) \pm \sum_{\eta=x,y} \frac{q_\eta}{2} \frac{\partial}{\partial k_\eta} \Lambda_{y;dc}(\mathbf{k}, i\epsilon_{m+n}, \mathbf{k}, i\epsilon_m). \quad (2.74)$$

For the three-point vector VF for the x component, we have

$$\Lambda_{x;AB}(\mathbf{k}_-, i\epsilon_m, \mathbf{k}_+, i\epsilon_{m+n}) = \Lambda_{x;AB}(\mathbf{k}, i\epsilon_m, \mathbf{k}, i\epsilon_{m+n}) + \Delta\Lambda_{x;AB}(\mathbf{k}, i\epsilon_m, \mathbf{k}, i\epsilon_{m+n}), \quad (2.75)$$

where $\Delta\Lambda_{x;AB}(\mathbf{k}, i\epsilon_m, \mathbf{k}, i\epsilon_{m+n})$ is determined by

$$\begin{aligned} \Delta\Lambda_{x;AB}(\mathbf{k}, i\epsilon_m, \mathbf{k}, i\epsilon_{m+n}) &= \frac{T}{N} \sum_{k'} \sum_{\{a\}} \Gamma_{ABcd}^{(1)}(\mathbf{k}, i\epsilon_m, \mathbf{k}, i\epsilon_{m+n}; \mathbf{k}', i\epsilon_{m'}, \mathbf{k}', i\epsilon_{m'+n}) \\ &\times \sum_{\eta=x,y} \frac{q_\eta}{2} \left[G_{bd}(\mathbf{k}', i\epsilon_{m'+n}) \overleftrightarrow{\frac{\partial}{\partial k_\eta}} G_{ca}(\mathbf{k}', i\epsilon_{m'}) \right] \Lambda_{x;ab}(\mathbf{k}', i\epsilon_{m'}, \mathbf{k}', i\epsilon_{m'+n}) \\ &+ \frac{T}{N} \sum_{k'} \sum_{\{a\}} \Gamma_{ABcd}^{(1)}(\mathbf{k}, i\epsilon_m, \mathbf{k}, i\epsilon_{m+n}; \mathbf{k}', i\epsilon_{m'}, \mathbf{k}', i\epsilon_{m'+n}) \\ &\times G_{bd}(\mathbf{k}', i\epsilon_{m'+n}) G_{ca}(\mathbf{k}', i\epsilon_{m'}) \Delta\Lambda_{x;ab}(\mathbf{k}', i\epsilon_{m'}, \mathbf{k}', i\epsilon_{m'+n}). \end{aligned} \quad (2.76)$$

In deriving Eq. (2.76) from Eq. (2.49), I neglect the \mathbf{q} -linear term originated from the irreducible four-point VF since this term gives the higher order contributions than the contributions from retarded-advanced pairs [9]. For the three-point vector VF for the α component, there is no \mathbf{q} -linear term since the Matsubara frequencies of the outgoing and the incoming lines are the same. Thus, we have

$$\begin{aligned} &\sum_{f,g} G_{fb}(\mathbf{k}_-, i\epsilon_m) \Lambda_{\alpha;gf}(\mathbf{k}_+, i\epsilon_m, \mathbf{k}_-, i\epsilon_m) G_{cg}(\mathbf{k}_+, i\epsilon_m) \\ &= \sum_{f,g} G_{fb}(\mathbf{k}, i\epsilon_m) \Lambda_{\alpha;gf}(\mathbf{k}, i\epsilon_m, \mathbf{k}, i\epsilon_m) G_{cg}(\mathbf{k}, i\epsilon_m) \\ &= \frac{\partial G_{cb}(\mathbf{k}, i\epsilon_m)}{\partial k_\alpha}. \end{aligned} \quad (2.77)$$

In the final line, one of the Ward identities [10, 72] has been used. Note that in Eq. (2.77), the Matsubara frequencies of the pair of the single-particle Green's functions are the same, while in Eq. (2.72), those are different. Namely, the contributions of the \mathbf{q} -linear terms arising from the pair with the same Matsubara frequencies are negligible since these terms are proportional to the retarded-retarded or the advanced-advanced pair. For the irreducible six-point VFs, we neglect the \mathbf{q} -linear term due to the same reason why the irreducible four-point VF is neglected [9], as described above.

Substituting Eqs. (2.72), (2.74), (2.75), and (2.77) into Eq. (2.71) and neglecting the \mathbf{q} -linear terms of the irreducible four-point and the irreducible six-point VFs, we have

$$\begin{aligned}
& \Phi_{xy\alpha}(q) \\
&= \delta_{\alpha,y} \frac{T}{N} \sum_k \sum_{a,b,A,B} \frac{\partial(v_{\mathbf{k}y})_{ba}}{\partial k_\alpha} G_{aA}(\mathbf{k}, i\epsilon_m) \Delta\Lambda_{x;AB}(\mathbf{k}, i\epsilon_m, \mathbf{k}, i\epsilon_{m+n}) G_{Bb}(\mathbf{k}, i\epsilon_{m+n}) \\
&+ \delta_{\alpha,y} \frac{T}{N} \sum_k \sum_{a,b,A,B} \frac{\partial(v_{\mathbf{k}y})_{ba}}{\partial k_\alpha} \Lambda_{x;AB}(\mathbf{k}, i\epsilon_m, \mathbf{k}, i\epsilon_{m+n}) \sum_\eta \frac{q_\eta}{2} \left[G_{aA}(\mathbf{k}, i\epsilon_m) \overleftrightarrow{\frac{\partial}{\partial k_\eta}} G_{Bb}(\mathbf{k}, i\epsilon_{m+n}) \right] \\
&+ \frac{T}{N} \sum_k \sum_{\{a\}} \Delta\Lambda_{x;ba}(\mathbf{k}, i\epsilon_m, \mathbf{k}, i\epsilon_{m+n}) G_{ad}(\mathbf{k}, i\epsilon_{m+n}) \frac{\partial G_{cb}(\mathbf{k}, i\epsilon_m)}{\partial k_\alpha} \Lambda_{y;dc}(\mathbf{k}, i\epsilon_{m+n}, \mathbf{k}, i\epsilon_m) \\
&+ \frac{T}{N} \sum_k \sum_{\{a\}} \Lambda_{x;ba}(\mathbf{k}, i\epsilon_m, \mathbf{k}, i\epsilon_{m+n}) \sum_\eta \frac{q_\eta}{2} \frac{\partial G_{ad}(\mathbf{k}, i\epsilon_{m+n})}{\partial k_\eta} \frac{\partial G_{cb}(\mathbf{k}, i\epsilon_m)}{\partial k_\alpha} \Lambda_{y;dc}(\mathbf{k}, i\epsilon_{m+n}, \mathbf{k}, i\epsilon_m) \\
&+ \frac{T}{N} \sum_k \sum_{\{a\}} \Lambda_{x;ba}(\mathbf{k}, i\epsilon_m, \mathbf{k}, i\epsilon_{m+n}) G_{ad}(\mathbf{k}, i\epsilon_{m+n}) \frac{\partial G_{cb}(\mathbf{k}, i\epsilon_m)}{\partial k_\alpha} \sum_\eta \frac{q_\eta}{2} \frac{\partial \Lambda_{y;dc}(\mathbf{k}, i\epsilon_{m+n}, \mathbf{k}, i\epsilon_m)}{\partial k_\eta} \\
&+ \frac{T}{N} \sum_k \sum_{\{a\}} \Delta\Lambda_{x;ba}(\mathbf{k}, i\epsilon_m, \mathbf{k}, i\epsilon_{m+n}) G_{cb}(\mathbf{k}, i\epsilon_m) \frac{\partial G_{ad}(\mathbf{k}, i\epsilon_{m+n})}{\partial k_\alpha} \Lambda_{y;dc}(\mathbf{k}, i\epsilon_{m+n}, \mathbf{k}, i\epsilon_m) \\
&- \frac{T}{N} \sum_k \sum_{\{a\}} \Lambda_{x;ba}(\mathbf{k}, i\epsilon_m, \mathbf{k}, i\epsilon_{m+n}) \sum_\eta \frac{q_\eta}{2} \frac{\partial G_{cb}(\mathbf{k}, i\epsilon_m)}{\partial k_\eta} \frac{\partial G_{ad}(\mathbf{k}, i\epsilon_{m+n})}{\partial k_\alpha} \Lambda_{y;dc}(\mathbf{k}, i\epsilon_{m+n}, \mathbf{k}, i\epsilon_m) \\
&- \frac{T}{N} \sum_k \sum_{\{a\}} \Lambda_{x;ba}(\mathbf{k}, i\epsilon_m, \mathbf{k}, i\epsilon_{m+n}) G_{cb}(\mathbf{k}, i\epsilon_m) \frac{\partial G_{ad}(\mathbf{k}, i\epsilon_{m+n})}{\partial k_\alpha} \sum_\eta \frac{q_\eta}{2} \frac{\partial \Lambda_{y;dc}(\mathbf{k}, i\epsilon_{m+n}, \mathbf{k}, i\epsilon_m)}{\partial k_\eta} \\
&+ \left(\frac{T}{N}\right)^3 \sum_{k,k',k''} \sum_{\{a\}} \sum_{\{A\},F,G} G_{Bb}(\mathbf{k}, i\epsilon_m) \Delta\Lambda_{x;ba}(\mathbf{k}, i\epsilon_m, \mathbf{k}, i\epsilon_{m+n}) G_{aA}(\mathbf{k}, i\epsilon_{m+n}) \\
&\times \frac{\partial G_{GF}(\mathbf{k}'', i\epsilon_{m''})}{\partial k'_\alpha} G_{Dd}(\mathbf{k}', i\epsilon_{m'+n}) \Lambda_{y;dc}(\mathbf{k}', i\epsilon_{m'+n}, \mathbf{k}', i\epsilon_{m'}) G_{cC}(\mathbf{k}', i\epsilon_{m'}) \\
&\times \Gamma_{3;ABCD}^{(1)}(\mathbf{k}, i\epsilon_{m+n}, \mathbf{k}, i\epsilon_m; \mathbf{k}', i\epsilon_{m'}, \mathbf{k}', i\epsilon_{m'+n}; \mathbf{k}'', i\epsilon_{m''}, \mathbf{k}'', i\epsilon_{m''}) \\
&+ \left(\frac{T}{N}\right)^3 \sum_{k,k',k''} \sum_{\{a\}} \sum_{\{A\},F,G} \Lambda_{x;ba}(\mathbf{k}, i\epsilon_m, \mathbf{k}, i\epsilon_{m+n}) \sum_\eta \frac{q_\eta}{2} \left[G_{Bb}(\mathbf{k}, i\epsilon_m) \overleftrightarrow{\frac{\partial}{\partial k_\eta}} G_{aA}(\mathbf{k}, i\epsilon_{m+n}) \right] \\
&\times \frac{\partial G_{GF}(\mathbf{k}'', i\epsilon_{m''})}{\partial k'_\alpha} G_{Dd}(\mathbf{k}', i\epsilon_{m'+n}) \Lambda_{y;dc}(\mathbf{k}', i\epsilon_{m'+n}, \mathbf{k}', i\epsilon_{m'}) G_{cC}(\mathbf{k}', i\epsilon_{m'}) \\
&\times \Gamma_{3;ABCD}^{(1)}(\mathbf{k}, i\epsilon_{m+n}, \mathbf{k}, i\epsilon_m; \mathbf{k}', i\epsilon_{m'}, \mathbf{k}', i\epsilon_{m'+n}; \mathbf{k}'', i\epsilon_{m''}, \mathbf{k}'', i\epsilon_{m''}). \tag{2.78}
\end{aligned}$$

In addition, the ninth and tenth terms of Eq. (2.78) can be written in a simpler form by using Eqs. (2.49) and (2.76), the exchange symmetry of the irreducible four-point VF, used in deriving Eq. (2.53), and the relation between the irreducible six-point and the irreducible four-point VFs, which is

$$\begin{aligned}
& \left(\frac{\partial}{\partial k_\alpha} + \frac{\partial}{\partial k'_\alpha} \right) \Gamma_{ABDC}^{(1)}(\mathbf{k}, i\epsilon_{m+n}, \mathbf{k}, i\epsilon_m; \mathbf{k}', i\epsilon_{m'+n}, \mathbf{k}', i\epsilon_{m'}) \\
&= \frac{T}{N} \sum_{k''} \sum_{F,G} \Gamma_{3;ABCD}^{(1)}(\mathbf{k}, i\epsilon_{m+n}, \mathbf{k}, i\epsilon_m; \mathbf{k}', i\epsilon_{m'}, \mathbf{k}', i\epsilon_{m'+n}; \mathbf{k}'', i\epsilon_{m''}, \mathbf{k}'', i\epsilon_{m''}) \frac{\partial G_{GF}(\mathbf{k}'', i\epsilon_{m''})}{\partial k''_\alpha}. \tag{2.79}
\end{aligned}$$

After some straightforward calculations, the ninth and tenth terms of Eq. (2.78) become

$$\begin{aligned}
& \left(\frac{T}{N}\right)^2 \sum_{k,k'} \sum_{\{a\}} \sum_{\{A\}} G_{Bb}(\mathbf{k}, i\epsilon_m) \Delta\Lambda_{x;ba}(\mathbf{k}, i\epsilon_m, \mathbf{k}, i\epsilon_{m+n}) G_{aA}(\mathbf{k}, i\epsilon_{m+n}) \\
& \quad \times G_{Dd}(\mathbf{k}', i\epsilon_{m'+n}) \Lambda_{y;dc}(\mathbf{k}', i\epsilon_{m'+n}, \mathbf{k}', i\epsilon_{m'}) G_{cC}(\mathbf{k}', i\epsilon_{m'}) \\
& \quad \times \left(\frac{\partial}{\partial k_\alpha} + \frac{\partial}{\partial k'_\alpha}\right) \Gamma_{ABDC}^{(1)}(\mathbf{k}, i\epsilon_{m+n}, \mathbf{k}, i\epsilon_m; \mathbf{k}', i\epsilon_{m'+n}, \mathbf{k}', i\epsilon_{m'}) \\
& + \left(\frac{T}{N}\right)^2 \sum_{k,k'} \sum_{\{a\}} \sum_{\{A\}} \Lambda_{x;ba}(\mathbf{k}, i\epsilon_m, \mathbf{k}, i\epsilon_{m+n}) \sum_{\eta} \frac{q_\eta}{2} \left[G_{Bb}(\mathbf{k}, i\epsilon_m) \frac{\overleftrightarrow{\partial}}{\partial k_\eta} G_{aA}(\mathbf{k}, i\epsilon_{m+n}) \right] \\
& \quad \times G_{Dd}(\mathbf{k}', i\epsilon_{m'+n}) \Lambda_{y;dc}(\mathbf{k}', i\epsilon_{m'+n}, \mathbf{k}', i\epsilon_{m'}) G_{cC}(\mathbf{k}', i\epsilon_{m'}) \\
& \quad \times \left(\frac{\partial}{\partial k_\alpha} + \frac{\partial}{\partial k'_\alpha}\right) \Gamma_{ABDC}^{(1)}(\mathbf{k}, i\epsilon_{m+n}, \mathbf{k}, i\epsilon_m; \mathbf{k}', i\epsilon_{m'+n}, \mathbf{k}', i\epsilon_{m'}) \\
= & \frac{T}{N} \sum_k \sum_{a,b,A,B} G_{Bb}(\mathbf{k}, i\epsilon_m) \Delta\Lambda_{x;ba}(\mathbf{k}, i\epsilon_m, \mathbf{k}, i\epsilon_{m+n}) G_{aA}(\mathbf{k}, i\epsilon_{m+n}) \\
& \quad \times \frac{\partial}{\partial k_\alpha} \left[\Lambda_{y;AB}(\mathbf{k}, i\epsilon_{m+n}, \mathbf{k}, i\epsilon_m) - (v_{ky})_{AB} \right] \\
& - \left(\frac{T}{N}\right)^2 \sum_{k,k'} \sum_{\{a\}} \sum_{\{A\}} G_{Bb}(\mathbf{k}, i\epsilon_m) \Delta\Lambda_{x;ba}(\mathbf{k}, i\epsilon_m, \mathbf{k}, i\epsilon_{m+n}) G_{aA}(\mathbf{k}, i\epsilon_{m+n}) \\
& \quad \times \frac{\partial}{\partial k'_\alpha} \left[G_{Dd}(\mathbf{k}', i\epsilon_{m'+n}) \Lambda_{y;dc}(\mathbf{k}', i\epsilon_{m'+n}, \mathbf{k}', i\epsilon_{m'}) G_{cC}(\mathbf{k}', i\epsilon_{m'}) \right] \\
& \quad \times \Gamma_{ABDC}^{(1)}(\mathbf{k}, i\epsilon_{m+n}, \mathbf{k}, i\epsilon_m; \mathbf{k}', i\epsilon_{m'+n}, \mathbf{k}', i\epsilon_{m'}) \\
& + \frac{T}{N} \sum_k \sum_{a,b,A,B} \Lambda_{x;ba}(\mathbf{k}, i\epsilon_m, \mathbf{k}, i\epsilon_{m+n}) \sum_{\eta} \frac{q_\eta}{2} \left[G_{Bb}(\mathbf{k}, i\epsilon_m) \frac{\overleftrightarrow{\partial}}{\partial k_\eta} G_{aA}(\mathbf{k}, i\epsilon_{m+n}) \right] \\
& \quad \times \frac{\partial}{\partial k_\alpha} \left[\Lambda_{y;AB}(\mathbf{k}, i\epsilon_{m+n}, \mathbf{k}, i\epsilon_m) - (v_{ky})_{AB} \right] \\
& - \left(\frac{T}{N}\right)^2 \sum_{k,k'} \sum_{\{a\}} \sum_{\{A\}} \Lambda_{x;ba}(\mathbf{k}, i\epsilon_m, \mathbf{k}, i\epsilon_{m+n}) \sum_{\eta} \frac{q_\eta}{2} \left[G_{Bb}(\mathbf{k}, i\epsilon_m) \frac{\overleftrightarrow{\partial}}{\partial k_\eta} G_{aA}(\mathbf{k}, i\epsilon_{m+n}) \right] \\
& \quad \times \frac{\partial}{\partial k'_\alpha} \left[G_{Dd}(\mathbf{k}', i\epsilon_{m'+n}) \Lambda_{y;dc}(\mathbf{k}', i\epsilon_{m'+n}, \mathbf{k}', i\epsilon_{m'}) G_{cC}(\mathbf{k}', i\epsilon_{m'}) \right] \\
& \quad \times \Gamma_{ABDC}^{(1)}(\mathbf{k}, i\epsilon_{m+n}, \mathbf{k}, i\epsilon_m; \mathbf{k}', i\epsilon_{m'+n}, \mathbf{k}', i\epsilon_{m'}) \\
= & \frac{T}{N} \sum_k \sum_{a,b,A,B} \left\{ \Delta\Lambda_{x;ba}(\mathbf{k}, i\epsilon_m, \mathbf{k}, i\epsilon_{m+n}) G_{Bb}(\mathbf{k}, i\epsilon_m) G_{aA}(\mathbf{k}, i\epsilon_{m+n}) \right. \\
& \quad \left. + \Lambda_{x;ba}(\mathbf{k}, i\epsilon_m, \mathbf{k}, i\epsilon_{m+n}) \sum_{\eta} \frac{q_\eta}{2} \left[G_{Bb}(\mathbf{k}, i\epsilon_m) \frac{\overleftrightarrow{\partial}}{\partial k_\eta} G_{aA}(\mathbf{k}, i\epsilon_{m+n}) \right] \right\} \\
& \quad \times \frac{\partial}{\partial k_\alpha} \left[\Lambda_{y;AB}(\mathbf{k}, i\epsilon_{m+n}, \mathbf{k}, i\epsilon_m) - (v_{ky})_{AB} \right] \\
& - \frac{T}{N} \sum_k \sum_{c,d,C,D} \Delta\Lambda_{x;DC}(\mathbf{k}', i\epsilon_{m'+n}, \mathbf{k}', i\epsilon_{m'}) \\
& \quad \times \frac{\partial}{\partial k'_\alpha} \left[G_{Dd}(\mathbf{k}', i\epsilon_{m'+n}) \Lambda_{y;dc}(\mathbf{k}', i\epsilon_{m'+n}, \mathbf{k}', i\epsilon_{m'}) G_{cC}(\mathbf{k}', i\epsilon_{m'}) \right]. \tag{2.80}
\end{aligned}$$

Substituting Eq. (2.80) into Eq. (2.78), we obtain

$$\begin{aligned}
& \Phi_{xy\alpha}(q) \\
&= \frac{T}{N} \sum_k \sum_{\{a\}} \Lambda_{x;ba}(\mathbf{k}, i\epsilon_m, \mathbf{k}, i\epsilon_{m+n}) \sum_{\eta} \frac{q_{\eta}}{2} \frac{\partial G_{ad}(\mathbf{k}, i\epsilon_{m+n})}{\partial k_{\eta}} \frac{\partial G_{cb}(\mathbf{k}, i\epsilon_m)}{\partial k_{\alpha}} \Lambda_{y;dc}(\mathbf{k}, i\epsilon_{m+n}; \mathbf{k}, i\epsilon_m) \\
&+ \frac{T}{N} \sum_k \sum_{\{a\}} \Lambda_{x;ba}(\mathbf{k}, i\epsilon_m, \mathbf{k}, i\epsilon_{m+n}) G_{ad}(\mathbf{k}, i\epsilon_{m+n}) \frac{\partial G_{cb}(\mathbf{k}, i\epsilon_m)}{\partial k_{\alpha}} \sum_{\eta} \frac{q_{\eta}}{2} \frac{\partial \Lambda_{y;dc}(\mathbf{k}, i\epsilon_{m+n}, \mathbf{k}, i\epsilon_m)}{\partial k_{\eta}} \\
&- \frac{T}{N} \sum_k \sum_{\{a\}} \Lambda_{x;ba}(\mathbf{k}, i\epsilon_m, \mathbf{k}, i\epsilon_{m+n}) \sum_{\eta} \frac{q_{\eta}}{2} \frac{\partial G_{cb}(\mathbf{k}, i\epsilon_m)}{\partial k_{\eta}} \frac{\partial G_{ad}(\mathbf{k}, i\epsilon_{m+n})}{\partial k_{\alpha}} \Lambda_{y;dc}(\mathbf{k}, i\epsilon_{m+n}, \mathbf{k}, i\epsilon_m) \\
&- \frac{T}{N} \sum_k \sum_{\{a\}} \Lambda_{x;ba}(\mathbf{k}, i\epsilon_m, \mathbf{k}, i\epsilon_{m+n}) G_{cb}(\mathbf{k}, i\epsilon_m) \frac{\partial G_{ad}(\mathbf{k}, i\epsilon_{m+n})}{\partial k_{\alpha}} \sum_{\eta} \frac{q_{\eta}}{2} \frac{\partial \Lambda_{y;dc}(\mathbf{k}, i\epsilon_{m+n}, \mathbf{k}, i\epsilon_m)}{\partial k_{\eta}} \\
&+ \frac{T}{N} \sum_k \sum_{\{a\}} \Lambda_{x;ba}(\mathbf{k}, i\epsilon_m, \mathbf{k}, i\epsilon_{m+n}) \sum_{\eta} \frac{q_{\eta}}{2} \left[G_{cb}(\mathbf{k}, i\epsilon_m) \frac{\overleftrightarrow{\partial}}{\partial k_{\eta}} G_{ad}(\mathbf{k}, i\epsilon_{m+n}) \right] \\
&\quad \times \frac{\partial \Lambda_{y;dc}(\mathbf{k}, i\epsilon_{m+n}, \mathbf{k}, i\epsilon_m)}{\partial k_{\alpha}} \\
&= \frac{T}{N} \sum_k \sum_{\{a\}} \Lambda_{x;ba}(\mathbf{k}, i\epsilon_m, \mathbf{k}, i\epsilon_{m+n}) \Lambda_{y;dc}(\mathbf{k}, i\epsilon_{m+n}, \mathbf{k}, i\epsilon_m) \\
&\quad \times \sum_{\eta=x,y} \frac{q_{\eta}}{2} \left\{ \frac{\partial G_{ad}(\mathbf{k}, i\epsilon_{m+n})}{\partial k_{\eta}} \frac{\partial G_{cb}(\mathbf{k}, i\epsilon_m)}{\partial k_{\alpha}} - \frac{\partial G_{ad}(\mathbf{k}, i\epsilon_{m+n})}{\partial k_{\alpha}} \frac{\partial G_{cb}(\mathbf{k}, i\epsilon_m)}{\partial k_{\eta}} \right\} \\
&+ \frac{T}{N} \sum_k \sum_{\{a\}} \Lambda_{x;ba}(\mathbf{k}, i\epsilon_m, \mathbf{k}, i\epsilon_{m+n}) \\
&\quad \times \sum_{\eta=x,y} \frac{q_{\eta}}{2} \left\{ \left[G_{cb}(\mathbf{k}, i\epsilon_m) \frac{\overleftrightarrow{\partial}}{\partial k_{\eta}} G_{ad}(\mathbf{k}, i\epsilon_{m+n}) \right] \frac{\partial \Lambda_{y;dc}(\mathbf{k}, i\epsilon_{m+n}, \mathbf{k}, i\epsilon_m)}{\partial k_{\alpha}} \right. \\
&\quad \left. - \left[G_{cb}(\mathbf{k}, i\epsilon_m) \frac{\overleftrightarrow{\partial}}{\partial k_{\alpha}} G_{ad}(\mathbf{k}, i\epsilon_{m+n}) \right] \frac{\partial \Lambda_{y;dc}(\mathbf{k}, i\epsilon_{m+n}, \mathbf{k}, i\epsilon_m)}{\partial k_{\eta}} \right\} \\
&= \frac{1}{2} (q_x \delta_{\alpha,y} - q_y \delta_{\alpha,x}) \frac{T}{N} \sum_k \sum_{\{a\}} \Lambda_{x;ba}(\mathbf{k}, i\epsilon_m, \mathbf{k}, i\epsilon_{m+n}) \\
&\quad \times \left\{ \left[G_{cb}(\mathbf{k}, i\epsilon_m) \frac{\overleftrightarrow{\partial}}{\partial k_x} G_{ad}(\mathbf{k}, i\epsilon_{m+n}) \right] \frac{\partial \Lambda_{y;dc}(\mathbf{k}, i\epsilon_{m+n}, \mathbf{k}, i\epsilon_m)}{\partial k_y} \right. \\
&\quad \left. - \left[G_{cb}(\mathbf{k}, i\epsilon_m) \frac{\overleftrightarrow{\partial}}{\partial k_y} G_{ad}(\mathbf{k}, i\epsilon_{m+n}) \right] \frac{\partial \Lambda_{y;dc}(\mathbf{k}, i\epsilon_{m+n}, \mathbf{k}, i\epsilon_m)}{\partial k_x} \right\} \\
&+ \frac{1}{2} (q_x \delta_{\alpha,y} - q_y \delta_{\alpha,x}) \frac{T}{N} \sum_k \sum_{\{a\}} \Lambda_{x;ba}(\mathbf{k}, i\epsilon_m, \mathbf{k}, i\epsilon_{m+n}) \\
&\quad \times \left(\frac{\partial G_{cb}(\mathbf{k}, i\epsilon_m)}{\partial k_y} \frac{\partial G_{ad}(\mathbf{k}, i\epsilon_{m+n})}{\partial k_x} - \frac{\partial G_{cb}(\mathbf{k}, i\epsilon_m)}{\partial k_x} \frac{\partial G_{ad}(\mathbf{k}, i\epsilon_{m+n})}{\partial k_y} \right) \Lambda_{y;dc}(\mathbf{k}, i\epsilon_{m+n}; \mathbf{k}, i\epsilon_m).
\end{aligned} \tag{2.81}$$

Here I have used the fact that the surface integrals with respect to k_x and k_y are zero due to the periodicity of the Brillouin zone. Note that the replacement which has been used in Refs. [9, 73] is unnecessary to obtain the above equation.

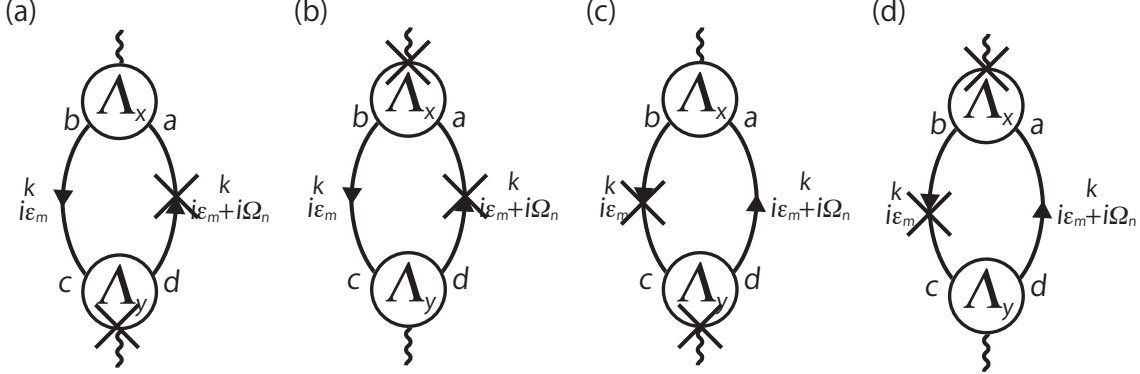


Figure 2.14: Diagrammatic representation of each term of Eq. (2.82), where the same coefficient, $(q_x \delta_{\alpha,y} - q_y \delta_{\alpha,x})/2$, and the minus signs in (b) and (c) are not shown explicitly. \times represents momentum derivative. Note that the reason why two momentum derivatives appear is to exclude the terms being both \mathbf{q} -linear and \mathbf{A} -linear.

Furthermore, using the equivalence between the x - and the y -directions, which is one of the assumptions, we have

$$\begin{aligned} \Phi_{xy\alpha}(q) &= \frac{1}{2}(q_x \delta_{\alpha,y} - q_y \delta_{\alpha,x}) \frac{T}{N} \sum_{\mathbf{k}} \sum_{\{a\}} \left[\Lambda_{x;ba}(\mathbf{k}, i\epsilon_m, \mathbf{k}, i\epsilon_{m+n}) \overleftrightarrow{\frac{\partial}{\partial k_y}} \Lambda_{y;dc}(\mathbf{k}, i\epsilon_{m+n}, \mathbf{k}, i\epsilon_m) \right] \\ &\quad \times \left[G_{cb}(\mathbf{k}, i\epsilon_m) \overleftrightarrow{\frac{\partial}{\partial k_x}} G_{ad}(\mathbf{k}, i\epsilon_{m+n}) \right]. \end{aligned} \quad (2.82)$$

The diagrammatic representation of each term is shown in Fig. 2.14.

I go on to explain the analytic continuation of $\Phi_{xy\alpha}(q)$ in Eq. (2.82).

Since momentum derivatives are irrelevant in the analytic continuation about frequency, we can easily carry out the analytic continuation of $\Phi_{xy\alpha}(q)$ by the same way used in §2.3.1 [compare Eqs. (2.46) and (2.82)]. Namely, within the linear order of ω/T , the result is

$$\begin{aligned} \Phi_{xy\alpha}^{(R)}(\mathbf{q}, \omega) - \Phi_{xy\alpha}^{(R)}(\mathbf{q}, 0) &= \frac{1}{2}(q_x \delta_{\alpha,y} - q_y \delta_{\alpha,x}) \frac{1}{N} \sum_{\mathbf{k}} \int_{-\infty}^{\infty} \frac{d\epsilon}{4\pi i} 2\omega \left(-\frac{\partial f(\epsilon)}{\partial \epsilon} \right) \\ &\quad \times \sum_{\{a\}} \left[\Lambda_{x;2;ba}(\mathbf{k}, \epsilon, \mathbf{k}, \epsilon) \overleftrightarrow{\frac{\partial}{\partial k_y}} \Lambda_{y;2;dc}(\mathbf{k}, \epsilon, \mathbf{k}, \epsilon) \right] \left[G_{cb}^{(A)}(\mathbf{k}, \epsilon) \overleftrightarrow{\frac{\partial}{\partial k_x}} G_{ad}^{(R)}(\mathbf{k}, \epsilon) \right]. \end{aligned} \quad (2.83)$$

Finally, from Eqs. (2.68), (2.69), and (2.83), we have the transverse conductivity being proportional to H on the basis of the microscopic FL theory:

$$\begin{aligned} \lim_{H \rightarrow 0} \frac{\sigma_{xy}^{(1)}}{H} &= -\frac{e^3}{N} \sum_{\mathbf{k}} \int_{-\infty}^{\infty} \frac{d\epsilon}{2\pi} \left(-\frac{\partial f(\epsilon)}{\partial \epsilon} \right) \sum_{\{a\}} \left[\Lambda_{x;2;ba}(\mathbf{k}, \epsilon, \mathbf{k}, \epsilon) \overleftrightarrow{\frac{\partial}{\partial k_y}} \Lambda_{y;2;dc}(\mathbf{k}, \epsilon, \mathbf{k}, \epsilon) \right] \\ &\quad \times \text{Im} \left[G_{cb}^{(A)}(\mathbf{k}, \epsilon) \overleftrightarrow{\frac{\partial}{\partial k_x}} G_{ad}^{(R)}(\mathbf{k}, \epsilon) \right]. \end{aligned} \quad (2.84)$$

Note that the reason why two momentum derivatives appear is to exclude the terms being both \mathbf{q} -linear and \mathbf{A} -linear. We see from Eq. (2.84) that $\lim_{H \rightarrow 0} (\sigma_{xy}^{(1)}/H)$ is proportional to the square term with respect to the QP lifetime since the retarded-advanced pair gives the linear

term and the momentum derivate of that leads to the additional term of the QP lifetime. As a result, the Hall coefficient Eq. (2.66) is independent of the QP lifetime. Also, we see from Eq. (2.84) that the difference between the result in the relaxation time approximation [57] and the present result is to replace the band velocities by the three-point vector VFs, which is the current including all the corrections due to electron correlation, as described in §2.3.1.

Therefore, we can calculate the Hall coefficient for multi-orbital systems in the weak-field limit by Eqs. (2.56), (2.57), (2.58), (2.66) and (2.84) if we give the form of $\mathcal{J}_{22;abcd}^{(0)}(k, k', 0)$.

2.4 Irreducible four-point VF in the FLEX approximation

In this section, I give the general derivation of the four-point VF of multi-orbital systems, which leads to the correction to the current, by the FLEX approximation. In particular, it is sufficient to consider the four-point VF which does not contain retarded-advanced pairs only in the cases of 22-II, 22-III, and 22-IV regions, which are shown in Fig. 2.10, since what we need to calculate is $\mathcal{J}_{22;abcd}^{(0)}(k, k', 0)$ of Eq. (2.57). This general derivation is just the extension of that [11] in the single-orbital Hubbard model.

This section is organized as follows. First, I show how to determine the irreducible four-point VF on the basis of conserving approximations [61, 62]. Before explaining the derivation of $\Gamma_{abcd}^{(0)}(k, k'; 0)$, by using the FLEX approximation, I present a simple example of the calculations for the second-order bubble type self-energy of electrons. Then, I turn to the case of the FLEX approximation, and calculate $\Gamma_{abcd}^{(0)}(k, k'; 0)$ in this approximation. After the analytic continuation in the cases of 22-II, 22-III, and 22-IV regions, we obtain finally $\mathcal{J}_{22;abcd}^{(0)}(k, k'; 0)$, which determines the three-point vector VF Eq. (2.57).

On the basis of conserving approximations [61, 62], the irreducible four-point VF is determined by the functional derivative of the self-energy of electrons with respect to the single-particle Green's function:

$$\Gamma_{abcd}^{(1)}(k, k'; q) = \Gamma_{abcd}^{(1)}(k + q, k; k' + q, k') = \frac{\delta \Sigma_{ac}(k)}{\delta G_{bd}(k')}. \quad (2.85)$$

For the actual derivations, it is necessary to label momentum and Matsubara frequency in each diagram correctly in order to satisfy conservation laws.

For exmaples of the calculations of $\Gamma_{abcd}^{(0)}(k, k'; 0)$, let us consider the case that the self-energy of electrons is given by the bubble type diagram in the second-order perturbation theory. In this case, as shown in Fig. 2.15, we can easily calculate $\Gamma_{abcd}^{(0)}(k, k'; 0)$ from Eq. (2.85). Note that the first and the second/third diagrams, shown in Fig. 2.15, are called the MT term [12, 13] and the AL term [14], respectively.

Similarly, we can calculate $\Gamma_{abcd}^{(0)}(k, k'; 0)$ in the case of the FLEX approximation whose self-energy of electrons is give by Eq. (2.17). As a result, we have

$$\begin{aligned} \Gamma_{abcd}^{(0)}(k, k'; q) &= \frac{T}{N} \sum_q \sum_{B,D} V_{aBcD}(q) \frac{\delta G_{BD}(k - q)}{G_{bd}(k')} + \frac{T}{N} \sum_q \sum_{B,D} \frac{\delta V_{aBcD}(q)}{G_{bd}(k')} G_{BD}(k - q) \\ &= \Gamma_{abcd}^{(0)\text{MT}}(k, k'; q) + \Gamma_{abcd}^{(0)\text{AL1}}(k, k'; q) + \Gamma_{abcd}^{(0)\text{AL2}}(k, k'; q), \end{aligned} \quad (2.86)$$

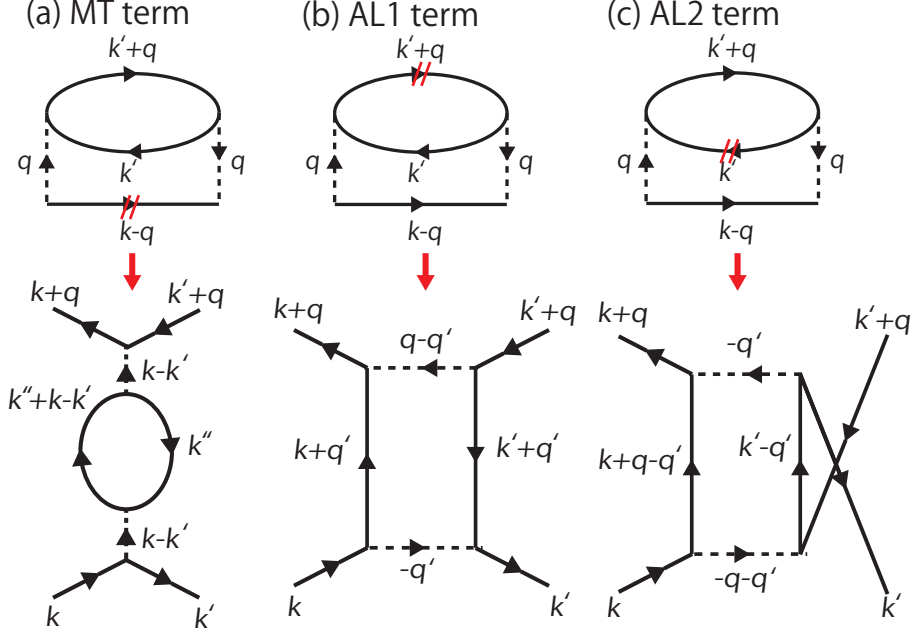


Figure 2.15: Diagrammatic representations of the second-order bubble type self-energy of electrons and the corresponding four-point VFs. Two red slashes denote the functional derivative of the single-particle Green's function in Eq. (2.85). First term and second/third term are called the MT term and the AL term, respectively.

where

$$\Gamma_{abcd}^{(0)\text{MT}}(k, k'; q) = V_{abcd}(k - k'), \quad (2.87)$$

$$\Gamma_{abcd}^{(0)\text{AL1}}(k, k'; q) = -\frac{T}{N} \sum_{q'} \sum_{\{A\}} G_{CA}(k' + q') G_{BD}(k + q') \tilde{W}_{\{A\};\{a\}}^{\text{AL1}}(-q', q - q'), \quad (2.88)$$

$$\Gamma_{abcd}^{(0)\text{AL2}}(k, k'; q) = -\frac{T}{N} \sum_{q'} \sum_{\{A\}} G_{AC}(k' - q') G_{BD}(k + q + q') \tilde{W}_{\{A\};\{a\}}^{\text{AL2}}(-q - q', -q'). \quad (2.89)$$

Here I have introduced two quantities

$$\begin{aligned} \tilde{W}_{\{A\};\{a\}}^{\text{AL1}}(-q', q - q') &= \frac{3}{2} \sum_{\{A'\}} \Gamma_{abA'B'}^{\text{S}}(M^{\text{S}})^{-1}_{A'B'bA}(-q')(N^{\text{S}})_{dCC'D'}(q - q') \Gamma_{C'D'cD}^{\text{S}} \\ &+ \frac{1}{2} \sum_{\{A'\}} \Gamma_{abA'B'}^{\text{C}}(M^{\text{C}})^{-1}_{A'B'bA}(-q')(N^{\text{C}})_{dCC'D'}(q - q') \Gamma_{C'D'cD}^{\text{C}} \\ &- \frac{1}{2} (\Gamma_{aBbA}^{\text{S}} + \Gamma_{aBbA}^{\text{C}}) \frac{1}{2} (\Gamma_{dCcD}^{\text{S}} + \Gamma_{dCcD}^{\text{C}}), \end{aligned} \quad (2.90)$$

$$\tilde{W}_{\{A\};\{a\}}^{\text{AL2}}(-q - q', -q') = \tilde{W}_{dBbD;aAcC}^{\text{AL1}}(-q - q', -q'), \quad (2.91)$$

where

$$(N^{\text{S/C}})_{abcd}(q) = \delta_{a,c} \delta_{b,d} \pm \sum_{a',b'} \Gamma_{aba'b'}^{\text{S/C}} \chi_{a'b'cd}^{(\text{S/C})}(q), \quad (2.92)$$

and $(M^{\text{S/C}})^{-1}_{abcd}(q)$ is the inverse matrix of $(M^{\text{S/C}})_{abcd}(q)$,

$$(M^{\text{S/C}})_{abcd}(q) = \delta_{a,c} \delta_{b,d} \mp \sum_{a',b'} \chi_{aba'b'}(q) \Gamma_{a'b'cd}^{\text{S/C}}. \quad (2.93)$$

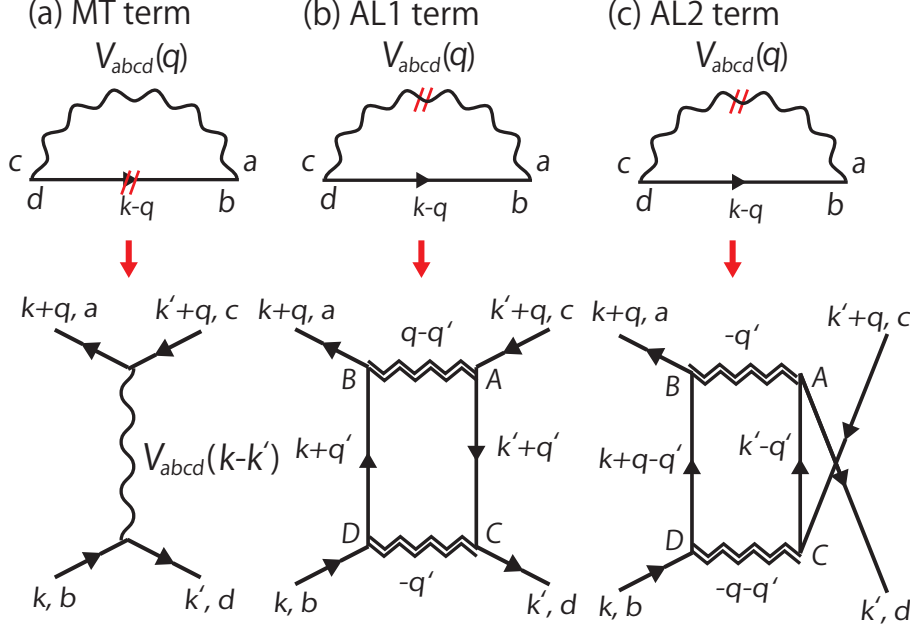


Figure 2.16: Diagrammatic representations of the self-energy of electrons of the FLEX approximation and the corresponding four-point VFs. Two red slashes denote the functional derivative of the single-particle Green's function in Eq. (2.85). First term and second/third term are called the MT term and the AL term, respectively. Two double lines in (b) and (c) correspond to $\tilde{W}_{\{A\};\{a\}}^{\text{AL1}}(-q', q - q')$ and $\tilde{W}_{\{A\};\{a\}}^{\text{AL2}}(-q - q', -q')$, respectively.

In deriving Eqs. (2.88) and (2.89), I have used the relations

$$\frac{\delta \chi_{a'b'c'd'}^{(\text{S/C})}(q')}{G_{bd}(k')} = \sum_{\{A'\}} (M^{\text{S/C}})_{a'b'A'B'}^{-1}(q') \frac{\delta \chi_{A'B'C'D'}(q')}{G_{bd}(k')} (N^{\text{S/C}})_{C'D'e'd'}(q'), \quad (2.94)$$

and

$$\frac{\delta \chi_{A'B'C'D'}(q')}{G_{bd}(k')} = -\delta_{A',b} \delta_{C',d} G_{D'B'}(k' - q') - \delta_{D',b} \delta_{B',d} G_{A'C'}(k' + q'). \quad (2.95)$$

It should be noted that in contrast to the case of a single-orbital system [11], it is impossible to write the AL terms by using the bare interaction vertices and $(M^{\text{S/C}})_{abcd}^{-1}(q)$ since $(N^{\text{S/C}})_{abcd}(q)$ is not equal to $(M^{\text{S/C}})_{abcd}^{-1}(q)$:

$$\begin{aligned} \chi_{abcd}^{(\text{S/C})}(q) &= \sum_{a',b'} (M^{\text{S/C}})_{aba'b'}^{-1}(q) \chi_{a'b'cd}(q) \\ &= \sum_{a',b'} \chi_{aba'b'}(q) (N^{\text{S/C}})_{a'b'cd}(q). \end{aligned} \quad (2.96)$$

I turn to the analytic continuations of $\Gamma_{abcd}^{(0)}(k, k'; 0)$ in the cases of 22-II, 22-III, and 22-IV regions and to calculate $\mathcal{J}_{22;abcd}^{(0)}(k, k'; 0)$ Eq. (2.34). Note that in contrast to the cases of the conductivities, the analytic continuation is about the bosonic Matsubara frequency [75].

After the analytic continuations, whose details are described below, we have

$$\mathcal{J}_{22;abcd}^{(0)}(k, k'; 0) = \mathcal{J}_{22;abcd}^{(0)\text{MT}}(k, k'; 0) + \mathcal{J}_{22;abcd}^{(0)\text{AL1}}(k, k'; 0) + \mathcal{J}_{22;abcd}^{(0)\text{AL2}}(k, k'; 0). \quad (2.97)$$

For the MT term Eq. (2.87), the procedure of the analytic continuation is simple, and the result is

$$\begin{aligned}\mathcal{J}_{22;\{a\}}^{(0)\text{MT}}(k, k'; 0) &= \coth \frac{\epsilon' - \epsilon}{2T} \left[\Gamma_{22;\{a\}}^{\text{II;MT}}(k, k'; 0) - \Gamma_{22;\{a\}}^{\text{III;MT}}(k, k'; 0) \right] \\ &\quad - \tanh \frac{\epsilon'}{2T} \left[\Gamma_{22;\{a\}}^{\text{II;MT}}(k, k'; 0) - \Gamma_{22;\{a\}}^{\text{IV;MT}}(k, k'; 0) \right] \\ &= \left(\coth \frac{\epsilon - \epsilon'}{2T} + \tanh \frac{\epsilon'}{2T} \right) 2i \text{Im} V_{abcd}^{(\text{R})}(k - k').\end{aligned}\quad (2.98)$$

We have used Eq. (2.34) and the relation $\Gamma_{22;\{a\}}^{\text{III;MT}}(k, k'; 0) = \Gamma_{22;\{a\}}^{\text{IV;MT}}(k, k'; 0)$. Note that $\Gamma_{\{a\}}^{(0)\text{MT}}(k, k'; 0)$ becomes $V_{\{a\}}^{(\text{A})}(k - k')$ in the region 22-II or $V_{\{a\}}^{(\text{R})}(k - k')$ in the regions 22-III and 22-IV since in the region 22-II, $\text{Im}\epsilon - \text{Im}\epsilon' < 0$, and in the regions 22-III and 22-IV, $\text{Im}\epsilon - \text{Im}\epsilon' > 0$ (see Fig. 2.10).

For the AL1 and the AL2 terms, the procedure of the analytic continuations is slightly complicated but straightforward. The results, whose detailed calculations are described below, are

$$\begin{aligned}\mathcal{J}_{22;\{a\}}^{(0)\text{AL1}}(k, k'; 0) &= \coth \frac{\epsilon' - \epsilon}{2T} \left[\Gamma_{22;\{a\}}^{\text{II;AL1}}(k, k'; 0) - \Gamma_{22;\{a\}}^{\text{III;AL1}}(k, k'; 0) \right] \\ &\quad - \tanh \frac{\epsilon'}{2T} \left[\Gamma_{22;\{a\}}^{\text{II;AL1}}(k, k'; 0) - \Gamma_{22;\{a\}}^{\text{IV;AL1}}(k, k'; 0) \right] \\ &= \left(\coth \frac{\epsilon' - \epsilon}{2T} - \tanh \frac{\epsilon'}{2T} \right) \left(\frac{-i}{\pi} \right) \frac{1}{N} \sum_{q'} \sum_{\{A\}} \int_{-\infty}^{\infty} d\omega' \left(\tanh \frac{\omega' + \epsilon}{2T} - \tanh \frac{\omega' + \epsilon'}{2T} \right) \\ &\quad \times W_{\{A\};\{a\}}^{\text{AL1}}(-q') \text{Im} G_{CA}^{(\text{R})}(k' + q') \text{Im} G_{BD}^{(\text{R})}(k + q'),\end{aligned}\quad (2.99)$$

$$\begin{aligned}\mathcal{J}_{22;\{a\}}^{(0)\text{AL2}}(k, k'; 0) &= \coth \frac{\epsilon' + \epsilon}{2T} \left[\Gamma_{22;\{a\}}^{\text{III;AL2}}(k, k'; 0) - \Gamma_{22;\{a\}}^{\text{IV;AL2}}(k, k'; 0) \right] \\ &\quad - \tanh \frac{\epsilon'}{2T} \left[\Gamma_{22;\{a\}}^{\text{II;AL2}}(k, k'; 0) - \Gamma_{22;\{a\}}^{\text{IV;AL2}}(k, k'; 0) \right] \\ &= \left(\coth \frac{\epsilon + \epsilon'}{2T} - \tanh \frac{\epsilon'}{2T} \right) \left(\frac{-i}{\pi} \right) \frac{1}{N} \sum_{q'} \sum_{\{A\}} \int_{-\infty}^{\infty} d\omega' \left(\tanh \frac{\omega' + \epsilon}{2T} - \tanh \frac{\omega' - \epsilon'}{2T} \right) \\ &\quad \times W_{\{A\};\{a\}}^{\text{AL2}}(-q') \text{Im} G_{AC}^{(\text{R})}(k' - q') \text{Im} G_{BD}^{(\text{R})}(k + q'),\end{aligned}\quad (2.100)$$

where

$$\begin{aligned}W_{\{A\};\{a\}}^{\text{AL1}}(-q') &= \frac{3}{2} \sum_{\{A'\}} \Gamma_{abA'B'}^{\text{S}} (M^{\text{S}(\text{A})})_{A'B'bA}^{-1}(-q') (N^{\text{S}(\text{R})})_{dCC'D'}(-q') \Gamma_{C'D'cD}^{\text{S}} \\ &\quad + \frac{1}{2} \sum_{\{A'\}} \Gamma_{abA'B'}^{\text{C}} (M^{\text{C}(\text{A})})_{A'B'bA}^{-1}(-q') (N^{\text{C}(\text{R})})_{dCC'D'}(-q') \Gamma_{C'D'cD}^{\text{C}} \\ &\quad - \frac{1}{2} (\Gamma_{aBbA}^{\text{S}} + \Gamma_{aBbA}^{\text{C}}) \frac{1}{2} (\Gamma_{dCcD}^{\text{S}} + \Gamma_{dCcD}^{\text{C}}),\end{aligned}\quad (2.101)$$

$$W_{\{A\};\{a\}}^{\text{AL2}}(-q') = W_{dBbD;aAcC}^{\text{AL1}}(-q'). \quad (2.102)$$

We have used Eq. (2.34) and the relations $\Gamma_{22;\{a\}}^{\text{III;AL1}}(k, k'; 0) = \Gamma_{22;\{a\}}^{\text{IV;AL1}}(k, k'; 0)$ and $\Gamma_{22;\{a\}}^{\text{II;AL2}}(k, k'; 0) = \Gamma_{22;\{a\}}^{\text{IV;AL2}}(k, k'; 0)$. We see from Eqs. (2.98), (2.99), and (2.100) that the AL VFs are of higher

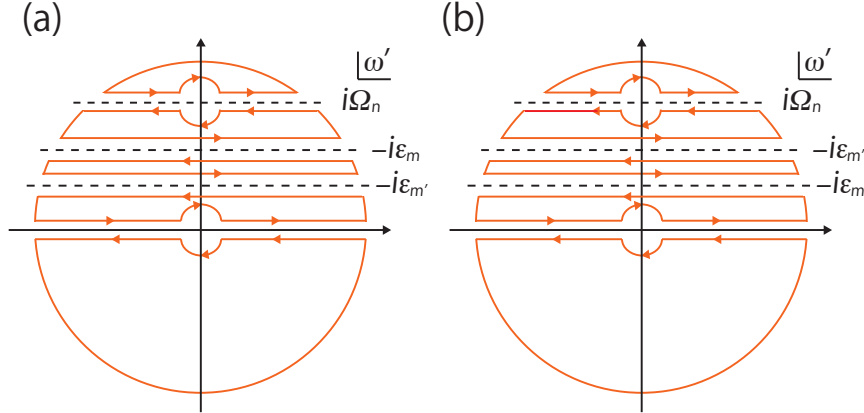


Figure 2.17: Contours used for the analytic continuations of the AL1 term Eq. (2.88) in (a) 22-II region and (b) 22-III and 22-IV regions. The difference between (a) and (b) is the relative location of $\omega' = -i\epsilon_m$ and $-i\epsilon_{m'}$.

order with respect to the QP damping than the MT VF since one of the two imaginary parts of the single-particle Green's function in the AL VFs gives the higher order contribution. It is noted that similarly to the case of a single-orbital system [11], $W_{\{A\};\{a\}}^{\text{AL1}/2}(-q')$ is real.

By using the contours shown in Fig. 2.17, we can carry out the analytic continuations of the AL1 term Eq. (2.88) in 22-II region and 22-III and 22-IV regions as follows:

$$\begin{aligned}
& \Gamma_{22;\{a\}}^{\text{II;AL1}}(k, k'; q) \\
&= -\frac{1}{N} \sum_{\mathbf{q}'} \sum_{\{A\}} \int_C \frac{d\omega'}{4\pi i} \coth \frac{\omega'}{2T} G_{CA}(\mathbf{k}' + \mathbf{q}', i\epsilon_{m'} + \omega') G_{BD}(\mathbf{k} + \mathbf{q}', i\epsilon_m + \omega') \\
&\quad \times \tilde{W}_{\{A\};\{a\}}^{\text{AL1}}(-\mathbf{q}', -\omega', \mathbf{q} - \mathbf{q}', i\Omega_n - \omega') \\
&\quad - \frac{T}{N} \sum_{\mathbf{q}'} \sum_{\{A\}} G_{CA}(\mathbf{k}' + \mathbf{q}', i\epsilon_{m'}) G_{BD}(\mathbf{k} + \mathbf{q}', i\epsilon_m) \tilde{W}_{\{A\};\{a\}}^{\text{AL1}}(-\mathbf{q}', 0, \mathbf{q} - \mathbf{q}', i\Omega_n) \\
&\quad - \frac{T}{N} \sum_{\mathbf{q}'} \sum_{\{A\}} G_{CA}(\mathbf{k}' + \mathbf{q}', i\epsilon_{m'} + i\Omega_n) G_{BD}(\mathbf{k} + \mathbf{q}', i\epsilon_m + i\Omega_n) \tilde{W}_{\{A\};\{a\}}^{\text{AL1}}(-\mathbf{q}', -\omega', \mathbf{q} - \mathbf{q}', 0) \\
&\rightarrow -\frac{1}{N} \sum_{\mathbf{q}'} \sum_{\{A\}} \int_{-\infty}^{\infty} \frac{d\omega'}{2\pi} \tanh \frac{\omega' + \epsilon'}{2T} \text{Im} G_{CA}^{(\text{R})}(k' + q') G_{BD}^{(\text{A})}(k + q') \tilde{W}_{\{A\};\{a\}}^{\text{AL1}}(-q', q - q') \\
&\quad - \frac{1}{N} \sum_{\mathbf{q}'} \sum_{\{A\}} \int_{-\infty}^{\infty} \frac{d\omega'}{2\pi} \tanh \frac{\omega' + \epsilon}{2T} G_{CA}^{(\text{R})}(k' + q') \text{Im} G_{BD}^{(\text{R})}(k + q') \tilde{W}_{\{A\};\{a\}}^{\text{AL1}}(-q', q - q') \\
&\quad + (\text{Principal integrals}), \tag{2.103}
\end{aligned}$$

and

$$\begin{aligned}
& \Gamma_{22;\{a\}}^{\text{III/IV;AL1}}(k, k'; q) \\
&\rightarrow -\frac{1}{N} \sum_{\mathbf{q}'} \sum_{\{A\}} \int_{-\infty}^{\infty} \frac{d\omega'}{2\pi} \tanh \frac{\omega' + \epsilon'}{2T} \text{Im} G_{CA}^{(\text{R})}(k' + q') G_{BD}^{(\text{R})}(k + q') \tilde{W}_{\{A\};\{a\}}^{\text{AL1}}(-q', q - q') \\
&\quad - \frac{1}{N} \sum_{\mathbf{q}'} \sum_{\{A\}} \int_{-\infty}^{\infty} \frac{d\omega'}{2\pi} \tanh \frac{\omega' + \epsilon}{2T} G_{CA}^{(\text{A})}(k' + q') \text{Im} G_{BD}^{(\text{R})}(k + q') \tilde{W}_{\{A\};\{a\}}^{\text{AL1}}(-q', q - q') \\
&\quad + (\text{Principal integrals}), \tag{2.104}
\end{aligned}$$

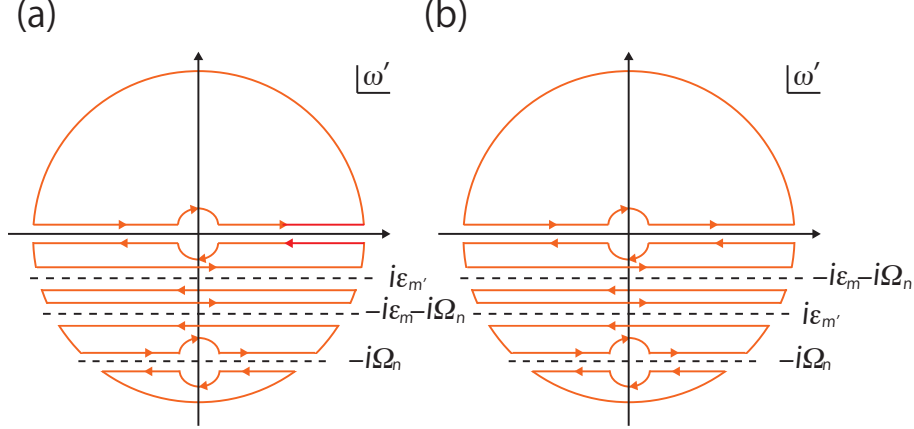


Figure 2.18: Contours used for the analytic continuations of the AL2 term Eq. (2.89) in (a) 22-II and 22-III regions and (b) 22-IV region. The difference between (a) and (b) is the relative location of $\omega' = i\epsilon_{m'}$ and $-i\epsilon_m - i\Omega_n$.

where (Principal integrals) are the contributions from $\omega' = i\Omega_n$ and 0, which are canceled out between the different regions due to Eq. (2.34), and \rightarrow represents the replacements of the three Matsubara frequencies, $i\epsilon_m$, $i\epsilon_{m'}$, and $i\Omega_n$, to the real frequencies satisfying the inequalities in each region (see Fig. 2.10).

Similarly, by using the contours shown in Fig. 2.18, we can carry out the analytic continuations of the AL2 term Eq. (2.89) in 22-II and 22-III regions and 22-IV region as follows:

$$\begin{aligned}
& \Gamma_{22;\{a\}}^{\text{II/III;AL2}}(k, k'; q) \\
&= -\frac{1}{N} \sum_{\mathbf{q}'} \sum_{\{A\}} \int_C \frac{d\omega'}{4\pi i} \coth \frac{\omega'}{2T} G_{AC}(\mathbf{k}' - \mathbf{q}', i\epsilon_{m'} - \omega') G_{BD}(\mathbf{k} + \mathbf{q} + \mathbf{q}', i\epsilon_m + i\Omega_n + \omega') \\
&\quad \times \tilde{W}_{\{A\};\{a\}}^{\text{AL2}}(-\mathbf{q} - \mathbf{q}', -i\Omega_n - \omega', -\mathbf{q}', -\omega') \\
&\quad - \frac{T}{N} \sum_{\mathbf{q}'} \sum_{\{A\}} G_{AC}(\mathbf{k}' - \mathbf{q}', i\epsilon_{m'}) G_{BD}(\mathbf{k} + \mathbf{q} + \mathbf{q}', i\epsilon_m + i\Omega_n) \tilde{W}_{\{A\};\{a\}}^{\text{AL2}}(-\mathbf{q} - \mathbf{q}', -i\Omega_n, -\mathbf{q}', 0) \\
&\quad - \frac{T}{N} \sum_{\mathbf{q}'} \sum_{\{A\}} G_{AC}(\mathbf{k}' - \mathbf{q}', i\epsilon_{m'} + i\Omega_n) G_{BD}(\mathbf{k} + \mathbf{q} + \mathbf{q}', i\epsilon_m) \tilde{W}_{\{A\};\{a\}}^{\text{AL2}}(-\mathbf{q} - \mathbf{q}', 0, -\mathbf{q}', i\Omega_n) \\
&\rightarrow -\frac{1}{N} \sum_{\mathbf{q}'} \sum_{\{A\}} \int_{-\infty}^{\infty} \frac{d\omega'}{2\pi} \tanh \frac{\omega' - \epsilon'}{2T} (-\text{Im} G_{AC}^{(\text{R})}(k' - q')) G_{BD}^{(\text{R})}(k + q + q') \tilde{W}_{\{A\};\{a\}}^{\text{AL2}}(-q - q', -q') \\
&\quad - \frac{1}{N} \sum_{\mathbf{q}'} \sum_{\{A\}} \int_{-\infty}^{\infty} \frac{d\omega'}{2\pi} \tanh \frac{\omega' + \epsilon + \omega}{2T} G_{AC}^{(\text{R})}(k' - q') \text{Im} G_{BD}^{(\text{R})}(k + q + q') \tilde{W}_{\{A\};\{a\}}^{\text{AL2}}(-q - q', -q') \\
&\quad + (\text{Principal integrals}), \tag{2.105}
\end{aligned}$$

and

$$\begin{aligned}
& \Gamma_{22;\{a\}}^{\text{IV;AL2}}(k, k'; q) \\
&\rightarrow -\frac{1}{N} \sum_{\mathbf{q}'} \sum_{\{A\}} \int_{-\infty}^{\infty} \frac{d\omega'}{2\pi} \tanh \frac{\omega' - \epsilon'}{2T} (-\text{Im} G_{AC}^{(\text{R})}(k' - q')) G_{BD}^{(\text{A})}(k + q + q') \tilde{W}_{\{A\};\{a\}}^{\text{AL2}}(-q - q', -q') \\
&\quad - \frac{1}{N} \sum_{\mathbf{q}'} \sum_{\{A\}} \int_{-\infty}^{\infty} \frac{d\omega'}{2\pi} \tanh \frac{\omega' + \epsilon + \omega}{2T} G_{AC}^{(\text{A})}(k' - q') \text{Im} G_{BD}^{(\text{R})}(k + q + q') \tilde{W}_{\{A\};\{a\}}^{\text{AL2}}(-q - q', -q') \\
&\quad + (\text{Principal integrals}), \tag{2.106}
\end{aligned}$$

where the contributions of (Principle integrals) to $\mathcal{J}_{22;abcd}^{(0)AL2}(k, k'; 0)$ are canceled out between the different regions due to Eq. (2.34). It should be noted that in the analytic continuation of the AL2 term, we have to pay attention to the minus sign of the bosonic Matsubara frequency in $G_{AC}^{(R)}(k' - q')$; in contrast to the case of the plus sign, that single-particle Green's function becomes advanced (retarded) in the upper (lower) path.

Therefore, we can determine the three-point vector VF from Eqs. (2.97), (2.98), (2.99), and (2.100), and can calculate the transport coefficients. Note that the three-point vector VF is real since the imaginary unit appearing in the CVC is canceled out with that appearing in the MT and the AL terms, i.e. Eqs. (2.98), (2.99), and (2.100).

Chapter 3

Results

In this chapter, I present the numerical results for the effective model of Sr_2RuO_4 near and away from the IC AF QCP by using the FLEX approximation including the MT CVC. After showing the momentum dependence of the QP damping in §3.1 and the dynamical property of SFs in §3.2, I present the temperature dependence of the in-plane resistivity and the Hall coefficient in the weak-field limit in §3.3 and §3.4, respectively.

Before presenting the numerical results, I explain how to choose the parameters and how to carry out the procedure for obtaining the quantities shown below.

The numerical calculations are carried out by using the following parameters. The BZ is divided into 64×64 meshes and 1024 Matsubara frequencies are taken for using the fast Fourier transformation. In this case, the numerical calculations for the analyses about not only static but also dynamic property can be safely carried out in the range of $T \geq 0.01$ eV since the non-interacting total bandwidth is about 4 eV. I set $J' = J_{\text{H}} = U/6$, $U' = U - 2J_{\text{H}}$, and consider the cases at $U = 1.6$ and 2.1 eV in $0.01 \leq T \leq 0.03$ (eV). For $U = 2.1$ eV ($U = 1.6$ eV), the system is located near (away from) the IC AF QCP since the spin susceptibility with $\mathbf{Q}_{\text{IC-AF}} = (2\pi/3, 2\pi/3)$, which is shown in Fig. 3.1, shows the CW like (the Pauli PM) temperature dependence. The reasons why I choose $U = 1.6$ eV as the case away from the QCP are that this value is lowest in the cases where the nesting vectors of the t_{2g} orbitals around $\mathbf{Q}_{\text{IC-AF}}$ coincide, and that it is possible to analyze the effects of the corresponding SFs of these orbitals, which are cooperatively enhanced near the QCP, on the transport properties by comparing with the results at $U = 2.1$ eV. For the integration with respect to real frequency, I approximate the upper and the lower values to $\epsilon_c = 0.2$ eV and $-\epsilon_c$, and discretize this integration with the interval being 0.0025 eV. This choice is sufficient to obtain the results without the numerical error in the cases considered since I have checked both the energy cut-off dependence for $\epsilon_c = 0.4, 0.6$ and 0.8 eV and the interval dependence for 0.002 and 0.005 eV and I have obtained the same results as those shown below within a few percent error.

By using these parameters, I calculate the quantities shown below as follows. The single-particle quantities, the susceptibilities, and the effective interaction are calculated by the self-consistent loop of the FLEX approximation Eqs. (2.12)–(2.17) until the relative error of the self-energy of electrons becomes less than 10^{-4} . In this procedure, the chemical potential is determined by Eq. (2.4) so as to hold $n_e = 4$ in each iteration. After the convergence of this self-consistent procedure, I carry out the analytic continuations of the self-energy of electrons, of the susceptibility in a spin sector, and of the effective interaction by the Padé approximation [76] using the lowest four Matsubara frequencies. Using these quantities, I calculate the three-point

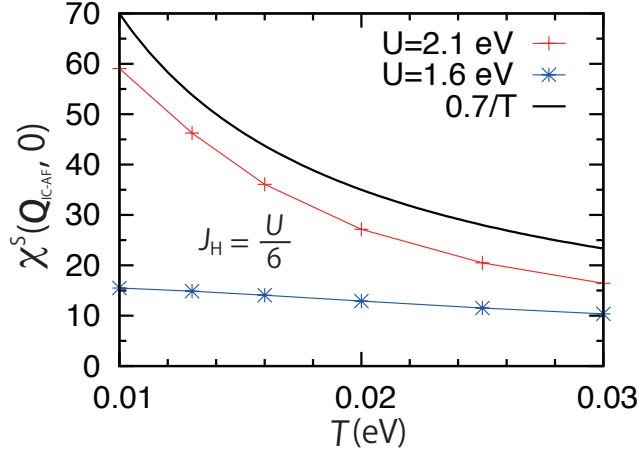


Figure 3.1: Temperature dependence of the static spin susceptibility at $U = 1.6$ and 2.1 eV in the FLEX approximation [2] for a 2D tight-binding model of Sr_2RuO_4 , where the non-interacting FS is the same as that obtained in the LDA [4, 5]. $\mathbf{Q}_{\text{IC-AF}}$ is $(2\pi/3, 2\pi/3)$, where the static spin susceptibility is most strongly enhanced at $U = 2.1$ eV. The data for $0.7/T$ is shown in order to compare the temperature dependence.

vector $\mathbf{V}\mathbf{F}$ by the iterative procedure for the BS equation Eq. (2.57) including only the MT CVC until its relative error becomes less than 10^{-4} . In this calculation, the principal integral with respect to real frequency is treated by subtracting and adding the numerator setting $\epsilon' = \epsilon$, i.e. the term except $[-1 + \exp(\epsilon' - \epsilon)/T]$. As a result, we can eliminate the singularity of the principal integral by the derivative with respect to real frequency as follows:

$$\begin{aligned} & \frac{1}{N} \sum_{\mathbf{k}'} \sum_{\{A\}} \int_{-\infty}^{\infty} \frac{d\epsilon'}{2\pi} \coth \frac{\epsilon - \epsilon'}{2T} \text{Im} V_{cdCD}^{(R)}(k - k') g_{2;CABD}(k'; 0) \Lambda_{\mu;2;AB}(k; 0) \\ &= \frac{1}{N} \sum_{\mathbf{k}'} \sum_{\{A\}} \int_{\epsilon' \neq \epsilon} \frac{d\epsilon'}{2\pi} \coth \frac{\epsilon - \epsilon'}{2T} \text{Im} V_{cdCD}^{(R)}(k - k') g_{2;CABD}(k'; 0) \Lambda_{\mu;2;AB}(k; 0) + T \left. \frac{\partial F_{cd}^{\text{MT}}(\mathbf{k}; \epsilon, \epsilon')}{\partial \epsilon'} \right|_{\epsilon' = \epsilon}, \end{aligned} \quad (3.1)$$

where the first term does not contain the contribution for $\epsilon' = \epsilon$ and

$$F_{cd}^{\text{MT}}(\mathbf{k}; \epsilon, \epsilon') = -\frac{1}{2\pi} (e^{(\epsilon' - \epsilon)/T} + 1) \frac{1}{N} \sum_{\mathbf{k}'} \sum_{\{A\}} \text{Im} V_{cdCD}^{(R)}(k - k') g_{2;CABD}(k'; 0) \Lambda_{\mu;2;AB}(k; 0). \quad (3.2)$$

Here I have used $\text{Im} V_{abcd}^{(R)}(\mathbf{q}, 0) = 0$.

3.1 QP damping

Here I present the momentum dependence of the QP damping near and away from the IC AF QCP at some temperatures. Hereafter the values of momentum of the damping are not restricted on those of the FS.

First, to analyze the role of each Ru t_{2g} orbital, I present the momentum dependence of the damping of each orbital, $\gamma_a(\mathbf{k}) = -\text{Im} \Sigma_{aa}^{(R)}(\mathbf{k}, 0)$, at $U = 2.1$ eV and $T = 0.01$ eV in Fig. 3.2 (a).

From this figure, there are two remarks to be drawn.

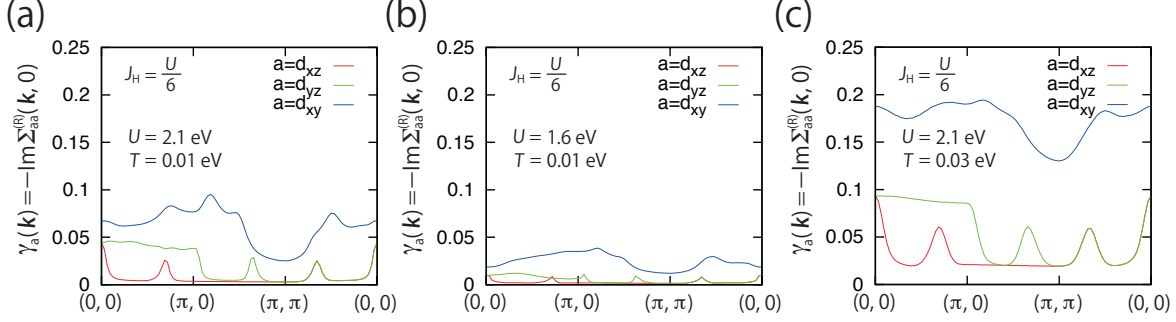


Figure 3.2: Momentum dependence of the damping obtained in the FLEX approximation [2] for a 2D tight-binding model of Sr_2RuO_4 , where the non-interacting FS is the same as that obtained in the LDA [4, 5].

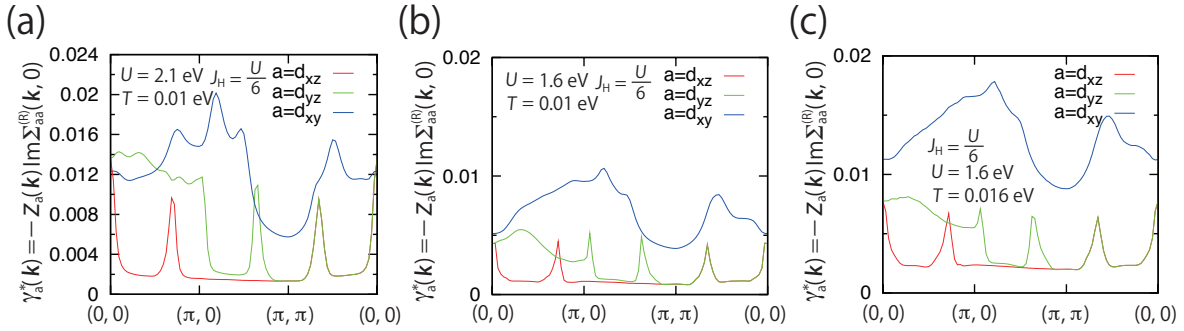


Figure 3.3: Momentum dependence of the QP damping in the FLEX approximation [2] for a 2D tight-binding model of Sr_2RuO_4 , where the non-interacting FS is the same as that obtained in the LDA [4, 5]. Note that the phenomenological FL description becomes valid when the QP damping is much smaller than temperature [10].

One is the orbital dependence: the damping of the d_{xy} orbital is much larger than that of the $d_{xz/yz}$ orbital. This indicates that the d_{xy} orbital is less coherent. This difference arises from the stronger SF of the d_{xy} orbital [see Fig. 1.12 (c)] since the self-energy of electrons is given by the convolution of the effective interaction, mediated by fluctuations, and the single-particle Green's function [see Eq. (2.17)]. As I will show in §3.3, due to this orbital dependence and the momentum dependence of the band velocities of the t_{2g} orbitals, the in-plane longitudinal conductivity arises mainly from the $d_{xz/yz}$ orbital, and the contribution from the d_{xy} orbital is very small.

The other is the momentum dependence: the peaks of the dampings of the t_{2g} orbitals arise from the corresponding SFs enhanced due to the nesting instability; e.g., SFs of the d_{xy} orbital located at $\mathbf{q} = (2\pi/3, 2\pi/3)$ and $(\pi, 3\pi/2)$ lead to the large dampings. In particular, the reason why the damping around $\mathbf{k} = (\pi, 3\pi/2)$ is larger than that around $\mathbf{k} = (2\pi/3, 2\pi/3)$ is due to the larger DOS since the vHs of the d_{xy} orbital exists around $\mathbf{k} \approx (\pi, 0)$. Note that in the case of Sr_2RuO_4 , the wave vector on the FS for the d_{xy} orbital around $\mathbf{k} = (\pi, 0)$ corresponds to $\mathbf{k} = (K, 0)$ with $K < \pi$ [see Fig. 2.3 (a)].

The similar result is obtained at a small value of U and at higher temperature. The results at $U = 1.6 \text{ eV}$ and $T = 0.01 \text{ eV}$ and at $U = 2.1 \text{ eV}$ and $T = 0.03 \text{ eV}$ are shown in Figs. 3.2 (b) and (c), respectively.

Thus, it is deduced from the results shown in Figs. 3.2 (a)–(c) that the larger damping of the d_{xy} orbital compared with that of the $d_{xz/yz}$ orbital and the very large peaks of the

damping of the d_{xy} orbital around $\mathbf{k} = (\pi, 3\pi/2)$ and $\mathbf{k} = (2\pi/3, 2\pi/3)$ are realized in all the cases considered in the analyses of this thesis.

Then, to discuss whether the phenomenological FL description works or not, I present the momentum dependence of the QP damping of each orbital, $\gamma_a^*(\mathbf{k}) = -z_a(\mathbf{k})\text{Im}\Sigma_{aa}^{(R)}(\mathbf{k}, 0)$, in the three cases considered above in Figs. 3.3 (a)–(c), where the renormalization factor, $z_a(\mathbf{k})$, is calculated by

$$z_a(\mathbf{k}) = \left[1 - \frac{\partial \Sigma_{aa}^{(R)}(\mathbf{k}, \omega)}{\partial \omega} \Big|_{\omega \rightarrow 0} \right]^{-1}. \quad (3.3)$$

In order that the phenomenological FL description works, it is necessary to turn on the interactions both sufficiently quickly so that the excitation is not damped and sufficiently slowly so that the energy resolution, the inverse of the interval of turning on the interactions, is smaller than the thermal excitation energy, which leads to the fading of the FS. These conditions are satisfied when the QP damping becomes smaller than temperature considered [10].

From Figs. 3.3 (a)–(c), we see two characteristic features related to the QCP. One is that at $U = 2.1$ eV, the phenomenological FL description is difficult since the QP damping is very large not only for the d_{xy} orbital but also for the $d_{xz/yz}$ orbital [Fig. 3.3 (a)]. The other is that at $U = 1.6$ eV, the phenomenological FL description is possible at $T = 0.01$ eV [Fig. 3.3 (b)], although that is difficult at $T = 0.016$ eV [Fig. 3.3 (c)]. As I will explain in §3.4, this difference between the cases near and away from the QCP plays an important role in discussing the effect of the MT CVC on the temperature dependence of the Hall coefficient in the weak-field limit.

These results about the QP damping suggest that the cases at $U = 1.6$ and 2.1 eV in $0.01 \leq T \leq 0.03$ (eV) are located in or very near red ellipse shown in Fig. 1.15. As described in §1.4, that red ellipse corresponds to the region where the treatment used is applicable.

Thus, I think that the transport properties in all the cases considered in this thesis can be analyzed by the method including only the MT CVC within the numerical accuracy.

Before going to the next section, I remark on the important difference between the phenomenological FL theory and microscopic perturbation theories. Microscopic perturbation theories do work even if the phenomenological FL description does not work. This difference is the reason why I calculate the transport coefficients by using the single-particle Green's function obtained in the FLEX approximation, which is one of the microscopic perturbation theories, instead of the standard FL type one. Note that this applicability of the microscopic perturbation theory is valid when the perturbation expansion with respect to electron correlation has good convergence. In other words, I assume that the convergence is good for all the cases considered in the analyses of this thesis.

3.2 Dynamical property of SFs

Here I present the dynamical property of SFs near and away from the IC AF QCP at $T = 0.01$ and 0.02 eV. In the following, I show the results for the SFs and the retarded effective interactions at $\mathbf{Q}_{\text{IC-AF}}$ and $\mathbf{Q}'_{\text{IC-AF}} = (\pi, 2\pi/3)$, and do not show the results for the other wave vectors and for the other fluctuations since in the model of Sr_2RuO_4 , the SFs at $\mathbf{Q}_{\text{IC-AF}}$ and $\mathbf{Q}'_{\text{IC-AF}}$ are strongly enhanced [Figs. 1.12 (b) and (c)] [2] and these give the dominant contribution to the effective interaction [see Eq. (2.16)]. Note that there are some symmetrically equivalent wave vectors with these wave vectors in Sr_2RuO_4 ; e.g., $\mathbf{q} = (2\pi/3, \pi)$ is equivalent to $\mathbf{Q}'_{\text{IC-AF}}$.

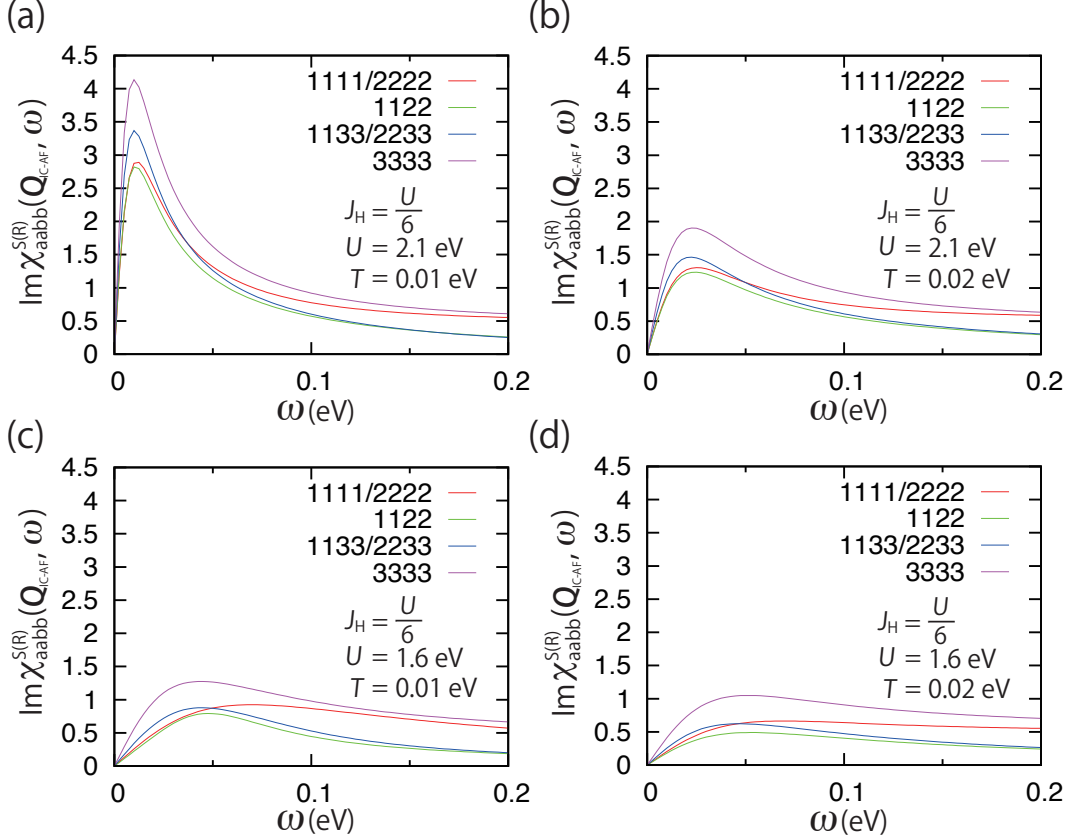


Figure 3.4: Real frequency dependence of the imaginary part of the retarded susceptibility in a spin sector at $\mathbf{Q}_{\text{IC-AF}}$ in the FLEX approximation [2] for a 2D tight-binding model of Sr_2RuO_4 , where the non-interacting FS is the same as that obtained in the LDA [4, 5]. As described in the beginning of §2, the d_{xz} , the d_{yz} , and the d_{xy} orbitals are labeled 1, 2, and 3, respectively.

First, I present the real frequency dependence of the imaginary part of the retarded susceptibilities in a spin sector at $\mathbf{Q}_{\text{IC-AF}}$ at $U = 2.1$ eV and $T = 0.01$ and 0.02 eV in Figs. 3.4 (a) and (b) and at $U = 1.6$ eV and $T = 0.01$ and 0.02 eV in Figs. 3.4 (c) and (d).

From these figures, there are two remarks about the dynamical property of SFs.

One is about the orbital dependence: in all the cases considered, the largest and the second largest contributions arise from the diagonal SF of the d_{xy} orbital (i.e. data for 3333) and the non-diagonal SF between the $d_{xz/yz}$ and the d_{xy} orbitals (i.e. data for 1133/2233), respectively, while the SFs of the $d_{xz/yz}$ orbital give smaller contributions. This result indicates that the SFs related to the d_{xy} orbital, i.e. the diagonal and the non-diagonal SFs, play more important roles in discussing the dynamical property of SFs than the others.

The other remark is about the characteristic properties due to quantum criticality [39]: as temperature decreases, at $U = 2.1$ eV, the peak position shifts to a lower energy and the value of the peak increases, while at $U = 1.6$ eV, the temperature dependence becomes very small and the peak position is located at not low energy. The former (latter) is a characteristic property near (away from) a QCP.

Next, the real frequency dependence of the imaginary part of the retarded susceptibilities in a spin sector at $\mathbf{Q}'_{\text{IC-AF}}$ is shown in Figs. 3.5 (a) and (b).

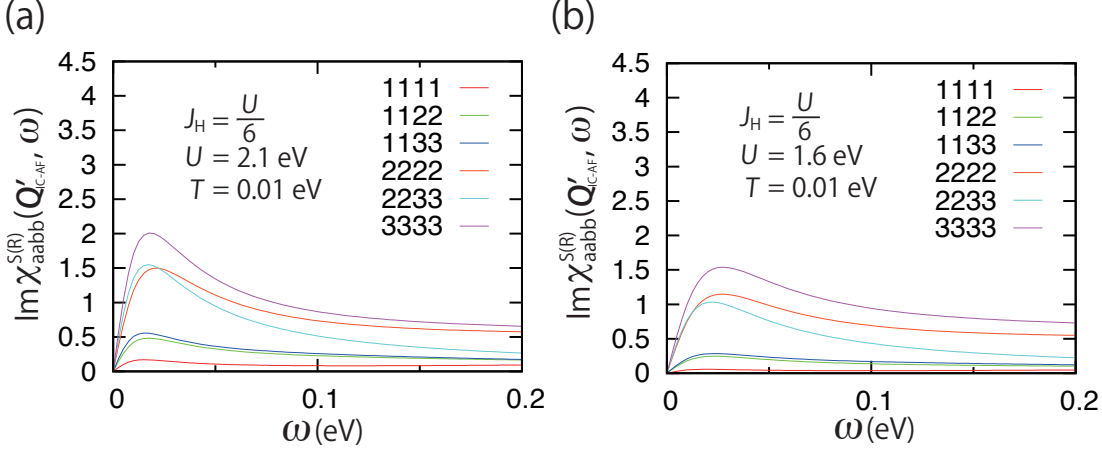


Figure 3.5: Real frequency dependence of the imaginary part of the retarded susceptibility in a spin sector at $\mathbf{Q}'_{\text{IC-AF}}$ in the FLEX approximation [2] for a 2D tight-binding model of Sr_2RuO_4 , where the non-interacting FS is the same as that obtained in the LDA [4, 5]. As described in the beginning of §2, the d_{xz} , the d_{yz} , and the d_{xy} orbitals are labeled 1, 2, and 3, respectively.

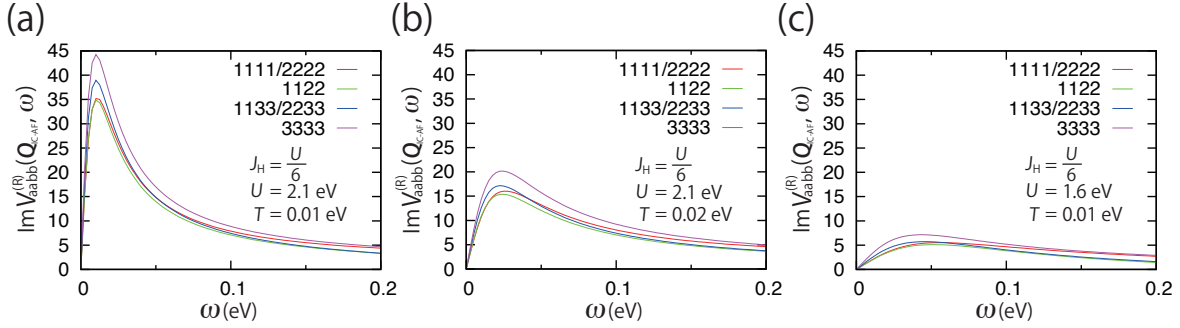


Figure 3.6: Real frequency dependence of the imaginary part of the retarded effective interaction at $\mathbf{Q}_{\text{IC-AF}}$ in the FLEX approximation [2] for a 2D tight-binding model of Sr_2RuO_4 , where the non-interacting FS is the same as that obtained in the LDA [4, 5]. As described in the beginning of §2, the d_{xz} , the d_{yz} , and the d_{xy} orbitals are labeled 1, 2, and 3, respectively.

From these figures, we see the similar results at $\mathbf{Q}_{\text{IC-AF}}$. Namely, the largest contribution arises from SFs related to the d_{xy} orbital, the peak position is located at lower energy at $U = 2.1$ eV than at $U = 1.6$ eV, and the value of the peak is larger at $U = 2.1$ eV. Note that in the case at $U = 2.1$ eV, the temperature dependence of the imaginary part of the retarded susceptibilities in a spin sector at $\mathbf{Q}'_{\text{IC-AF}}$ is weaker than that at $\mathbf{Q}_{\text{IC-AF}}$, although that temperature dependence at $\mathbf{Q}'_{\text{IC-AF}}$ is similar to that at $\mathbf{Q}_{\text{IC-AF}}$ (not shown here).

We also find that at $U = 1.6$ eV, the value of the peak for the diagonal SF of the d_{xy} orbital at $\mathbf{Q}'_{\text{IC-AF}}$ is larger than that at $\mathbf{Q}_{\text{IC-AF}}$ [Figs. 3.4 (c) and 3.5 (b)], while at $U = 2.1$ eV, the value of the peak at $\mathbf{Q}'_{\text{IC-AF}}$ becomes much smaller than that at $\mathbf{Q}_{\text{IC-AF}}$ [Figs. 3.4 (a) and 3.5 (a)].

Thus, these results indicate that away from the QCP, the dynamical property of SFs not only at $\mathbf{Q}_{\text{IC-AF}}$ but also at $\mathbf{Q}'_{\text{IC-AF}}$ is important, while near the QCP, the latter contribution becomes much smaller and the dynamical property of SFs only at $\mathbf{Q}_{\text{IC-AF}}$ is important.

Then, I turn to the real frequency dependence of the imaginary part of the retarded effective

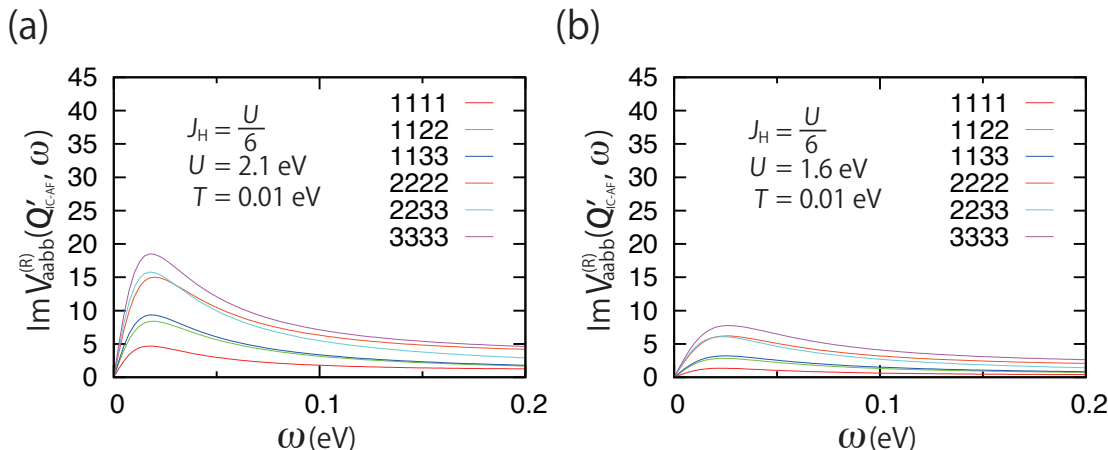


Figure 3.7: Real frequency dependence of the imaginary part of the retarded effective interaction at $Q'_{\text{IC-AF}}$ in the FLEX approximation [2] for a 2D tight-binding model of Sr_2RuO_4 , where the non-interacting FS is the same as that obtained in the LDA [4, 5]. As described in the beginning of §2, the d_{xz} , the d_{yz} , and the d_{xy} orbitals are labeled 1, 2, and 3, respectively.

interaction in the FLEX approximation, which is part of the kernel of the MT CVC and plays an important role in discussing the correction to the current due to electron correlation. The results for $Q_{\text{IC-AF}}$ and $Q'_{\text{IC-AF}}$ are shown in Figs. 3.6 (a)–(c) and 3.7 (a) and (b).

We see from these figures that the dependence of the imaginary part of the retarded effective interaction on U , T , orbital degrees of freedom and wave vector are the same as those of the retarded susceptibility in a spin sector. Namely, the diagonal and the non-diagonal components related to the d_{xy} orbital play very important roles. In particular, near the QCP, these diagonal and non-diagonal components only at $Q_{\text{IC-AF}}$ are important, while away from the QCP, those at $Q_{\text{IC-AF}}$ and $Q'_{\text{IC-AF}}$ are important. These results, which are similar to those of the retarded susceptibility in a spin sector, are due to the form of the effective interaction in the FLEX approximation: the effective interaction consists of the interaction mediated by fluctuations in spin and charge sectors [see Eq. (2.16)].

Finally, I discuss how the dynamical property of SFs shown above affects the current of each orbital through the MT CVC.

Before going to the detailed discussion, I explain the approximate solution of the BS equation for the three-point vector VF Eq. (2.57). (As described in §2.3.1, the three-point vector VF is the current including all the corrections due to electron correlation.) For simplicity, let us consider the three-point vector VF on the FS (i.e. $\epsilon = 0$ eV) since that near the FS plays an important role in determining the longitudinal and the transverse conductivities. Since SFs are dominant in the effective model of Sr_2RuO_4 [2] and the MT CVC in Eq. (2.98) contains the factor $\text{Im} V_{abcd}^{(R)}(\mathbf{k} - \mathbf{k}', 0 - \epsilon')$, the dominant corrections to the current due to the MT CVC arise from the regions where $\mathbf{k} - \mathbf{k}' = Q_{\text{IC-AF}}$ or $Q'_{\text{IC-AF}}$ satisfies and ϵ' is small. Considering only these dominant corrections due to the retarded effective interaction mediated by SFs, i.e. $\text{Im} V_{aabb}^{(R)}(\mathbf{k} - \mathbf{k}', 0 - \epsilon')$, we have the approximate solution within the linear order of the kernel

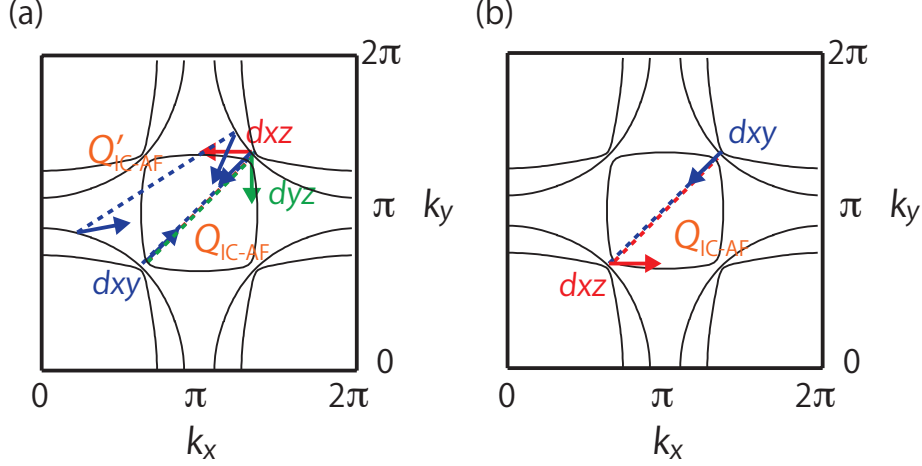


Figure 3.8: Schematic pictures how the currents of (a) the d_{xy} orbital and (b) the d_{xz} orbital on the Fermi level are affected by the MT CVC. The red, the green, and the blue arrows represent the band velocities of the d_{xz} , the d_{yz} , and the d_{xy} orbitals, respectively. The red, the green, and the blue dotted lines represent the nesting vectors of the d_{xz} , the d_{yz} , and the d_{xy} orbitals.

of the MT CVC, $\alpha_{ab}(\mathbf{Q}, \omega)$, of which the absolute value is smaller than an unity,

$$\begin{aligned} \Lambda_{x;2;aa}(\mathbf{k}, 0; 0) &\approx \Lambda_{x;2;aa}^{(0)}(\mathbf{k}, 0; 0) + \sum_{b=1}^3 \int_{-\infty}^{\infty} \frac{d\epsilon'}{2\pi} \alpha_{ab}(-\mathbf{Q}_{\text{IC-AF}}, -\epsilon') \Lambda_{x;2;bb}^{(0)}(\mathbf{k} + \mathbf{Q}_{\text{IC-AF}}, \epsilon'; 0) \\ &+ \sum_{b=1}^3 \int_{-\infty}^{\infty} \frac{d\epsilon'}{2\pi} \alpha_{ab}(-\mathbf{Q}'_{\text{IC-AF}}, -\epsilon') \Lambda_{x;2;bb}^{(0)}(\mathbf{k} + \mathbf{Q}'_{\text{IC-AF}}, \epsilon'; 0). \end{aligned} \quad (3.4)$$

Here I consider only the diagonal component of the three-point vector VF since that is larger than the non-diagonal one in the effective model of Sr_2RuO_4 . Thus, we see from Eq. (3.4) that the current of one orbital is renormalized by the MT CVC not only for itself but also for another orbital. In general, the renormalizations consist of the corrections to the absolute value of the current and to the angle between the current and the x -axis. (As I will explain in §3.3 and 3.4, the former correction is important in the case of the resistivity, and the latter correction is important in the case of the Hall coefficient in the weak-field limit.)

By using the results about the dynamical property of SFs and the above approximate solution, we can discuss how the current of each orbital is renormalized by the MT CVC.

For the d_{xy} orbital, in the case near the QCP, the dominant contributions of the CVC arise from $\text{Im}V_{3333}^{(\text{R})}(\mathbf{q}, \omega)$ at $\mathbf{q} = \mathbf{Q}_{\text{IC-AF}}$ and $\mathbf{Q}'_{\text{IC-AF}}$ and $\text{Im}V_{1133/2233}^{(\text{R})}(\mathbf{Q}_{\text{IC-AF}}, \omega)$, while away from the QCP, the dominant contributions arise from $\text{Im}V_{3333}^{(\text{R})}(\mathbf{q}, \omega)$ at $\mathbf{q} = \mathbf{Q}_{\text{IC-AF}}$ and $\mathbf{Q}'_{\text{IC-AF}}$. Combining these results with the direction of the current of each orbital on the FS, we find from Fig. 3.8 (a) that only the contribution of $\text{Im}V_{3333}^{(\text{R})}(\mathbf{Q}'_{\text{IC-AF}}, \omega)$ leads to the bend of the current, and the others just lead to the corrections to the absolute value of the current. It is noted that the bend of the current due to the non-diagonal SF with the d_{xz} orbital at $\mathbf{Q}_{\text{IC-AF}}$ is canceled out with that due to the orbital non-diagonal SF with d_{yz} orbital at $\mathbf{Q}_{\text{IC-AF}}$ [see Fig. 3.8 (a)].

For the d_{xz}/yz orbital, near the QCP, the largest and the second largest contributions of the CVC arise from $\text{Im}V_{1133/2233}^{(\text{R})}(\mathbf{Q}_{\text{IC-AF}}, \omega)$ and $\text{Im}V_{1111/2222}^{(\text{R})}(\mathbf{Q}_{\text{IC-AF}}, \omega)$, while away from the QCP, the dominant contributions arise from $\text{Im}V_{1133/2233}^{(\text{R})}(\mathbf{Q}_{\text{IC-AF}}, \omega)$, $\text{Im}V_{1111/2222}^{(\text{R})}(\mathbf{Q}_{\text{IC-AF}}, \omega)$,

$\text{Im}V_{2233}^{(R)}(\mathbf{Q}'_{\text{IC-AF}}, \omega)$, and $\text{Im}V_{2222}^{(R)}(\mathbf{Q}'_{\text{IC-AF}}, \omega)$. Similarly to the case for the d_{xy} orbital, we find from Fig. 3.8 (b) that the contributions related to the d_{xy} orbital [e.g., $\text{Im}V_{1133/2233}^{(R)}(\mathbf{Q}_{\text{IC-AF}}, \omega)$] leads to the bend of the current, and the others just lead to the corrections to the absolute value of the current. Note that the bend of the current of the $d_{xz/yz}$ orbital due to the diagonal SF of that orbital is very small since t_2 , the NN hopping integral due to the direct hopping process, is very small in the model of Sr_2RuO_4 (see Fig. 2.2).

Thus, we can expect that the current of the d_{xy} orbital is bent due to the MT CVC of the diagonal SF of that orbital at $\mathbf{Q}'_{\text{IC-AF}}$ and the current of the $d_{xz/yz}$ orbital is bent due to the MT CVC of the non-diagonal SF between that and the d_{xy} orbital at $\mathbf{Q}_{\text{IC-AF}}$, and that the other contributions of the MT CVC lead to corrections to the absolute values of the currents of these t_{2g} orbitals.

3.3 In-plane resistivity

Here I present the temperature dependence of the in-plane resistivity near and away from the IC AF QCP; hereafter, the constant factor due to e is neglected for brevity.

Before showing the numerical results, I briefly explain how the resistivity is modified by the MT CVC. (The following explanation holds even including the AL CVCs.) The longitudinal conductivity along the x -direction contains the factor

$$\begin{aligned}
& \Lambda_{x;2;ba}^{(0)}(k; 0)\Lambda_{x;2;cd}(k; 0) \\
&= |\Lambda_{2;ba}^{(0)}(k)| \cos \varphi_{ba}^0(k) |\Lambda_{2;cd}(k)| \cos \varphi_{cd}(k) \\
&= |\Lambda_{2;ba}^{(0)}(k)| \cos \varphi_{ba}^0(k) \left[|\Lambda_{2;cd}^{(0)}(k)| + \Delta |\Lambda_{2;cd}(k)| \right] \cos \left(\varphi_{cd}^0(k) + \Delta \varphi_{cd}(k) \right) \\
&\sim |\Lambda_{2;ba}^{(0)}(k)| \left[|\Lambda_{2;cd}^{(0)}(k)| + \Delta |\Lambda_{2;cd}(k)| \right] \cos \varphi_{ba}^0(k) \cos \varphi_{cd}^0(k) \left[1 - \frac{(\Delta \varphi_{cd}(k))^2}{2} \right], \quad (3.5)
\end{aligned}$$

where $\Delta |\Lambda_{2;cd}(k; 0)|$ and $\Delta \varphi_{cd}(k)$ represent the corrections to the absolute value and to the angle due to the MT CVC. Here only the finite terms are considered, i.e. the vanishing terms after the summations with respect to momentum are neglected. Similarly, the longitudinal conductivity along the y -direction contains the factor,

$$\begin{aligned}
& \Lambda_{y;2;ba}^{(0)}(k; 0)\Lambda_{y;2;cd}(k; 0) \\
&\sim |\Lambda_{2;ba}^{(0)}(k)| \left[|\Lambda_{2;cd}^{(0)}(k)| + \Delta |\Lambda_{2;cd}(k)| \right] \sin \varphi_{ba}^0(k) \sin \varphi_{cd}^0(k) \left[1 - \frac{(\Delta \varphi_{cd}(k))^2}{2} \right]. \quad (3.6)
\end{aligned}$$

From Eqs. (3.5) and (3.6), we see that in case of the longitudinal conductivity, the dominant effect of CVCs is the correction to the absolute value of the current, $\Delta |\Lambda_{2;cd}(k)|$, and that the effect of the correction to the angle due to CVCs, $\Delta \varphi_{cd}(k)$, is very small. Thus, the renormalization of the temperature dependence of the resistivity due to electron correlation arises mainly from the change of the absolute value of the current. In contrast, as I will describe in §3.4, the correction to the angle of the current due to the MT CVC at a certain wave vector plays important roles in discussing the temperature dependence of the Hall coefficient in the weak-field limit.

First, I present the temperature dependence of the in-plane resistivity with and without the MT CVC at $U = 2.1$ and 1.6 eV in Fig. 3.9 in order to analyze effects of both the momentum

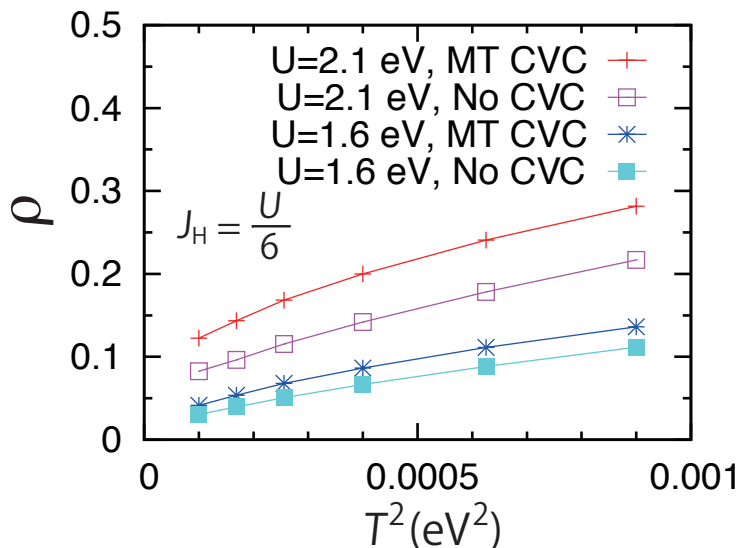


Figure 3.9: Temperature dependence of the in-plane resistivity at $U = 2.1$ and 1.6 eV with and without the MT CVC. As described in the text in detail, the reason for very small but finite asymptotic value of the in-plane resistivity at $T = 0$ eV in the cases of $U = 2.1$ and 1.6 eV with the MT CVC is due to very small but finite contributions of the AL CVCs, which are neglected in this calculation.

dependence of the self-energy of electrons and the temperature dependence of the MT four-point VF.

From this figure, there are two remarks to be drawn.

One is about the effects of the self-energy of electrons: the power of the temperature dependence of the in-plane resistivity changes from square at $U = 1.6$ eV to linear at $U = 2.1$ eV. Since this change occurs in both cases with and without the MT CVC, we find that this change of the power arises from the characteristic momentum dependence of the QP damping near the IC AF QCP. This sensitivity of the resistivity on the QP damping can be understood that the resistivity, formulated on the basis of the microscopic FL theory, is proportional to the QP damping [see Eq. (2.56)].

The other is about the effects of the MT CVC: the MT CVC leads to an increase of the in-plane resistivity, although this does not affect the power of the temperature dependence. This increase is mainly due to a decrease of the absolute value of the current since, as explained in the beginning of this section, the correction to the absolute value due to the MT CVC is more important in the longitudinal conductivity than that of the angle between the current and the x -axis. As I will present in Fig. 3.11, this decrease arises mainly from SF of the $d_{xz/yz}$ orbital.

Before going to the results about the role of each Ru t_{2g} orbital, I remark that the reason why the asymptotic value of the in-plane resistivity at $T = 0$ eV in the cases of $U = 2.1$ and 1.6 eV with the MT CVC seems to be very small but finite is that the contributions of the AL CVCs, which are neglected in this calculation, are very small but finite. Since very small but finite value strongly affects whether a certain value is zero or not, it is necessary to include not only the MT CVC but also the AL CVCs to discuss the value of the resistivity at very low temperature. However, I believe that such very small contributions do not lead to drastic changes from the obtained results.

Next, to analyze the role of each Ru t_{2g} orbital, I present the orbital dependence of the

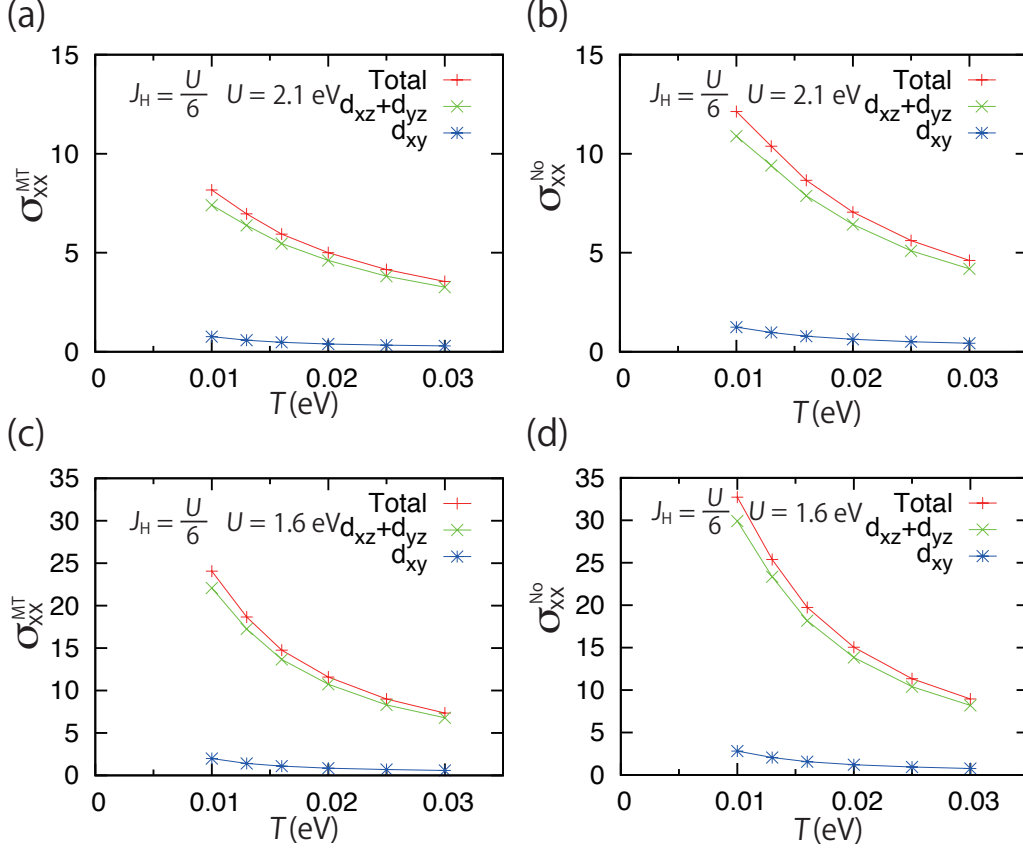


Figure 3.10: Temperature dependence of the in-plane longitudinal conductivities with and without the MT CVC. The data for the $d_{xz/yz}$ orbital and for the d_{xy} orbital represent the corresponding components in the longitudinal conductivity, whose definitions are given by Eqs. (3.7) and (3.8).

in-plane longitudinal conductivity in the cases considered above in Figs. 3.10 (a)–(d). Here I introduce the longitudinal conductivities of the $d_{xz/yz}$ and of the d_{xy} orbitals, which are defined as

$$\frac{2}{N} \sum_{\mathbf{k}} \sum_{a,b,c,d=1,2} \int_{-\infty}^{\infty} \frac{d\epsilon}{2\pi} \Lambda_{x;2;ba}^{(0)}(k;0) g_{2;acdb}(k;0) \Lambda_{x;2;cd}(k;0) \left(-\frac{\partial f(\epsilon)}{\partial \epsilon} \right), \quad (3.7)$$

and

$$\frac{2}{N} \sum_{\mathbf{k}} \sum_{a,b,c,d=3} \int_{-\infty}^{\infty} \frac{d\epsilon}{2\pi} \Lambda_{x;2;ba}^{(0)}(k;0) g_{2;acdb}(k;0) \Lambda_{x;2;cd}(k;0) \left(-\frac{\partial f(\epsilon)}{\partial \epsilon} \right), \quad (3.8)$$

respectively.

We see from Figs. 3.10 (a)–(d) that the in-plane longitudinal conductivity arises mainly from the $d_{xz/yz}$ orbital, and that the contribution from the d_{xy} orbital is very small. In particular, the d_{xz} orbital gives the primary contribution to the longitudinal conductivity along the x -direction. Also, from the equivalence between the x - and the y -directions, it is deduced that the primary contribution to the longitudinal conductivity along the y -direction arises from the d_{yz} orbital.

These results can be understood as the smaller QP damping of the $d_{xz/yz}$ orbital compared with that of the d_{xy} orbital and the momentum dependence of the band velocities of the Ru

t_{2g} orbitals along the x/y -direction. The detailed explanation is as follows. As shown in §3.1, the QP damping of the $d_{xz/yz}$ orbital is smaller than that of the d_{xy} orbital. In addition, the dominant contribution to the longitudinal conductivity along the x -direction arises from the band velocities around $k_x = \pi/2$ since the band velocities for the dispersions given by Eqs. (2.7)–(2.11) are

$$(v_{\mathbf{k}x})_{11} = 2t_1 \sin k_x, \quad (3.9)$$

$$(v_{\mathbf{k}x})_{12} = (v_{\mathbf{k}x})_{21} = -4t' \cos k_x \sin k_y, \quad (3.10)$$

$$(v_{\mathbf{k}x})_{22} = 2t_2 \sin k_x, \quad (3.11)$$

$$(v_{\mathbf{k}x})_{33} = 2t_3 \sin k_x + 4t_4 \sin k_x \cos k_y, \quad (3.12)$$

$$(v_{\mathbf{k}x})_{ab} = 0 \quad \text{otherwise} . \quad (3.13)$$

Although the band velocity of the d_{xy} orbital becomes comparable with that of the d_{xz} orbital only around $k_y = 0$ or π , there are no states related to the d_{xy} orbital around $k_x = \pi/2$ and $k_y = 0$ or π near the Fermi level [see Fig. 2.3 (a)]. As a result, the contribution of the d_{xy} orbital becomes smaller than that of the d_{xz} orbital. The similar discussion holds for the longitudinal conductivity along the y -direction. Thus, I conclude that the dominant contribution to the in-plane longitudinal conductivity arises mainly from the $d_{xz/yz}$ orbital in the model of Sr_2RuO_4 since in general the longitudinal conductivity becomes large for the small QP damping and for the large band velocity.

Finally, to analyze the role of each fluctuation, let us consider several special cases, where only some components of the retarded effective interaction with respect to orbital indices are taken into account as the MT CVC. To be precise, I introduce three cases other than the full MT CVC where all the components of the retarded effective interaction are included. These three cases are named SF-MT CVC, d_{xy} -SF-MT CVC, and $d_{xz/yz}$ -SF-MT CVC. Each definition is as follows. For the SF-MT CVC, only $\text{Im}V_{abb}^{(R)}(k - k')$ is taken into account. As a result, this retarded effective interaction arises mainly from SFs. Note that although the contribution from charge fluctuation is also taken into account in principle, the contribution is negligible compared with that from SF [2]. For the d_{xy} -SF-MT ($d_{xz/yz}$ -SF-MT) CVC, only $\text{Im}V_{aaa}^{(R)}(k - k')$ for $a = d_{xy}$ ($a = d_{xz}, d_{yz}$) is taken into account. It should be noted that by comparing the cases of the SF-MT CVC with the cases of the d_{xy} -SF-MT and the $d_{xz/yz}$ -SF-MT CVCs, we can analyze the effects of the non-diagonal SF between the $d_{xz/yz}$ and the d_{xy} orbitals since the difference between the former case and the latter cases from the contributions of that non-diagonal SF.

Figure 3.11 shows the temperature dependence of the in-plane resistivity in several cases of the MT CVCs at $U = 2.1$ eV.

From this figure, there are three remarks to be drawn.

First, the dominant contributions of the full MT CVC arise from SFs since the temperature dependence in the case including the full MT CVC can be reproduced by considering only SF: the data named MT CVC is reproducible by that named SF-MT CVC. (As I will show in §3.4, the same result is obtained in the Hall coefficient in the weak-field limit.) This result is due to the fact that the dominant fluctuations of the model of Sr_2RuO_4 are SFs [2].

Second, the MT CVC due to the diagonal SF of the $d_{xz/yz}$ orbital gives the dominant contribution, while that due to the diagonal SF of the d_{xy} orbital little change on the values of the in-plane resistivity from that without the MT CVC. This result can be understood that

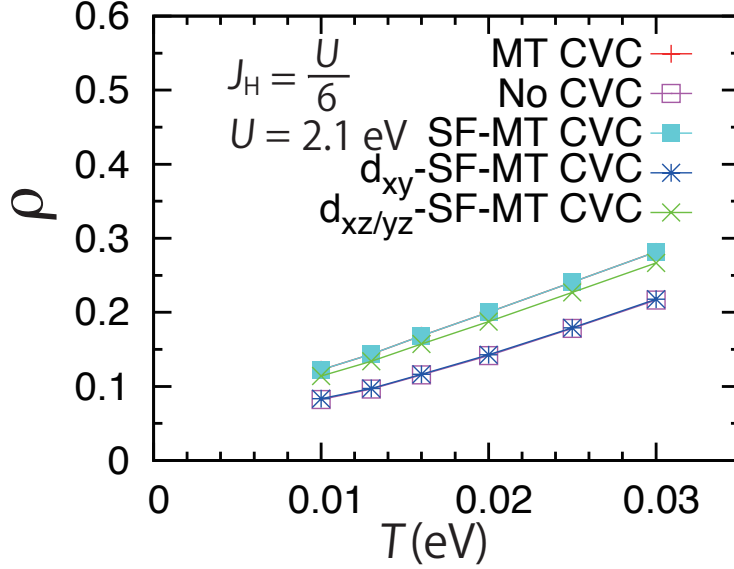


Figure 3.11: Temperature dependence of the in-plane resistivity at $U = 2.1$ eV in several cases of the MT CVCs; the definitions are given in the text. We see that the data for the full MT CVC can be reproduced by the data for the MT CVC considering only SFs. In particular, the primary contribution arises from the diagonal component of the $d_{xz/yz}$ orbital. As described in the text in detail, the reason for very small but finite asymptotic value of the in-plane resistivity at $T = 0$ eV in the cases with the full MT CVC is due to very small but finite contributions of the AL CVCs, which are neglected in this calculation.

the in-plane longitudinal conductivity arises mainly from the $d_{xz/yz}$ orbital, and the MT CVC only of that orbital leads to considerable effects on the longitudinal conductivity by changing the absolute value of the current.

Third, the MT CVC due to the non-diagonal SF gives small effects on the value of the in-plane resistivity since the contributions from the diagonal SF of the d_{xy} orbital are negligible and the difference between the values for SF-MT CVC and for $d_{xz/yz}$ -SF-MT CVC is small. This result can be understood that the MT CVC due to the non-diagonal SF gives rise to a small change of the absolute value of the current. [As I will show in §3.4, this CVC gives a considerable change of the angle for the current around $\mathbf{k} = (2\pi/3, 2\pi/3)$, resulting in the renormalization of the temperature dependence of the Hall coefficient in the weak-field limit.]

3.4 Hall coefficient in the weak-field limit

Here I present the temperature dependence of the Hall coefficient in the weak-field limit near and away from the IC AF QCP. (As described in §3.3, the constant factor due to e is neglected for brevity.)

Before showing the numerical results, I briefly explain how the MT CVC modifies the Hall coefficient in the weak-field limit. (The following explanation holds even including the AL CVCs.) Similarly to the case of the longitudinal conductivity [Eqs. (3.5) and (3.6)], the transverse

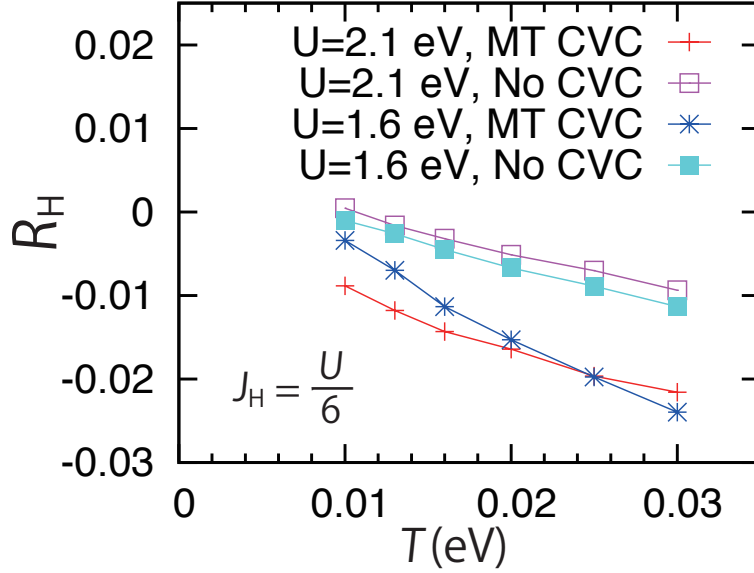


Figure 3.12: Temperature dependence of the Hall coefficient in the weak-field limit at $U = 2.1$ and 1.6 eV with and without the MT CVC.

conductivity divided by the magnetic field contains the factor

$$\begin{aligned}
\left[\Lambda_{x;2;ba}(k;0) \frac{\overleftrightarrow{\partial}}{\partial k_y} \Lambda_{y;2;dc}(k;0) \right] &= \left[|\Lambda_{2;ba}^{(0)}(k)| + \Delta |\Lambda_{2;ba}(k)| \right] \left[|\Lambda_{2;dc}^{(0)}(k)| + \Delta |\Lambda_{2;dc}(k)| \right] \\
&\times \left[\cos \varphi_{ba}(k) \cos \varphi_{dc}(k) \frac{\partial \varphi_{dc}(k)}{\partial k_y} + \sin \varphi_{ba}(k) \frac{\partial \varphi_{ba}(k)}{\partial k_y} \sin \varphi_{dc}(k) \right] \\
&\sim \left[|\Lambda_{2;ba}^{(0)}(k)| + \Delta |\Lambda_{2;ba}(k)| \right] \left[|\Lambda_{2;dc}^{(0)}(k)| + \Delta |\Lambda_{2;dc}(k)| \right] \\
&\times \left[\cos \varphi_{ba}^{(0)}(k) \cos \varphi_{dc}^{(0)}(k) \left(\frac{\partial \varphi_{dc}^{(0)}(k)}{\partial k_y} + \frac{\partial \Delta \varphi_{dc}(k)}{\partial k_y} \right) \right. \\
&\quad \left. + \sin \varphi_{ba}^{(0)}(k) \left(\frac{\partial \varphi_{ba}^{(0)}(k)}{\partial k_y} + \frac{\partial \Delta \varphi_{ba}(k)}{\partial k_y} \right) \sin \varphi_{dc}^{(0)}(k) \right]. \quad (3.14)
\end{aligned}$$

Here the notation of each quantity is the same as that used in §3.3, and the vanishing terms after the summations with respect to momentum are neglected. From this equation, we see that the transverse conductivity divided by the magnetic field is affected not only by the change of the absolute value of the current, $\Delta |\Lambda_{2;ab}(k;0)| = |\Lambda_{2;ab}(k;0)| - |\Lambda_{2;ab}^{(0)}(k;0)|$, but also by the change of the angle of the current due to CVCs, $\Delta \varphi_{ab}(k) = \varphi_{ab}(k) - \varphi_{ab}^{(0)}(k)$, in part of the \mathbf{k} -space. (As described in §3.3, the latter change little affects the longitudinal conductivity since the order becomes higher and that does not contain momentum derivatives.) Since the Hall coefficient in the weak-field limit is given by Eq. (2.66), the corrections to the absolute value of the current, appearing in the transverse conductivity, are nearly cancelled out with that, appearing in the square of the longitudinal conductivity. Thus, the renormalization of the temperature dependence of the Hall coefficient in the weak-field limit due to electron correlation arises mainly from the change of the angle for the current in part of the \mathbf{k} -space.

First, I present the temperature dependence of the Hall coefficient in the weak-field limit with and without the MT CVC in Fig. 3.12.

There are three principal remarks.

First remark is about the effect of the self-energy of electrons: without the MT CVC, the value of the Hall coefficient in the weak-field limit at $U = 2.1$ eV is nearly the same as that at $U = 1.6$ eV, although the QP dampings are different in between. This result indicates that the self-energy of electrons gives a small effect on the value of the Hall coefficient in the weak-field limit. This can be understood that the Hall coefficient in the weak-field limit, which is formulated on the basis of the microscopic FL theory, is independent of the QP damping [see Eqs. (2.56), (2.66) and (2.84)].

Second and third remarks are about the effects of the MT CVC.

Second one is that near the IC AF QCP, the MT CVC gives rise to the negative enhancement of the Hall coefficient in the weak-field limit, and this enhancement persists even at low temperature. As I will explain below by using this figure and the other figures in detail, this enhancement arises mainly from the bend of the current of the $d_{xz/yz}$ orbital due to the MT CVC of the non-diagonal SF with the d_{xy} orbital located at $\mathbf{Q}_{\text{IC-AF}}$. Actually, as I will show in Fig. 3.14, when we consider only the MT CVC of the diagonal SF of the $d_{xz/yz}$ or the d_{xy} orbital, the enhancement is very small and cannot reproduce the value obtained for the full MT CVC. Thus, this enhancement is due to a multi-orbital effect and cannot be understood within single-orbital descriptions.

Third one is that away from the QCP (i.e. $U = 1.6$ eV), the negative enhancement of the Hall coefficient in the weak-field limit is induced by the MT CVC, and this enhancement is strongly suppressed at low temperatures. The former can be understood as the same mechanism as that in the case near the QCP, and the latter can be understood that there is another considerable contribution, whose sign is opposite compared with one contribution, from the bend of the current of the d_{xy} orbital at low temperature. As I will show below, the signs of the transverse conductivities of the $d_{xz/yz}$ and the d_{xy} orbitals are opposite.

Next, to analyze the role of each Ru t_{2g} orbital, I present each component of the transverse conductivity divided by the magnetic field in Figs. 3.13 (a)–(d). Each component of the Ru t_{2g} orbital is obtained by the same replacement used in the analyses of the in-plane resistivity: the transverse conductivities of the $d_{xz/yz}$ and of the d_{xy} orbitals divided by the magnetic field are defined as

$$-\frac{1}{N} \sum_{\mathbf{k}} \int_{-\infty}^{\infty} \frac{d\epsilon}{2\pi} \left(-\frac{\partial f(\epsilon)}{\partial \epsilon} \right) \sum_{a,b,c,d=1,2} \left[\Lambda_{x;2;ba}(k;0) \frac{\overleftrightarrow{\partial}}{\partial k_y} \Lambda_{y;2;dc}(k;0) \right] \text{Im} \left[G_{cb}^{(A)}(k) \frac{\overleftrightarrow{\partial}}{\partial k_x} G_{ad}^{(R)}(k) \right], \quad (3.15)$$

and

$$-\frac{1}{N} \sum_{\mathbf{k}} \int_{-\infty}^{\infty} \frac{d\epsilon}{2\pi} \left(-\frac{\partial f(\epsilon)}{\partial \epsilon} \right) \sum_{a,b,c,d=3} \left[\Lambda_{x;2;ba}(k;0) \frac{\overleftrightarrow{\partial}}{\partial k_y} \Lambda_{y;2;dc}(k;0) \right] \text{Im} \left[G_{cb}^{(A)}(k) \frac{\overleftrightarrow{\partial}}{\partial k_x} G_{ad}^{(R)}(k) \right], \quad (3.16)$$

respectively.

From Figs. 3.13 (a)–(d), we find three characteristic properties.

One is about the sign of the transverse conductivity of each orbital divided by the magnetic field: the signs for the $d_{xz/yz}$ and the d_{xy} orbitals are opposite. This arises from the details of the band structure and the occupation number of each orbital.

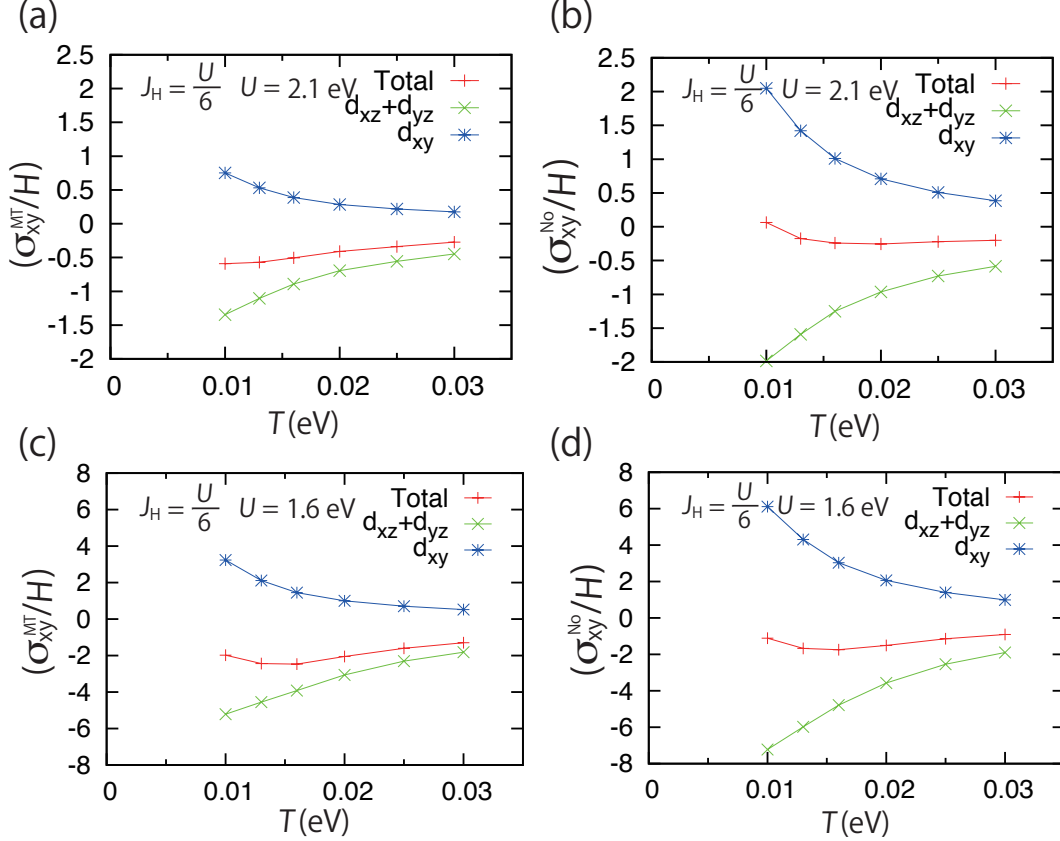


Figure 3.13: Temperature dependence of the transverse conductivities divided magnetic field at $U = 2.1$ and 1.6 eV with and without the MT CVC. The data for the $d_{xz/yz}$ and the d_{xy} orbitals represent the corresponding components in the transverse conductivity divided magnetic field, whose definitions are given by Eqs. (3.15) and (3.16).

The others are about the magnitude of the transverse conductivity of each orbital divided by the magnetic field without and with the MT CVC: although without the MT CVC, the absolute values of the transverse conductivities of the $d_{xz/yz}$ and the d_{xy} orbitals are comparable, the MT CVC gives rise to a larger suppression of the absolute value of the transverse conductivity of the d_{xy} orbital. This difference of the effect of the MT CVC between these orbitals can be understood that the MT CVC gives rise to a larger decrease of the magnitude of the transverse conductivity of the d_{xy} orbital due to the combination of a decrease of the current, which decreases the magnitude, and a change of the angle for the current, which increases the magnitude. As I will show in Fig. 3.14, in the case of the current of the d_{xy} orbital, the increase of the magnitude due to a change of the angle for the current is smaller compared with the case of the current of the $d_{xz/yz}$ orbital.

Thus, from these three characteristic properties, we can understand the reasons why the values of the Hall coefficients at $U = 2.1$ and 1.6 eV without the MT CVC are nearly zero and why the MT CVC gives rise to the negative enhancement.

Finally, to analyze the role of each fluctuation, I present the temperature dependence of the Hall coefficient in the weak-field limit in the same cases considered in the analysis of the resistivity in Fig. 3.14.

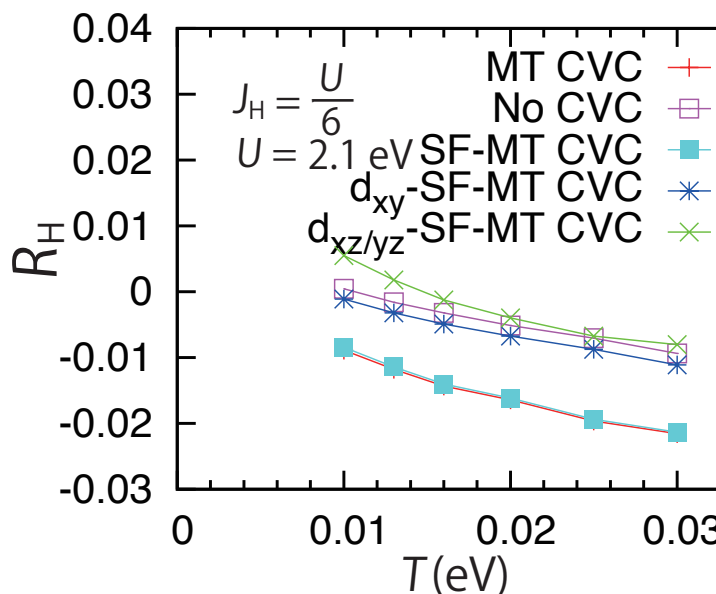


Figure 3.14: Temperature dependence of the Hall coefficient in the weak-field limit at $U = 2.1$ eV in several cases of the MT CVCs; the definitions are given in the text of §3.3. We see that the data for the full MT CVC can be reproduced by the data for the MT CVC considering only SFs, and that the dominant contributions to the full MT CVC arises not from the diagonal SFs of the $d_{xz/yz}$ or the d_{xy} orbital but from the non-diagonal SF between these orbitals.

From this figure, we find three principal results.

First one is that similarly to the result of the in-plane resistivity, the dominant contributions of the full MT CVC arise from SFs. The origin is the same as the case of the in-plane resistivity: SFs are dominant fluctuations of the model of Sr_2RuO_4 [2].

Second and third principal results are qualitatively different from the result of the in-plane resistivity.

Second one is that the diagonal SF of the $d_{xz/yz}$ (d_{xy}) orbital gives a slightly positive (negative) shift from that without the MT CVC. This result can be understood that the MT CVC due to that diagonal SF leads to a decrease of the current of that orbital, resulting in a decrease of the magnitude of the transverse conductivity of that orbital. As described above, the signs of the transverse conductivities of the $d_{xz/yz}$ and the d_{xy} orbital are negative and positive, respectively, and the MT CVC suppresses the value from that without the MT CVC. Note that the reasons why the difference between data without the MT CVC and with the $d_{xz/yz}$ -SF-MT CVC is enhanced at lower temperature is that the contributions from the d_{xy} orbital, whose sign is positive, become more considerable due to the combination of decreases both of the QP damping of the d_{xy} orbital at lower temperature and of the transverse conductivity of the $d_{xz/yz}$ orbital, which is induced by the $d_{xz/yz}$ -SF-MT CVC.

Third one is that the change of the Hall coefficient due the MT CVC arises not from the diagonal SF of the $d_{xz/yz}$ or the d_{xy} orbital but from the non-diagonal SF in between. It should be noted that if the non-diagonal component were not important and the diagonal component were important, the data for d_{xy} -SF-MT CVC or/and $d_{xz/yz}$ -SF-MT CVC would appear near the data for MT CVC.

These results can be understood as follows. The largest contribution of the renormalization

of the Hall coefficient due to the MT CVC arises from the bend of the current of the $d_{xz/yz}$ orbital due the non-diagonal SF between that and the d_{xy} orbital at $\mathbf{Q}_{\text{IC-AF}}$. The second largest contribution is the bend of the current of the d_{xy} orbital due the diagonal SF of that orbital at $\mathbf{Q}'_{\text{IC-AF}}$. The signs of these contributions are opposite.

Chapter 4

Discussion

In this chapter, I compare the obtained results with previous theoretical results in §4.1 and address their correspondences with the experimental results in §4.2. It should be noted that pure Sr_2RuO_4 is located not near the IC AF QCP but away from the IC AF QCP since the spin susceptibility observed experimentally shows Pauli paramagnetism [27]. Thus, it is better to compare the obtained results in the cases away from the IC AF QCP with the results for Sr_2RuO_4 .

4.1 Comparisons with other theoretical results

First, let us compare the obtained results with the previous study [11] for a single-orbital Hubbard model on a 2D square lattice by using the same method used in this thesis, i.e. the FLEX approximation including the MT CVC. Note that the qualitatively same result as this previous study has been obtained in larger meshes of the Brillouin zone [15].

The authors of this previous study [11] have found that near the AF QCP, where SF around $\mathbf{q} = (\pi, \pi)$ is strongly enhanced, the in-plane resistivity shows the T -linear dependence and the Hall coefficient in the weak-field limit shows the CW like temperature dependence. The former and the latter arise from the characteristic momentum dependence of the QP damping and the temperature dependence of the MT four-point VF, respectively. In addition to these principal results, they have shown that the MT CVC leads to an increase of the in-plane resistivity as a result of a decrease of the current, and that the asymptotic value of the in-plane resistivity at $T = 0$ eV becomes finite but very small in some cases considered [11]. Note that there are the other cases where the asymptotic value at $T = 0$ eV is zero only including the MT CVC.

For the in-plane resistivity, I have obtained the similar results for the Ru t_{2g} orbital Hubbard model on a 2D square lattice. The obtained results are that the power of the temperature dependence of the in-plane resistivity becomes linear at $U = 2.1$ eV (i.e. near the IC AF QCP), that the value of the in-plane resistivity increases by the MT CVC not only at $U = 2.1$ eV but also at $U = 1.6$ eV (i.e. away from the IC AF QCP), and that the asymptotic value of the in-plane resistivity at $T = 0$ eV becomes finite but very small.

This similarity between the results of the in-plane resistivity is due to the facts that the resistivity is strongly affected by the momentum dependence of the QP damping, and that the fluctuation of the orbital that gives the dominant contribution to the in-plane longitudinal conductivity is AF SF.

However, there is a considerable difference of the relation between the resistivity and the dominant fluctuation between single-orbital and multi-orbital systems. This difference is that in multi-orbital systems, the orbital giving the dominant contribution to the structure of fluctuations does not always give the dominant contribution to the longitudinal conductivity. The reasons are that the dominant contribution to the conduction arises from the orbital having the small QP damping, and that the QP damping becomes large for the orbital of which the fluctuation is strongly enhanced. Thus, the power of the temperature dependence of the in-plane resistivity just gives information about fluctuation of the orbital giving the dominant contribution to the longitudinal conductivity.

For the Hall coefficient in the weak-field limit, I have obtained the different result. The obtained result is that the temperature dependence of the Hall coefficient does not show the CW behavior even near the IC AF QCP, although the magnitude of the Hall coefficient enhances due to the MT CVC. As explained in §3.4, this result arises from two opposite-sign contributions to the Hall coefficient from the bends of the currents of the $d_{xz/yz}$ and the d_{xy} orbitals due to the MT CVC. Although the bend of the $d_{xz/yz}$ orbital is due to a multi-orbital effect, that of the d_{xy} orbital is similar to that in the single-orbital case [11].

This difference between the results of the temperature dependence of the Hall coefficient can be understood that in multi-orbital systems, the signs of the transverse conductivities of several orbitals are not always the same and there are several contributions of the MT CVC to the renormalization of the Hall coefficient in general.

Thus, I deduce from this comparison the same properties as those of the single-orbital case and the different properties. These same properties are the change of the power of the temperature dependence of the in-plane resistivity near the QCP, an increase of the value of the resistivity due to the MT CVC, and finite but very small asymptotic value of the in-plane resistivity at $T = 0$ eV. The different properties from those of the single-orbital case are the relation between the resistivity and the dominant fluctuation and the temperature dependence of the Hall coefficient in the weak-field limit near the QCP.

I turn to the comparison with the previous study [18] about the transport properties of Sr_2RuO_4 within the relaxation time approximation. It should be noted that in contrast to this previous theory [18], I do not use any ad hoc parameters about the QP damping.

As explained in §1.3, the authors of this previous theory [18] has shown that the experimental results of the in-plane resistivity and the Hall coefficient in the weak-field limit can be reproduced within the relaxation time approximation for the tight-binding model of Sr_2RuO_4 by using the momentum independent QP damping with some ad hoc parameters.

For the in-plane resistivity, I have obtained the similar result, i.e. the T^2 dependence at $U = 1.6$ eV. The similar result will be obtained in the other cases not near the IC AF QCP (e.g., $U = 1.8$ eV).

For the Hall coefficient in the weak-field limit, I have obtained the similar temperature dependence in the range of $100 \leq T \leq 150$ (K) but the smaller absolute value at $U = 1.6$ eV than that obtained in this previous theory [18]. This difference in the value is due to the experimentally inconsistent occupation number of each orbital in the theory used in this thesis.

However, I think that if the Hall coefficient is calculated in the same method as that used in this thesis by the model having the experimentally consistent occupation number of each orbital, the difference in the value of the Hall coefficient becomes smaller. The reasons are that the smaller absolute value of the Hall coefficient without the CVCs at $U = 2.1$ eV compared with that at $U = 1.6$ eV arises mainly from the change of the occupation number of each orbital,

and that the occupation number at $U = 2.1$ eV is nearer to the experimentally observed value than that at $U = 1.6$ eV.

Thus, I conclude that the similar temperature dependence of the in-plane resistivity and the Hall coefficient in the weak-field limit can be obtained in the more correct approximation for the effective model of Sr_2RuO_4 without any ad hoc parameters about the QP damping. In particular, two factors lacking in the previous phenomenological theory [18] of Sr_2RuO_4 , i.e. the momentum dependence of the self-energy of electrons and the temperature dependence of the electron-hole four-point VF, are not so important away from the IC AF QCP at low temperatures.

4.2 Correspondences with experimental results

First, I address the correspondence between the obtained results and the experimental results [22, 30] of pure Sr_2RuO_4 .

As shown in Figs. 1.3 (a) and (b), the in-plane resistivity [22] shows the T^2 -dependence at low temperatures, and the Hall coefficient [30] in the weak-field limit, which becomes zero at $T = 150$ K, shows the upward shift in the range of $100 \leq T \leq 300$ (K) as temperature decreases.

For the in-plane resistivity, the obtained results are consistent with this experimental result [22] since the T^2 behavior of the in-plane resistivity has been obtained at $U = 1.6$ eV.

For the Hall coefficient in the weak-field limit, the temperature dependence is qualitatively consistent with the experimental result [30], but the obtained value is inconsistent; e.g. the value including the MT CVC at $U = 1.6$ eV and $T = 150$ K ~ 0.013 eV is not equal to zero. The reason for this inconsistency can be understood as the experimentally inconsistent occupation number of each orbital in the theory used in this thesis. As described in §4.1, this inconsistency will be improved by using the model having the experimentally consistent occupation number of each orbital since the value of the Hall coefficient will shift upward compared with that obtained in this thesis.

Thus, I conclude that the obtained results are qualitatively consistent with the experimental results [22, 30] of pure Sr_2RuO_4 , although there is a remaining issue about the quantitative comparison of the value of the Hall coefficient in the weak-field limit by using the model having the experimentally consistent occupation number.

Next, I turn to the discussions about the correspondences between the obtained results and three unusual transport properties [22, 23, 24] of Sr_2RuO_4 .

As described in §1.4, I focus only on the in-plane transport and do not analyze the out-of-plane transport due to the difficulties of the treatments both of the three-dimensionality and of the incoherent conduction. Thus, the analysis about the out-of-plane resistivity is a future problem.

The mechanism for the negative enhancement [23] of the Hall coefficient due to tiny amount of nonmagnetic Al impurities can be qualitatively explained by the combination of the obtained results and the knowledge about the effect of the impurity scattering in the Born approximation, although the nonmagnetic impurity scattering is not taken into account for the actual calculations. As I will explain below in detail, that mechanism is that the dilute and weak nonmagnetic impurity scattering enhances a ratio of the QP damping of the d_{xy} orbital to that of the $d_{xz/yz}$ orbital, resulting in a suppression of the positive enhancement to the Hall coefficient due to the bend of the current of the d_{xy} orbital. As shown in §3.4, there are two opposite-sign

contributions to the Hall coefficient from the MT CVC, which are the bend of the current of the $d_{xz/yz}$ orbital due to the MT CVC of the non-diagonal SF between that and the d_{xy} orbital at $Q_{\text{IC-AF}}$ and that of the d_{xy} orbital due to the MT CVC of the diagonal SF of that orbital at $Q'_{\text{IC-AF}}$. If the dilute and weak impurity scattering is introduced in Sr_2RuO_4 , the QP damping of the d_{xy} orbital is more strongly enhanced compared with that of the $d_{xz/yz}$ orbital due to the larger DOS of the d_{xy} orbital near the Fermi level. Note that in the Born approximation [16], the self-energy of an orbital due to the impurity scattering is proportional to the DOS of that orbital. Since the kernel of the MT CVC contains the QP damping, this enhancement of a ratio of the QP damping of the d_{xy} orbital to that of the $d_{xz/yz}$ orbital leads to a larger suppression of the contribution of the bend of the current of the d_{xy} orbital than that of the $d_{xz/yz}$ orbital. As a result, the negative enhancement of the Hall coefficient is induced by the dilute and weak nonmagnetic impurity scattering. Since the above argument is just qualitative discussion, it is necessary to carry out the actual calculation in the presence of the dilute and weak nonmagnetic impurity scattering.

Similarly, the T -linear in-plane resistivity [24] in the case of small substitution of Ti^{4+} for Ru^{4+} can be understood by one of the obtained results, which is the T -linear dependence near the IC AF QCP. As described in §1.2.2, $\text{Sr}_2\text{Ru}_{1-y}\text{Ti}_y\text{O}_4$ at $y = 0.025$, which is located near the IC AF QCP, shows the T -linear dependence of the in-plane resistivity [24, 40]. Since the concentration of Ti is not so large compared with that of Ru, I think that the effect of the Ti substitution on the total occupation number is small. Although the mechanism that small substitution of Ti^{4+} for Ru^{4+} leads to the system being nearer to the IC AF QCP compared with Sr_2RuO_4 , I think that the obtained results can explain the experimental fact [24] that the power of the temperature dependence of the in-plane resistivity becomes linear near the IC AF QCP.

Thus, the obtained results can give the qualitative explanations about the mechanisms for two of the three unusual transport properties of Sr_2RuO_4 , although the actual calculations about the out-of-plane resistivity and the effects of nonmagnetic impurities are remaining future problems.

Chapter 5

Conclusions and remaining issues

In this chapter, I summarize the principal results and the conclusions and explain the remaining issues for future study.

There are the six principal results drawn from this study. Three of them are about the in-plane resistivity, and the others are about the Hall coefficient in the weak-field limit.

First one is about the effects of the self-energy of electrons on the in-plane resistivity: the power of the temperature dependence of the in-plane resistivity is strongly affected by the momentum dependent self-energy of electrons. Actually, we see from Figs. 3.9 and 3.11 that the power at $U = 1.6$ eV (i.e. away from the IC AF QCP) is square, while the power becomes linear at $U = 2.1$ eV (i.e. near the IC AF QCP).

Second one is about the effects of the MT CVC on the in-plane resistivity: the MT CVC little affects the power of the temperature dependence of the in-plane resistivity, although the value of the in-plane resistivity increases due to a decrease of the current, induced by the MT CVC. For the model of Sr_2RuO_4 , the main contribution to the MT CVC arises from SFs, and the contributions from the other fluctuations (e.g., orbital fluctuation) are negligible. In particular, the MT CVC of the diagonal SF of the $d_{xz/yz}$ orbital gives the primary effect on the in-plane resistivity.

Third one is about the role of each Ru t_{2g} orbital in the in-plane conduction: the longitudinal conductivity arises mainly from the $d_{xz/yz}$ orbital due to the smaller QP damping compared with that of the d_{xy} orbital and the momentum dependence of the band velocities. In particular, the d_{xz} (d_{yz}) orbital gives the primary contribution to conduction along the x -direction (y -direction). This larger contribution of the $d_{xz/yz}$ orbital compared with that of the d_{xy} orbital is the origin that the primary effect of the MT CVC on the in-plane resistivity arises from the diagonal component of SF of the $d_{xz/yz}$ orbital. In addition, this result suggests that the orbital giving the dominant contribution to the in-plane conduction is not equal to that giving the dominant contribution to the structure of magnetic fluctuations.

Fourth one is about the effect of the self-energy of electrons on the Hall coefficient in the weak-field limit: the self-energy of electrons gives a small effect on the value of the Hall coefficient. Actually, I have found that the difference between the values without the MT CVC at $U = 2.1$ and 1.6 eV is very small. This result arises from the dependence of the Hall coefficient on the self-energy of electrons. Instead, this small difference between the values of the Hall coefficient without the MT CVC at $U = 2.1$ and 1.6 eV arises from the small difference in the occupation number of each orbital.

Fifth one is about the role of each Ru t_{2g} orbital in the Hall coefficient in the weak-field limit:

the signs of the transverse conductivities of the $d_{xz/yz}$ and the d_{xy} orbitals divided by H are opposite, and the absolute value of the $d_{xz/yz}$ orbital without (with) the MT CVC is comparable with (larger than) that of the d_{xy} orbital. These opposite signs are due to the details of the band structure and the occupation number of each orbital, and the larger suppression of the transverse conductivity of the d_{xy} orbital arises from a combination of a decrease of the current, which decreases the magnitude of the transverse conductivity, and a bend of the current, which increases the magnitude.

Sixth one is about the effects of the MT CVC on the Hall coefficient in the weak-field limit: the MT CVC gives rise to the negative enhancement of the Hall coefficient not only near but also away from the IC AF QCP, although in the case away from the QCP the value reaches that without the MT CVC at low temperatures. This negative enhancement arises from the bend of the current of the $d_{xz/yz}$ orbital due to the MT CVC of the non-diagonal SF between that and the d_{xy} orbitals at $Q_{\text{IC-AF}}$. The suppression of the negative enhancement of the Hall coefficient away from the QCP arises from the opposite-sign contributions of that bend and the bend of the current of the d_{xy} orbital due to the MT CVC of the diagonal SF of that orbital at $Q'_{\text{IC-AF}}$. Since the former contribution, whose sign is negative, is primary near the IC AF QCP, the MT CVC gives rise to the negative enhancement of the Hall coefficient. On the other hand, in the case away from the IC AF QCP, since the latter contribution becomes nearly the same as the former contribution at low temperatures, these enhancements of the Hall coefficient are cancelled out at low temperatures.

From these principal results, we can deduce the following conclusions.

One is that the in-plane resistivity of Ru oxides is determined almost by the $d_{xz/yz}$ orbital since the QP damping of that orbital will remain smaller than that of the d_{xy} orbital. In particular, near the IC AF QCP, the characteristic momentum dependence of the QP damping of the $d_{xz/yz}$ orbital leads to the T -linear in-plane resistivity. As described in §4.2, I think that this result can explain the mechanism for the T -linear in-plane resistivity [24] in $\text{Sr}_2\text{Ru}_{1-y}\text{Ti}_y\text{O}_4$ at $y = 0.025$.

The other conclusion is that even near the IC AF QCP, the Hall coefficient of the model of Sr_2RuO_4 does not show the CW-like temperature dependence, which is obtained in the single-orbital case [11]. This arises from two opposite-sign contributions of the bends of the currents of the $d_{xz/yz}$ and of the d_{xy} orbitals due to the MT CVC. However, as explained in §4.2, the situation will be changed in the presence of dilute nonmagnetic impurities. In this case, an additional QP damping due to the nonmagnetic impurity scattering will lead to a negative enhancement of the Hall coefficient from the value in the absence of impurities as a result of an increase of a ratio of the QP damping of the d_{xy} orbital to that of the $d_{xz/yz}$ orbital. I think that this is the origin of the negative enhancement [23] of the Hall coefficient due to tiny amount of nonmagnetic Al impurities.

I believe that the obtained results lead to a deeper understanding of the transport properties of Ru oxides since the basis of the electronic structure of other Ru oxides is similar to that of Sr_2RuO_4 .

Also, I believe that the similar mechanism is realized in other multi-orbital SCES where several sheets of the FS's are located near each other and the dimensionalities of the orbital characters are different. The reasons are as follows. If several sheets of the FS's are located near each other, there are several nesting vectors, which are nearly the same. In the case of Sr_2RuO_4 , three sheets of the FS's are located near each other around $\mathbf{k} = (2\pi/3, 2\pi/3)$. In addition, if electron correlation becomes strong or moderately strong, these nesting vectors will coincide

due to the deformation of the FS. In particular, when the system is located near a QCP, the orbital cooperative fluctuation is most strongly enhanced and the temperature dependence of that is strong and leads to the CW like temperature dependence. Correspondingly, the effective interaction, mediated by this orbital cooperative fluctuation, shows the similar enhancement and strong temperature dependence. Furthermore, if there are some orbitals, whose dimensionalities are different in between, the current of one orbital can be bent through the MT CVC due to the non-diagonal fluctuations with another orbital. Finally, this bend of the current leads to the drastic renormalization of the temperature dependence of the Hall coefficient in the weak-field limit.

Finally, I explain six remaining issues for future study.

First one is about the actual calculations including the AL CVCs, which are neglected. The actual calculations including the AL CVCs are necessary to carry out since I have obtained very small but finite asymptotic value of the in-plane resistivity at $T = 0$ eV. It should be noted that as described in §3.3, there will be no drastic changes from the results obtained in this thesis even including the AL CVCs since it is known for the single-orbital Hubbard model on a 2D square lattice that the AL CVCs are very small near the AF QCP and the similar result will hold even in multi-orbital cases.

In addition, in the vicinity of a SC QCP, it is necessary to analyze the roles of the AL CVCs in multi-orbital systems since these roles have not been clarified yet. Note that the roles in a single-orbital system have been clarified and the importance of the AL CVCs near a SC QCP has been shown [14]. I believe that the analysis about the roles of the AL CVC in multi-orbital systems leads to a understanding of the origin of the unusual behavior in the Nernst coefficient of CeCoIn₅ [77] near a SC QCP since this compound is categorized into one of the multi-orbital SCES and has several sheets of the FS's being located near each other.

Second one is about the out-of-plane resistivity. As described in §1.4, the out-of-plane resistivity is not analyzed due to the difficulties of the treatments of the three-dimensionality and the incoherent conduction. Since it has been pointed out the importance of the role of the large QP damping due the vHs in cuprates [58], it is highly desirable to analyze the out-of-plane resistivity of Sr₂RuO₄ on the basis of the microscopic theory including the three-dimensionality and the momentum dependence of the QP damping.

Third one is about the dependence of the Hall coefficient on the occupation number of each orbital or on the total filling. Even for the same total filling as that of Sr₂RuO₄, the temperature dependence of the Hall coefficient will change in cases where the occupation number of each orbital is different from that considered in this thesis. Thus, it is necessary to investigate the effects of the change of the occupation number of each orbital in discussing the Hall coefficient in the weak-field limit. In addition, the analysis about the dependence of the occupation number of each orbital is needed for the quantitative comparison of the value of the Hall coefficient with the experimental result [30], as described in §4.1. Furthermore, the analysis about this dependence including the effects of the RuO₆ distortions (e.g. rotation) is highly desirable to clarify the origins of the unusual transport properties [23, 59] of Ca_{2-x}Sr_xRuO₄ around $x = 0.5$, where the occupation number of each orbital is changed by the rotation [48, 78] from that of Sr₂RuO₄. Then, since the change of the total filling gives a drastic change of the temperature dependence of the Hall coefficient, the analysis about the effects of the change of the total filling is needed. I believe that this analysis will lead to a deep understanding about the transport properties of other SCESs (e.g. CeCoIn₅ [77] in the case near the AF QCP).

Fourth one is about the difference between the present case, where SF is primary, and

another case, where another fluctuation becomes primary. For example, if orbital fluctuation becomes dominant, we will obtain different transport properties from those obtained in this thesis. In that case, there will be other contributions of the bend of the current. Since there are some candidates where not SF but orbital fluctuation is dominant (e.g. PrIrZn₂₀ [79]), the analysis about this issue is highly desirable.

Fifth one is about the effects of dilute nonmagnetic impurities on the transport properties of multi-orbital SCES. Although I have given the qualitative explanations about the mechanisms for the unusual transport properties induced by nonmagnetic impurities in §4.2, it is necessary to carry out the actual calculations in the presence of dilute nonmagnetic impurities. In addition, from a theoretical point of view, the effects of dilute nonmagnetic impurities on the transport properties of multi-orbital SCESs have not been clarified yet. Thus, I believe that the analysis about the effects of dilute nonmagnetic impurities leads to not only a understanding of the origin of the unusual transport properties [23, 24] of Sr₂RuO₄ but also a deep understanding of the roles of dilute nonmagnetic impurities in the transport properties of multi-orbital SCESs.

Sixth one is about the roles of local correlation in the transport properties of SCESs: how are the obtained results modified in case that local correlation also becomes strong. This issue is important from a theoretical point of view since both spatial and local correlations play important roles in discussing the electronic structures of SCESs [39, 52]. In addition, it is highly desirable to clarify the effects of local fluctuation for a spin-chiral degree of freedom on the transport properties since there is a previous theoretical study based on the cellular DMFT, showing the importance of this fluctuation at low energy in discussing the electronic structure for the single-orbital Hubbard model on a Kagome lattice [80]. In order to analyze these, it is necessary to use another theory where conservation laws satisfy and both spatial and local correlations are taken into account.

Acknowledgements

I would like to thank M. Ogata, Y. Yanase, T. Kariyado, H. Kontani, T. Nomura, T. Mizoguchi, and R. Morii due to the following reasons. M. Ogata, my supervisor, has taught me a lot of things about how to do a study, how to explain results obtained, and how to write a document; these are the basis of the present study. Y. Yanase has given me a lot of fruitful advices not only about the studies but also about the spirits of how to do a primary and intriguing study. T. Kariyado has given me a lot of useful advices about the numerical calculations. H. Kontani has shared the good opportunities of the fruitful discussions not only about my previous studies but also about my future studies. T. Nomura has given me a good question, resulting in the understanding of the mechanism of the unusual structure of magnetic fluctuations of Sr_2RuO_4 . T. Mizoguchi and R. Morii have shared valuable discussions in other studies, giving rise to my new way of thinking.

In addition, I would like to thank K. Ueda, H. Tsunetsugu, M. Imada, A. Fujimori, and S. Nakatsuji for giving me a lot of meaningful questions, which lead to my deeper understanding not only of the results obtained but also of other results for $\text{Ca}_{2-x}\text{Sr}_x\text{RuO}_4$, and several useful comments from theoretical and experimental points of view. As a result, I enjoy the discussions and the oral presentation.

Furthermore, I am grateful to all people who discussed and gave me a lot of useful comments for the poster and the oral presentations at several conferences because these comments lead to my deeper understanding of the results.

Finally, I have my parents and family to thank for my growth. In particular, they gave me a good opportunity to do what I want to do as much as I want without any anxieties.

Bibliography

- [1] Y. Maeno, H. Hashimoto, K. Yoshida, S. Nishizaki, T. Fujita, J. G. Bednorz, and F. Lichtenberg, *Superconductivity in a layered perovskite without copper*, Nature (London) **372**, 532 (1994).
- [2] N. Arakawa, in preparation. This is about the single-particle and the magnetic quantities of $\text{Ca}_{2-x}\text{Sr}_x\text{RuO}_4$ in $0.5 \leq x \leq 2$ in the FLEX approximation, where μ is self-consistently determined in each iteration so as to satisfy $n_e = 4$. This treatment will be better than the case where μ is determined after the self-consistent loop. In the latter treatment, which had been used previously (e.g., the results presented at the conference of 7th ISSP International Workshop and Symposium EQPCM 2013), U_c becomes smaller, the wave vector of the primary instability is slightly shifted, and the mass enhancement of each orbital becomes smaller. The others are qualitatively the same.
- [3] N. E. Bickers, D. J. Scalapino, and S. R. White, *Conserving Approximations for Strongly Correlated Electron Systems: Bethe-Salpeter Equation and Dynamics for the Two-Dimensional Hubbard Model*, Phys. Rev. Lett. **62**, 961 (1989).
- [4] T. Oguchi, *Electronic band structure of the superconductor Sr_2RuO_4* , Phys. Rev. B **51**, 1385 (1995).
- [5] I. I. Mazin and D. J. Singh, *Ferromagnetic Spin Fluctuation Induced Superconductivity in Sr_2RuO_4* , Phys. Rev. Lett. **79**, 733 (1997).
- [6] T. Takimoto, T. Hotta, and K. Ueda, *Strong-coupling theory of superconductivity in a degenerate Hubbard model*, Phys. Rev. B **69**, 104504 (2004).
- [7] H. Ikeda, R. Arita, and J. Kuneš, *Phase diagram and gap anisotropy in iron-pnictide superconductors*, Phys. Rev. B **81**, 054502 (2010).
- [8] G. M. Éliashberg, *TRANSPORT EQUATION FOR A DEGENERATE SYSTEM OF FERMI PARTICLES*, Sov. Phys. JETP **14**, 886 (1962).
- [9] H. Kohno and K. Yamada, *A General Expression for Hall Coefficient Based on Fermi Liquid Theory*, Prog. Theor. Phys. **80**, 623 (1988).
- [10] P. Nozières, *Theory of Interacting Fermi Systems* (Addison-Wesley, MA, 1997).
- [11] H. Kontani, K. Kanki, and K. Ueda, *Hall effect and resistivity in high- T_c superconductors: The conserving approximation*, Phys. Rev. B **59**, 723 (1999).

- [12] K. Maki, *Critical Fluctuation of the Order Parameter in a Superconductor. I*, Prog. Theor. Phys. **40**, 193 (1968).
- [13] R. S. Thompson, *Microwave, Flux Flow, and Fluctuation Resistance of Dirty Type-II Superconductors*, Phys. Rev. B **1**, 327 (1970).
- [14] L. G. Aslamasov and A. I. Larkin, *EFFECT OF FLUCTUATIONS ON THE PROPERTIES OF A SUPERCONDUCTOR ABOVE THE CRITICAL TEMPERATURE*, Sov. Phys. Solid State **10**, 875 (1968).
- [15] Y. Yanase, *Theory of Electric Transport in the Pseudogap State of High- T_c Cuprates*, J. Phys. Soc. Jpn. **71**, 278 (2002).
- [16] A. A. Abrikosov, L. P. Gorkov, I. E. Dyaloshinski, *Methods of Quantum Field Theory in Statistical Physics* (Dover Publications, INC., New York, 1963).
- [17] Y. Yamashita and K. Ueda, *Spin-orbital fluctuations and a large mass enhancement in LiV_2O_4* , Phys. Rev. B **67**, 195107 (2003).
- [18] C. Noce and M. Cuoco, *Phenomenological model for magnetotransport in a multiorbital system*, Phys. Rev. B **62**, 9884 (2000).
- [19] For an experimental review, see A. P. Mackenzie and Y. Maeno, *The superconductivity of Sr_2RuO_4 and the physics of spin-triplet pairing*, Rev. Mod. Phys. **75**, 657 (2003).
- [20] Y. Sidis, M. Braden, P. Bourges, B. Hennion, S. NishiZaki, Y. Maeno, and Y. Mori, *Evidence for Incommensurate Spin Fluctuations in Sr_2RuO_4* , Phys. Rev. Lett. **83**, 3320 (1999).
- [21] A. P. Mackenzie, S. R. Julian, A. J. Diver, G. J. McMullan, M. P. Ray, G. G. Lonzarich, Y. Maeno, S. Nishizaki, and T. Fujita, *Quantum Oscillations in the Layered Perovskite Superconductor Sr_2RuO_4* , Phys. Rev. Lett. **76**, 3786 (1996).
- [22] N. E. Hussey, A. P. Mackenzie, J. R. Cooper, Y. Maeno, S. Nishizaki, and T. Fujita, *Normal-state magnetoresistance of Sr_2RuO_4* , Phys. Rev. B **57**, 5505 (1998).
- [23] L. M. Galvin, R. S. Perry, A. W. Tyler, A. P. Mackenzie, S. Nakatsuji, and Y. Maeno, *Hall effect in single crystal $Ca_{2-x}Sr_xRuO_4$* , Phys. Rev. B **63**, 161102(R) (2001).
- [24] N. Kikugawa and Y. Maeno, *Non-Fermi-Liquid Behavior in Sr_2RuO_4 with Nonmagnetic Impurities*, Phys. Rev. Lett. **89**, 117001 (2002).
- [25] A. Damascelli, D. H. Lu, K. M. Shen, N. P. Armitage, F. Ronning, D. L. Feng, C. Kim, Z.-X. Shen, T. Kimura, Y. Tokura, Z. Q. Mao, and Y. Maeno, *Fermi Surface, Surface States, and Surface Reconstruction in Sr_2RuO_4* , Phys. Rev. Lett. **85**, 5194 (2000).
- [26] T. Katsufuji, M. Kasai, and Y. Tokura, *In-Plane and Out-of-Plane Optical Spectra of Sr_2RuO_4* , Phys. Rev. Lett. **76**, 126 (1995).
- [27] Y. Maeno, K. Yoshida, H. Hashimoto, S. Nishizaki, S. Ikeda, M. Nohara, T. Fujita, A. P. Mackenzie, N. E. Hussey, J. G. Bednorz, and F. Lichtenberg, *Two-Dimensional Fermi Liquid Behavior of the Superconductor Sr_2RuO_4* , J. Phys. Soc. Jpn. **66**, 1405 (1997).

- [28] H.-J. Noh, S.-J. Oh, B.-G. Park, J.-H. Park, J.-Y. Kim, H.-D. Kim, T. Mizokawa, L. H. Tjeng, H.-J. Lin, C. T. Chen, S. Schuppler, S. Nakatsuji, H. Fukazawa, and Y. Maeno, *Electronic structure and evolution of the orbital state in metallic $Ca_{2-x}Sr_xRuO_4$* , Phys. Rev. B **72**, 052411 (2005).
- [29] S. J. Moon, M. W. Kim, K. W. Kim, Y. S. Lee, J.-Y. Kim, J.-H. Park, B. J. Kim, S.-J. Oh, S. Nakatsuji, Y. Maeno, I. Nagai, S. I. Ikeda, G. Cao, and T. W. Noh, *Electronic structures of layered perovskite Sr_2MO_4 ($M=Ru, Rh, \text{ and } Ir$)*, Phys. Rev. B **74**, 113104 (2006).
- [30] A. P. Mackenzie, N. E. Hussey, A. J. Diver, S. R. Julian, Y. Maeno, S. Nishizaki, and T. Fujita, *Hall effect in the two-dimensional metal Sr_2RuO_4* , Phys. Rev. B **54**, 7425 (1996).
- [31] K. Ishida, Y. Kitaoka, K. Asayama, S. Ikeda, S. Nishizaki, Y. Maeno, K. Yoshida, and T. Fujita, *Anisotropic pairing in superconducting Sr_2RuO_4 : Ru NMR and NQR studies*, Phys. Rev. B **56**, R505 (1997).
- [32] I. I. Mazin and D. J. Singh, *Competitions in Layered Ruthenates: Ferromagnetism versus Antiferromagnetism and Triplet versus Singlet Pairing*, Phys. Rev. Lett. **82**, 4324 (1999).
- [33] A. Gukasov, M. Braden, R. J. Papoular, S. Nakatsuji, and Y. Maeno, *Anomalous Spin-Density Distribution on Oxygen and Ru in $Ca_{1.5}Sr_{0.5}RuO_4$: Polarized Neutron Diffraction Study*, Phys. Rev. Lett. **89**, 087202 (2002).
- [34] J. A. Duffy, S. M. Hayden, Y. Maeno, Z. Mao, J. Kulda, and G. J. McIntyre, *Polarized-Neutron Scattering Study of the Cooper-Pair Moment in Sr_2RuO_4* , Phys. Rev. Lett. **85**, 5412 (2000).
- [35] T. Imai, A. W. Hunt, K. R. Thurber, and F. C. Chou, *^{17}O NMR Evidence for Orbital Dependent Ferromagnetic Correlation in Sr_2RuO_4* , Phys. Rev. Lett. **81**, 3006 (1998).
- [36] K. Ishida, H. Mukuda, Y. Minami, Y. Kitaoka, Z. Q. Mao, H. Fukazawa, and Y. Maeno, *Normal-state spin dynamics in the spin-triplet superconductor Sr_2RuO_4* , Phys. Rev. B **64**, 100501(R) (2001).
- [37] H. Kontani, *Anomalous transport phenomena in Fermi liquids with strong magnetic fluctuations*, Rep. Prog. Phys. **71**, 026501 (2008).
- [38] O. Friedt, M. Braden, G. André, P. Adelman, S. Nakatsuji, and Y. Maeno, *Structural and magnetic aspects of the metal-insulator transition in $Ca_{2-x}Sr_xRuO_4$* , Phys. Rev. B **63**, 174432 (2001).
- [39] T. Moriya, *RECENT PROGRESS IN THE THEORY OF ITINERANT ELECTRON MAGNETISM*, J. Magn. Magn. Mater. **14**, 1 (1979).
- [40] K. Ishida, Y. Minami, Y. Kitaoka, S. Nakatsuji, N. Kikugawa, and Y. Maeno, *Evolution of normal-state magnetic fluctuations by Ca and Ti substitutions in Sr_2RuO_4 : ^{87}Sr -NMR study*, Phys. Rev. B **67**, 214412 (2003).
- [41] M. Braden, O. Friedt, Y. Sidis, P. Bourges, M. Minakata, and Y. Maeno, *Incommensurate Magnetic Ordering in $Sr_2Ru_{1-x}Ti_xO_4$* , Phys. Rev. Lett. **88**, 197002 (2002).

- [42] Y. Yanase and M. Ogata, *Microscopic Identification of the D-vector in Triplet Superconductor Sr_2RuO_4* , J. Phys. Soc. Jpn. **72**, 673 (2003).
- [43] D. J. Singh, *Relationship of Sr_2RuO_4 to the superconducting layered cuprates*, Phys. Rev. B **52**, 1358 (1995).
- [44] T. Oguchi, *Spin-Orbit Effects on the Ru-d Orbital Hybridization and Fermi Surface in $Ca_{2-x}Sr_xRuO_4$* , J. Phys. Soc. Jpn. **78**, 044702 (2009).
- [45] J. Mravlje, M. Aichhorn, T. Miyake, K. Haule, G. Kotliar, and A. Georges, *Coherence-Incoherence Crossover and the Mass-Renormalization Puzzles in Sr_2RuO_4* , Phys. Rev. Lett. **106**, 096401 (2011).
- [46] A. Liebsch and H. Ishida, *Subband Filling and Mott Transition in $Ca_{2-x}Sr_xRuO_4$* , Phys. Rev. Lett. **98**, 216403 (2007).
- [47] T. Nomura and K. Yamada, *Magnetic Properties of Quasi-Two-Dimensional Ruthenates Studied by Mean Field Theoretical Approach*, J. Phys. Soc. Jpn. **69**, 1856 (2000).
- [48] N. Arakawa and M. Ogata, *Competition between spin fluctuations in $Ca_{2-x}Sr_xRuO_4$ around $x = 0.5$* , Phys. Rev. B **87**, 195110 (2013).
- [49] T. Takimoto, *Orbital fluctuation-induced triplet superconductivity: Mechanism of superconductivity in Sr_2RuO_4* , Phys. Rev. B **62**, R14641 (2000).
- [50] K. Haule and G. Kotliar, *Coherence-incoherence crossover in the normal state of iron oxynictides and importance of Hund's rule coupling*, New J. Phys. **11**, 025021 (2009).
- [51] L. de' Medici, J. Mravlje, and A. Georges, *Janus-Faced Influence of Hund's Rule Coupling in Strongly Correlated Materials*, Phys. Rev. Lett. **107**, 256401 (2011).
- [52] A. Georges and W. Krauth, *Physical properties of the half-filled Hubbard model in infinite dimensions*, Phys. Rev. B **48**, 7167 (1993).
- [53] O. Parcollet, G. Biroli, and G. Kotliar, *Cluster Dynamical Mean Field Analysis of the Mott Transition*, Phys. Rev. Lett. **92**, 226402 (2004).
- [54] Y. Z. Zhang and M. Imada, *Pseudogap and Mott transition studied by cellular dynamical mean-field theory*, Phys. Rev. B **76**, 045108 (2007).
- [55] T. Maier, M. Jarrel, T. Pruschke, and J. Keller, *A non-crossing approximation for the study of intersite correlations*, Eur. Phys. J. B **13**, 613 (2000).
- [56] H. Ikeda, S. Shinkai, and K. Yamada, *Fourth-Order Perturbation Expansion for Hubbard Model on a Two-Dimensional Square Lattice*, J. Phys. Soc. Jpn. **77**, 064707 (2008).
- [57] J. M. Ziman, *Principles of the Theory of Solids* (Cambridge University Press, Cambridge, 1979).
- [58] Y. Yanase and K. Yamada, *Theory of Transport Phenomena in High- T_c Cuprates*, J. Phys. Soc. Jpn. **68**, 548 (1999).

- [59] S. Nakatsuji and Y. Maeno, *Quasi-Two-Dimensional Mott Transition System $Ca_{2-x}Sr_xRuO_4$* , Phys. Rev. Lett. **84**, 2666 (2000).
- [60] N. E. Bickers and S. R. White, *Conserving approximations for strongly fluctuating electron systems. II. Numerical results and parquet extension*, Phys. Rev. B **43**, 8044 (1991).
- [61] J. M. Luttinger and J. C. Ward, *Ground-State Energy of a Many-Ferimion System. II*, Phys. Rev. **118**, 1417 (1960).
- [62] G. Baym and L. P. Kadanoff, *Conserving Laws and Correlation Functions*, Phys. Rev. **124**, 287 (1961).
- [63] Y. Yanase and K. Yamada, *Pseudogap Phenomena and Superconducting Fluctuations in Hubbard Model for High- T_c Cuprates*, J. Phys. Soc. Jpn. **70**, 1659 (2001).
- [64] X. Y. Zhang, M. J. Rozenberg, and G. Kotliar, *Mott Transition in the $d = \infty$ Hubbard Model at Zero Temperature*, Phys. Rev. Lett. **70**, 1666 (1993).
- [65] N. Furukawa and M. Imada, *Two-Dimensional Hubbard Model–Metal Insulator Transition Studied by Monte Carlo Calculation–*, J. Phys. Soc. Jpn. **62**, 2557 (1993).
- [66] K. Morita, H. Maebashi, and K. Miyake, *FLEX study on Enhanced Charge Susceptibility near Antiferromagnetic Mott Transition in Two-Dimensional t - t' Hubbard Model*, J. Phys. Soc. Jpn. **72**, 3164 (2003).
- [67] R. Kubo, *Statistical-Mechanical Theory of Irreversible Processes. I. General Theory and Simple Applications to Magnetic and Conduction Problems*, J. Phys. Soc. Jpn. **12**, 570 (1957).
- [68] K. Yamada and Y. Yosida, *Fermi Liquid Theory on the Basis of the Periodic Anderson Hamiltonian*, Prog. Theor. Phys. **76**, 621 (1986).
- [69] H. Maebashi and H. Fukuyama, *Electrical Conductivity of Interacting Fermions. I. General Formulation*, J. Phys. Soc. Jpn. **66**, 3577 (1997).
- [70] W. Kohn, *Cyclotron Resonance and de Haas-van Alphen Oscillations of an Interacting Electron Gas*, Phys. Rev. **123**, 1242 (1961).
- [71] K. Kanki and K. Yamada, *Theory of Cyclotron Resonance in Interacting Electron Systems on the Basis of the Fermi Liquid Theory*, J. Phys. Soc. Jpn. **66**, 1103 (1997).
- [72] Y. Kuroda and A. D. S. Nagi, *Fermi-liquid theory and phase transitions*, Phys. Rev. **15**, 4460 (1977).
- [73] H. Fukuyama, H. Ebisawa, and Y. Wada, *Theory of Hall Effect. I –Nearly Free Electron–*, Prog. Theor. Phys. **42**, 494 (1969).
- [74] K. Yamada, *Densisoukan* (Iwanami shoten, Tokyo, 2000) [in Japanese].
- [75] Y. Takada, *Tatai modai* (Asakura shoten, Tokyo, 1999) [in Japanese].

-
- [76] H. J. Vildberg and J. W. Serene, *Solving the Eliashberg Equations by Means of N -Point Padé Approximants*, J. Low Temp. Phys. **29**, 179 (1977).
- [77] K. Izawa, K. Behnia, Y. Matsuda, H. Shishido, R. Settai, Y. Onuki, and J. Floquet, *Thermoelectric Response Near a Quantum Critical Point: The Case of $CeCoIn_5$* , Phys. Rev. Lett. **99**, 147005 (2007).
- [78] N. Arakawa and M. Ogata, *Origin of the heavy fermion behavior in $Ca_{2-x}Sr_xRuO_4$: Roles of Coulomb interaction and the rotation of RuO_6 octahedra*, Phys. Rev. B **86**, 125126 (2012).
- [79] K. Izawa *et al.*, unpublished.
- [80] M. Udagawa and Y. Motome, *Chirality-Driven Mass Enhancement in the Kagome Hubbard Model*, Phys. Rev. Lett. **104**, 106409 (2010).